Hasse Diagrams and Quiver Gauge Theory

Samuel BENNETT - September 2022

Supervisor: Amihay HANANY

Abstract. This report presents some recent advancements in the field of quiver gauge theory, focusing primarily on the application of Hasse diagrams to elucidate the structure of Higgs and Coulomb branches of various theories. A mathematical and physical background to the field is given before brane methods are introduced for Type IIB constructions, including the use of orientifold planes. The Hasse diagrams for particular classes of 3d $\mathcal{N} = 4$ theories are given and Hasse diagram inversion is shown to give the full moduli space of a particular set of theories. Type IIA brane constructions are used to present new computations regarding the Hasse diagram for a set of theories with enhanced global symmetry. The same brane calculations yield new electric quivers for some theories.

Contents

0.1. Introduction. Quantum field theory, for all its predictive power, remains an incomplete description of nature. Superstring theory, an enemy to all other joys, postulates the fundamental objects and symmetries of spacetime anew.

This report aims to delineate the reach of a novel technique that describes the behaviour of supersymmetric gauge theories under the only mechanism that gives them dynamics, the Higgs mechanism. Broadly, we consider a graphical representation, termed the *Hasse diagram*, of the singularity structure of transitions between different broken phases of an original theory. Such a diagram allows us to characterise the space of inequivalent vacua, called the moduli space, which is parametrised by the vacuum expectation values (VEVs) of the theory's scalar fields.

Despite their utility in gauge theory, Hasse diagrams are merely a diagrammatic way of representing a partial order imposed between various elements of a set. A *partial order* means that we may have elements in the set that do not have an ordering between them. For instance, in the set {A,B,C} we may institute a partial order $\prec$ between elements as {A $\prec$ C, B $\prec$ C} without making reference to any order between A and C. The Hasse diagram represents this by denoting each element of the set as a node and assigning an arrow between nodes (or otherwise directed line) to denote an order relation between them.

For supersymmetric gauge theories, the structure of the moduli space is often a symplectic singularity. We can foliate this into a set of symplectic *leaves*, each giving a different configuration of the theory under partial Higgsing to a subgroup of the gauge group.

This report will assume familiarity with 4d $\mathcal{N} = 1$ supersymmetry - further detail can be found in [1].

This report is arranged so as to show the motivations and development of the subject of Hasse diagrams in quiver gauge theory over the past several years. We will begin, - after an introduction to the mathematics and physics of the topic - by considering the brane methods which allow us to create Hasse diagrams and how we can associate them - in some cases - to nilpotent orbits of classical Lie algebras. We will also briefly consider the method by which we can associate particular Coulomb branches to transverse slices in an abstract mathematical object called the affine Grassmannian before considering a method to compute the Hasse diagram of the full moduli space of some 3d $\mathcal{N} = 4$ theories. We will then come to the main body of the work, which considers Hasse diagrams computed from recent work on quivers that have an enhanced global symmetry for their Coulomb branch. We present new calculations related to brane constructions of some of these theories and present electric quivers for particular magnetic quivers and associated brane systems.

0.2. Preliminaries. This chapter aims to provide a grounding in the mathematical and physical prerequisites that will be used in subsequent discussion. We begin with a description

of various configurations of extended supersymmetry, before relating these to quiver diagrams and exploring the technology required for the study of their vacuum configurations. Of particular importance is the difference in our approach between the *Coulomb* and *Higgs* branches of a theory - an outgrowth of the *nonrenormalisation theorem*. The "branch" structure of the moduli space will be discussed in due course.

The first insight we need is to see the moduli space of a theory as an *algebraic variety*, do be defined in this chapter. From here, we can straightforwardly use the refined Hilbert series to treat the Higgs branch and account for the quantum corrections to the Coulomb branch using *monopole operators*.

0.2.1. SUPERSYMMETRY & QUIVERS. Supersymmetry is often introduced as an extension of the four-dimensional Poincaré group via the introduction of two supercharges Q_α and $\bar{Q}_{\dot{\beta}}$ for spinorial indices $\alpha, \beta = 1,2$ - a setup termed 4d $\mathcal{N} = 1$. In this report, we will exclusively consider extended supersymmetries, where we introduce a further index A on our generators for $A = 1,..., \mathcal{N}$.

We shall also consider systems of dimension other than four, giving particular attention to $3d$ cases. Despite much of the analysis carrying over from the 4d case, there are significant differences we must take into account. For instance, in odd-dimension, the action picks up a *Chern-Simons term* (1) - containing a field strength multiplet F^b - on top of those from the Kähler potential and the superpotential [2].

$$S_{CS} = \frac{K_{ab}}{4\pi} \int d^d x d^{2\mathcal{N}} \theta \underbrace{(\epsilon^{ab} \bar{D}_\alpha V_a)}_{F^b} V_b \tag{1}$$

Further differences between the $3d$ and 4d cases concern the presence of monopole operators in the former [2]. These will be treated later.

0.2.1.1. $3d$ $\mathcal{N} = 4$. Three dimensional theories with eight supercharges are completely defined through their gauge groups and matter content. We hence see that the theory will contain only vector multiplets (Vplets) and hypermultiplets (Hplets), the former containing a vector field, three real scalar fields and their superpartners and the latter containing four real scalar fields and their superpartners [2]. A non-Abelian R-symmetry $SU(2)_C \times SU(2)_H$ transforms the three scalars in the Vplet as an SU(2) triplet and transforms the complex scalar and its complex conjugate in the Hplet as an SU(2) doublet [2]. In other words, the three scalars in the Vplet transform in the adjoint representation of the $SU(2)_C$ group and the trivial representation of the $SU(2)_H$ while the four scalars in the Hplet transform in the trivial representation of $SU(2)_C$ and the direct product of the trivial and adjoint representations of $SU(2)_H$.

We can also turn multiplets in $3d$ $\mathcal{N} = 4$ into multiplets in $3d$ $\mathcal{N} = 2$. Each Hplet in $\mathcal{N} = 4$ becomes two chiral multiplets (Cplets) in $3d$ $\mathcal{N} = 2$, one transforming in the fundamental representation of $SU(N)$ and the other transforming in the antifundamental representation [3]. As for Vplets in $3d$ $\mathcal{N} = 4$, they transform into one Vplet and one Cplet in $3d$ $\mathcal{N} = 2$. Quivers for $3d$ $\mathcal{N} = 4$ theories consist of round nodes depicting Vplets in the adjoint representation of the gauge group denoted by the node and square nodes depicting flavour groups. Lines between nodes depict an Hplet in the bifundamental representation of the two nodes it links. In analogy to the language of Dynkin diagrams, we define *simply laced quivers* to be those that contain only long nodes; we define *framed quivers* as those that have flavour groups (square nodes).

So for the case of $3d$ $\mathcal{N} = 4$ quivers decomposing into $3d$ $\mathcal{N} = 2$ quivers, we replace each $3d$ $\mathcal{N} = 4$ (undirected) edge representing an Hplet with two edges directed in opposite directions (representing the fundamental and antifundamental Cplets) and add to each gauge node in $3d$ $\mathcal{N} = 4$ a directed loop, representing the Cplet for the $3d$ $\mathcal{N} = 2$ case [4] [3].

We we also mention here the conventions for writing quivers with orthosymplectic groups. For a gauge or flavour node corresponding to the group $SO(k)$, we write the label O_k. For a gauge or flavour node corresponding to the group $Sp(k)$, we write the label C_k.

0.2.1.2. $6d$ $\mathcal{N} = (1, 0)$. We will also consider six-dimensional supersymmetric theories and the brane systems on which they can arise. The general interest of these theories notwithstanding, we will concern ourselves here with their uses in the correspondence between electric and magnetic quivers - we will see later that $3d$ $\mathcal{N} = 4$ quivers can be dualised to $6d$ $\mathcal{N} = (1, 0)$ theories in which the Higgs branch of the former is the Coulomb branch of the latter. We shall note that while such six-dimensional theories can be introduced through various compactifications, we will focus exclusively with Type IIA case derived from M5- and M9-branes on A-type singularities (D-type singularities give us the orthosymplectic case).

First, let us treat $6d$ $\mathcal{N} = (1, 0)$ theories in more detail. One of the main differences between three-dimensional and six-dimensional theories with eight supercharges is that we must introduce a *tensor multiplets* (Tplets) in the latter in order to cancel anomalies [5]. The Tplets contain scalars that can obtain non-zero VEVs and induce the *tensor branch* moduli space. For Vplets, in six dimensional they no longer contain scalar fields and so we no longer have a Coulomb branch. Some authors call the tensor branch in six dimensions a 'Coulomb branch' because the Tplets become Vplets under dimensional reduction to four or five dimensions [6]. In order to cancel gravitational anomalies we find that our different multiplets must obey,

$$n_h + 29n_t - n_v = const. \tag{2}$$

where n_h, n_t and n_v are the number of Hplets, Tplets and Vplets respectively. [6].

0.2.2. ROOTS, WEIGHTS AND DUAL SYSTEMS. We now turn to root and weight systems and their dual coroot and coweight systems. These are important concepts in the theory of Lie algebras and their representations; broadly, root and weight systems allow us to categorise the irreducible representations of classical Lie groups and are integral to the vocabulary and technology of modern theoretical physics. In this work we will use root and weight systems (and their duals, the *coroot* and *coweight* systems in the monopole formula for the Coulomb branch as well as the identification of transverse slices in the affine Grassmannian with the Coulomb branches of good quivers of type ADE. The following aims to provide a brief reminder of the concepts of root and weight systems before introducing the dualised coweight and coroot systems. We note that it is expected that the reader is familiar with the basic concepts and uses of roots and weights in the representation theory of semi-simple Lie algebras. Let us begin with a few definitions from [7].

- A *Root System* (V, R) is a real vector space V of finite dimension together with an inner product $\langle \cdot, \cdot \rangle$ and a finite subset $R \subset V$ such that $r \neq 0 \ \forall \ r \in R$ for which:

    - $\text{span}(R) = E$

    - For $b \in R$ and $\alpha \in \mathbb{R}$, $\alpha \cdot b \in R$ iff $|\alpha| = 1$

    - For $\alpha, \beta \in R$ then $S_\alpha \cdot \beta = \beta - 2\frac{\langle \beta, \alpha \rangle}{\langle \alpha, \alpha, \rangle}\alpha \in R$

    - For $\alpha, \beta \in R$ then $2\frac{\langle \beta, \alpha, \rangle}{\langle \alpha, \alpha, \rangle} \in \mathbb{Z}$

    The set of all S_α, for $\alpha \in R$, generate the *Weyl group* of R.

- The *root lattice* $\mathscr{R}_R$ corresponding to a root system (V, R) is the set $\mathscr{R}_R = \left\{ \sum_{i=1}^{|R|} a_i \alpha^i \Big| a_i \in \mathbb{Z}, \alpha^i \in R \right\}$.

- For a root system (V, R) we associate to each $\alpha \in R$ a $\beta^\vee \in R^\vee$. such that $\beta^\vee = 2\frac{\alpha}{\langle \alpha, \alpha \rangle}$. We call $R^\vee$ the *coroot system* or *dual root system* to R.

- The *coroot lattice* $\mathscr{R}_R^\vee$ corresponding to a root system (V, R) is the set $\mathscr{R}_R^\vee = \left\{ \sum_{i=1}^{|R^\vee|} a_i \alpha^{\vee i} \Big| a_i \in \mathbb{Z}, \alpha^{\vee i} \in R^\vee \right\}$

The reader will recall that in Lie theory we take $V = \mathfrak{g}$ for some semi-simple Lie algebra $\mathfrak{g}$ and use the fundamental roots in the theorem of the highest weight to construct the associated representation given a highest weight $\boldsymbol{w}$. As for the coroot system $R^\vee$, we see from our definition of the root system (V, R) that for all $\beta \in R^\vee$, any inner product with an $\alpha \in R$ will yield an integer. Although we won't prove it here, it is simple to show that $R^\vee$ will also

be a root system with the same Weyl group as R.

Similarly, we remind the reader of the weight lattice using the definition of [8],

- For a root system (V, R), the *weight lattice* is the set
  $\mathscr{W}_R = \left\{ y \in V \middle| \langle \beta^\vee, y \rangle \in \mathbb{Z} \ \forall \ \beta^\vee \in R^\vee \right\}$. The elements of the weight lattice are *weights*.

- For a root system (V, R), the *coweight lattice* is the set
  $\mathscr{W}_R^\vee = \left\{ y \in V \middle| \langle \beta, y \rangle \in \mathbb{Z} \ \forall \ \beta \in R \right\}$. The elements of the coweight lattice are *coweights*.

We can also define *fundamental roots* and *fundamental weights* in the usual fashion. For the coroot and coweight cases, the definitions follow naturally.

We now introduce a concept that will be of particular use in understanding the relationship between the representation theory of a particular group and the quivers that can be constructed from it. This is the *Weyl chamber*. [7],

- For a root system (V, R), remove the hyperplanes orthogonal to each root in R from the root space. Each connected component is then a *Weyl chamber* of (V, R). We define the *principal Weyl chamber* as that for which, for any set of fundamental roots Φ, we have that $\forall \ x \in R$ and $\alpha_i \in \Phi$, $\langle \alpha_i, x, \rangle > 0$.

The definition above might seem to verge on the abstract - in fact, the principal Weyl chamber is easily seen to be the points between the fundamental weights of V when we extend them from the origin to infinity.

0.2.3. ALGEBRAIC VARIETIES & MODULI BRANCHES. The principal objects of interest in the study of quiver gauge theories are their moduli spaces, formally described as *algebraic varieties*.

Consider a set of m polynomials in n variables $\{p_1(x_1, \cdots, x_n), \ \cdots, \ p_m(x_1, \cdots, x_n)\}$ such that $p_i = 0 \ \forall \ 1 \le i \le m$. The set of all complex n-tuples $x = (x_1, \cdots, x_n)$ that satisfy these polynomial equations is called an *affine algebraic set* [9]. We then define an *algebraic variety* as an affine algebraic set that cannot be written as a union of algebraic sets [10].

0.2.3.1. MODULI SPACES. For $3d \ \mathcal{N} = 4$ theories both the Coulomb and Higgs branches are hyper-Kähler spaces [11]. In this section we will give an exposition on these moduli spaces and provide a context for their use and reference in this report.

First let us clear up some matters of terminology. We have seen that for a $3d \ \mathcal{N} = 4$ theory we have scalar fields in the Higgs and Coulomb branches that admit non-zero VEVs. In general, we use the term *moduli space* to refer to the space of all non-zero VEVs associated to a particular *type* of multiplet. In the case of $3d \ \mathcal{N} = 4$ theories, we speak of the *Higgs branch* of the full moduli space - in which scalars in the Hplet have non-zero VEVs and all

9

scalars in the Vplet have zero VEV - and the *Coulomb branch* of the full moduli space - in which scalars in the Vplet will have non-zero VEV and scalars in the Hplet will have zero VEV. In the case where both scalars in the Hplet and Vplet have non-zero VEV, we speak of the *mixed branch*. The full moduli space is a reducible algebraic variety - denoting the Higgs branch $\mathcal{M}_H$, the Coulomb branch $\mathcal{M}_C$ and the full moduli space $\mathcal{M}$ we have the relation given in (3).

$$\mathcal{M} = \mathcal{M}_C \cup \mathcal{M}_H \tag{3}$$

The moduli space of vacua, as an algebraic variety, is in practice difficult to determine directly for a general theory. Instead, we arrive at it indirectly by leveraging our belief that the expectation values of chiral operators on a given moduli space are in one-to-one correspondence with the ring of holomorphic functions on the variety (its structure ring) [2]. Enumerating each operator is again not in general possible under current methods, and so we instead use the Hilbert series to count the number of operators and the charges of each under their various global symmetries.

It is perhaps not surprising then that when considering a specific theory our interest often converges on trying to find the precise structure of its moduli space, along with any further statements that can be made linking its moduli space to those of other theories. To this end, many techniques have been developed over the past few decades, including the monopole forumula [12] [13], Hasse diagrams [14] [15] and magnetic quivers [16] [17] [18] [19] amongst others.

We should stress here that much of this discussion is particualar to the case of three dimensions. As aforementioned, in six dimensions, we find that the Vplets no longer contain scalar fields and so the Coulomb branch is undefined. Instead, we introduce the tensor branch from the non-zero VEVs of scalar fields in the tensor multiplet representation of the supersymmetry algebra. In the following two sections we will only make three-dimensional considerations [4].

0.2.3.2. CHIRAL OPERATORS. We mentioned that chiral operators are important in allowing us to characterise the moduli space of a theory. Let us now define these objects properly. Chiral operators $O_i(x)$ are half-BPS operators that satisfy the relation given in (4) [2].

$$\bar{\mathcal{Q}}_{\dot{\alpha}} O_i(x) = 0 \tag{4}$$

Furthermore, the set of all chiral operators for a given theory naturally form a ring. We can see this by noting, as given in [2], that the product of two chiral operators is as given in (5). Applying $\bar{\mathcal{Q}}_{\dot{\alpha}}$ to this causes the two terms on the right hand side of the expression to vanish

(the first due to the condition (4) and the second due to the nilpotency of $\bar{\mathcal{Q}}_{\dot{\alpha}}$).

Hence if we stipulate that two chiral operators $O_i(x)$ and $O_j(x)$ are equivalent if they differ by a term that is $\bar{\mathcal{Q}}$-exact (in other words if we work at the level of $\bar{\mathcal{Q}}$-cohomology) then we can identify the resulting equivalence classes with holomorphic functions on the moduli space as an algebraic set [2].

$$O_i(x)O_j(x) = A_{ij}^k O_k(x) + \bar{\mathcal{Q}}_{\dot{\alpha}}(\cdots)^{\dot{\alpha}} \tag{5}$$

We thus define the *chiral ring* for a theory as the ring of chiral operators under the equivalence relation we've defined here.

0.2.3.3. HIGGS BRANCH. The Higgs branch is a symplectic singularity. The interested reader is directed towards [20] for a more mathematical treatment of symplectic singularities; here we will give a less rigorous account and define a symplectic variety somewhat heuristically, as in [15], as an algebraic variety with a non-degenerate two-form.

One of the main mathematical insights that underpins the use of Hasse diagrams is the fact that Higgs branches, as symplectic singularities, admit a *foliation* into *leaves*. To understand this further let's begin by considering an algebraic variety T. Following [15], we can promote this to a *Poisson variety* if there exists a Poisson bracket that obeys the conditions in (3), where f and g are elements of the coordinate ring of the variety.

1. $\{f, g\} + \{g, f\} = 0$

2. $\{f, \{g, h\}\} + \{g, \{h, f\}\} + \{h, \{f, g\}\} = 0$

3. $\{f, g \cdot h\} = \{f, g\} \cdot h + g \cdot \{f, h\}$

We can take the dual of this bracket to find a two-form and, keeping in mind that this two-form must be non-degenerate, define a symplectic variety. We can think of a symplectic singularity as arising from further considerations being made on this symplectic variety.

Perhaps most important is to consider how the structure of the Higgs branch is reflected in the Hasse diagram. For the Higgs branch we know that for $3d$ $\mathcal{N} = 4$ theories we are protected from quantum corrections and so can work classically. Historically, the closures of nilpotent orbits associated with classical algebras provide a clear example of symplectic singularities that are easy to find Hasse diagrams for (we show this explicitly in later sections). As mentioned in [15], when we consider the Hasse diagrams for theories in which the Higgs branch corresponds to the closure of a nipotent orbit, we find that we can exactly reproduce the structure of the Higgs branch by simply performing the technique of partial Higgsing. We do this explicitly later for the theory of $SU(5)$ with 10 fundamental Hplets. In [15]

the authors then conjectured that we can find the Hasse diagram for the Higgs branches of further theories by extending our use of the technique of partial Higgsing. Furthermore, in [15] it was conjectured that we can find Hasse diagrams for far more Higgs branches by using the technology of quiver subtraction (to be defined later) and stipulating that the only allowed subtractions are the magnetic quivers corresponding to (closures of) minimal nilpotent orbits (with some further cases given in [21]).

These terms will be defined in the coming sections. It remains to note that even though there is remarkable agreement between the Hasse diagrams computed from partial Higgsing and those from nilpotent orbits, in every new case that does not follow from previous ones the agreement must be checked. In this report we will present some new calculations for a type of quiver that has recently been introduced (called a 'decorated quiver'). Checking this agreement between the partial Higgsing (that takes the form of brane manipulations) and the calculations we get from leveraging the conjectures we've mentioned here is essential.

0.2.3.4. COULOMB BRANCH: SYMMETRY & MONOPOLES. Symmetries in field theories are intimately associated with Noether's theorem; the prescription for finding conserved currents due to the presence of continuous symmetry is well-known. It is an interesting fact however that Noether's theorem does not alone capture the total symmetries relating to a theory - in three-dimensional cases for instance we can observe the presence of hidden symmetries (more often called *topological symmetries*) that are constructed out of a field-strength 2-form.

Let's consider the specific example of The Hilbert series is a generating function for an algebraic variety that allows us to encode useful information pertaining to the variety in the form of an infinite series. In its simplest form, the *unrefined* Hilbert series counts the number of linearly-independent monomials in the structure ring of an algebraic variety [10].

Chiral operators corresponding to the Higgs branch are power series in the fields of the theory. For the Coulomb branch, we must also consider quantum corrections provided by chiral monopole operators which do not admit this power series description [22] [12].

The Hilbert series for the Coulomb branch of a quiver gauge theory is hence [4] [12],

$$HS_{\mathcal{M}_C} = \sum_{\boldsymbol{m} \in \Gamma_{G^V}/W} t^{2\Delta(\boldsymbol{m})} P_G(\boldsymbol{m}; t) \tag{6}$$

where we define the *conformal dimension* as,

$$\Delta(\boldsymbol{m}) = \underbrace{\frac{1}{2} \sum_{i=1}^{n} \sum_{\rho_i \in R_i} |\rho_i(\boldsymbol{m})|}_{\text{Hplet Contribution}} - \underbrace{\sum_{\alpha \in \Delta_+} |\alpha(\boldsymbol{m})|}_{\text{Vplet Contribution}} \tag{7}$$

where ρ_i is a weight in the representation R_i of the ith Hplet and α is a root in Δ_+, the set of all positive roots of the gauge group. As explained in [13], the reason we sum over points in the weight lattice of the Langlands dual group Γ_{G^V} is because we can associate a BPS monopole operator to each.

The factor $P_G(\mathbf{m}; t)$ is called a *dressing function* and is introduced by the Casmimir invariants of the subgroups of the gauge group.

The dimension of the $3d$ $\mathcal{N} = 4$ Coulomb branch for gauge group G is simply $d = rk(G)$. [2].

0.2.4. SINGULARITIES & NILPOTENT ORBITS. Much of the work in characterising moduli spaces for quivers consists in understanding the structure of the moduli space as a hyper-Kähler singularity. For $3d$ $\mathcal{N} = 4$ unitary quivers the singularities that will appear in the Hasse diagrams will be Kleinian ADE-singularites and minimal nilpotent orbits. The Kleinian singularity we will most often encounter will be the A_n singularity,

$$A_n = \frac{\mathbb{C}^2}{\mathbb{Z}_{n+1}}, \tag{8}$$

and more information on Kleinian, or 'surface' singularities is available from [23] [24]. The other set of singularities we are interested in are (minimal) nilpotent orbits. We can understand nilpotent orbits through their relation to classical Lie algebras and we make this explicit below by constructing the nilpotent orbits for the A, B, C and D-type algebras through partitions of the rank of the corresponding Lie groups [25]. We can then use the quivers corresponding to these orbits in the quiver subtraction algorithm to find the Hasse diagram of the moduli spaces of various theories. The construction of nilpotent orbits below is by no means exhaustive, there exist the minimal nilpotent orbits associated to the E_6, E_7 & E_8 algebras that we do not derive here, as well as *twisted* cousins of the nilpotent orbits that can all be used in the quiver subtraction algorithm. We point the reader toward [26] for more information on these.

0.2.4.1. $\mathfrak{sl}_n$. Let us begin by considering the nilpotent orbits of the algebra $\mathfrak{sl}_n$. Each orbit is in one-to-one correpsondence with ordered partitions of n, denoted by $\lambda = (\lambda_1, \lambda_2, ..., \lambda_r)$, which we can represent with a Young tableau. Consider the following prescription.

Define an element of a semi-simple Lie algebra $X \in \mathfrak{g}$ to be *nilpotent* in some finite representation $\rho(X)$ if for some $N \in \mathbb{N}^+$ $\underbrace{\rho(X) \cdot ... \cdot \rho(X)}_{N} = 0$ [3] [25]. Now consider the partition $\lambda = (\lambda_1, \lambda_2, ..., \lambda_r)$ into non-decreasing integers, defined such that $\sum_{i=1}^{r} \lambda_i = n$. We use the

$N \times N$ matrix,

$$
Y_N = \begin{pmatrix}
0 & 1 & 0 & 0 & \ldots & 0 & 0 \\
0 & 0 & 1 & 0 & \ldots & 0 & 0 \\
\vdots & \vdots & \vdots & \vdots & \ddots & \vdots & \vdots \\
0 & 0 & 0 & 0 & \ldots & 0 & 1 \\
0 & 0 & 0 & 0 & \ldots & 0 & 0
\end{pmatrix}
\tag{9}
$$

to construct the $n \times n$ Jordan normal form,

$$
X_\lambda = \begin{pmatrix}
Y_{\lambda_1} & 0 & 0 & \ldots & 0 \\
0 & Y_{\lambda_2} & 0 & \ldots & 0 \\
0 & 0 & Y_{\lambda_3} & \ldots & 0 \\
\vdots & \vdots & \vdots & \ddots & \vdots \\
0 & 0 & 0 & \ldots & Y_{\lambda_r}
\end{pmatrix}.
\tag{10}
$$

From this we can straightforwardly construct the nilpotent orbit $\mathcal{O}_\lambda$ of $\mathfrak{sl}_n$ corresponding to the partition λ [3] [25].

$$
\mathcal{O}_\lambda = \{ M \cdot X \cdot M^{-1} | M \in \mathrm{End}(\mathfrak{sl}_n) \}
\tag{11}
$$

That these can be interpreted as algebraic varieties and singularities is perhaps not immediately obvious. Consider the following example for $\mathfrak{sl}_3$.

First we specify the possible partitions: (1^3), $(1, 2)$ and (3) (we've introduced an exponential notation here such that (1^3) corresponds to $(1, 1, 1)$). We find the matrices,

$$
X_{(1^3)} = \begin{pmatrix} 0 & 0 & 0 \\ 0 & 0 & 0 \\ 0 & 0 & 0 \end{pmatrix}, \quad
X_{(1,2)} = \begin{pmatrix} 0 & 0 & 0 \\ 0 & 0 & 1 \\ 0 & 0 & 0 \end{pmatrix}, \quad
X_3 = \begin{pmatrix} 0 & 1 & 0 \\ 0 & 0 & 1 \\ 0 & 0 & 0 \end{pmatrix}.
\tag{12}
$$

By imposing a partial order on the partitions of $\mathfrak{sl}_n$ we can directly relate them to the structure of the Hasse diagrams we will later construct for $3d$ $\mathcal{N} = 4$ theories. We simply note here, as in [4], that for two partitions λ_1 and λ_2 we impose the partial order $\lambda_1 > \lambda_2$ iff all n^{th} partial sums of λ_1 are larger than or equal to the nth partial sums of λ_2. We define an nth *partial sum* here to be the sum of he first n elements of the partition. Of course, if $\lambda_1 > \lambda_2$ and $\lambda_2 > \lambda_1$ then there is no ordering between the two partitions. Hence for the example of $\mathfrak{sl}_6$ we can put the partitions in the partial order given in (13) below [4].

$$
\begin{array}{c}
[6] \\
\bullet \\
| \\
[1,5] \bullet \\
| \\
[2,4] \bullet \\
\diagup \quad \diagdown \\
[3^2] \bullet \qquad \bullet [1^2,4] \\
\diagdown \quad \diagup \\
[1,2,3] \bullet \\
\diagup \quad \diagdown \\
[2^3] \bullet \qquad \bullet [1^3,3] \\
\diagdown \quad \diagup \\
[1^2,2^2] \bullet \\
| \\
\bullet [1^4,2] \\
| \\
[1^6] \bullet
\end{array}
\tag{13}
$$
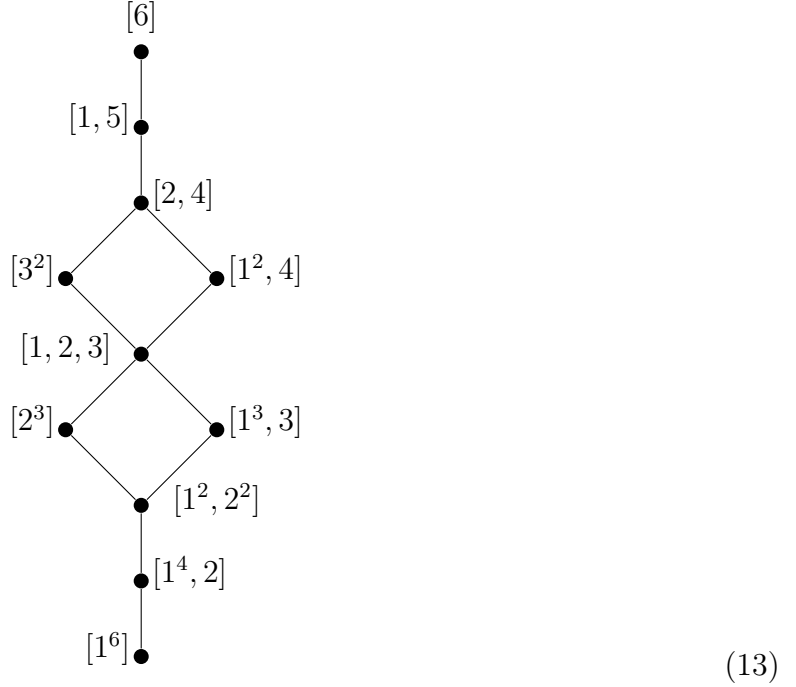
Now we define the *closure* of a nilpotent orbit. For a given nilpotent orbit $\mathcal{O}_\lambda$ we know that this is merely one rung on a partially-ordered ladder of partitions. We thus define the *closure* of this nilpotent orbit to be the union of $\mathcal{O}_\lambda$ with all nilpotent orbits whose partitions are lower on the ladder than λ. We denote the closure of $\mathcal{O}_\lambda$ as $\bar{\mathcal{O}}_\lambda$. For example, the closure of the minimal nilpotent orbit, a_n, is defined as,

$$
a_n = \mathcal{O}_{(1^{n-1},2)} \cup \mathcal{O}_{(1^n)}.
\tag{14}
$$

Furthermore, we define the *maximal* nilpotent orbit to be the nilpotent orbit corresponding to the partition $\lambda = (1, N-1)$ [3].

We can also define the quaternionic dimension of the closure of a minimal nilpotent orbit to be [27],

$$
h^\vee - 1
\tag{15}
$$

where $h^\vee$ is the dual Coxeter number corresponding to a particular Coxeter group (or equivalently, Dynkin diagram) and are easily accessible for classical groups [28].

0.2.4.2. $\mathfrak{so}_n$ & $\mathfrak{sp}_n$. The nilpotent orbits correspoding to partitions in orthosymplectic algebras can be similarly constructed as for the special linear case with some further refinements. We will give a cursory treatment of this, however the reader is instructed to consult [29]. Instead, we will focus on the *use* of these in the context of brane systems (now involving orientifold planes) and give examples.

For the algebra $\mathfrak{so}_{2n+1}$, we have a similar relation between partitions and nilpotent orbits, except now we add an additional condition to obtain a one-to-one mapping. This condition is that all even numbers in the partitions $\lambda \in P(n)$ must now have even multiplicity [25]. For instance, the partition $\lambda = (1^3, 2^2, 4^6)$ of $\mathfrak{so}_{31}$ labels a nilpotent orbit (since the elements 2 and 4 of its partition have even multiplicities) but $\lambda = (1^5, 2^1, 4^6)$ does not. Using the notation of [25], we define the set of partitions of $\mathfrak{so}_{2n+1}$ that correspond to nilpotent orbits $P_{+1}(n)$. For the $\mathfrak{so}_{2n}$ case we have the same condition as for the $\mathfrak{so}_{2n+1}$ case save for the additional complication of *very even partitions* which contain even numbers only. For very even partitions, we have two nilpotent orbits [30] [25].

For the case of $\mathfrak{sp}_n$ we now have that there is a one-to-one mapping between nilpotent orbits and partitions of $2n$ where odd numbers occur with even multiplicity [25]. As before we can build up the Hasse diagrams for these algebras taking into account the fact that we have restrictions on the partitions that will give nilpotent orbits.

0.2.5. HASSE DIAGRAMS. As previously mentioned, Hasse digrams allow us to represent a partial order between elements. For our present purposes, this will entail the structure of the Higgs and Coulomb branches for a particular theory.

The partial order in our Hasse diagrams can be thought of as the progressive breaking of the gauge group of an original quiver under the Higgs mechanism. In these Hasse diagrams, each node corresponds to a quiver and can be called a *leaf*, while each link between adjacent nodes is called an *elementary transverse slice* and will consist mainly of either nilpotent orbit closures or Kleinian singularities. The term *transverse slice* can be used more generally in the context of Hasse diagrams as the moduli that need to be tuned to move from from the theory represented by the closure of the higher leaf to that represented by the lower. Let's consider some further terminology.

To begin with, we will consider in this report Hasse diagrams showing the structure of the moduli spaces for the Higgs branches of various theories - in some cases these can be related to the Coulomb branch using an operation called *inversion*. The inversion operation maps between the Hasse diagrams of the Coulomb and Higgs branches when the only elementary slices are ADE-type Kleinian singularities or minimal nilpotent orbits of type a_n, d_n or e-type exceptional. We will explain precisely why this is the case in the following section, however it is a straightforward consequence of the Coulomb and Higgs branches of a particular set of quivers and can be extended using the technique of quiver subtraction.

0.2.5.1. INVERSION. The technique of Hasse diagram inversion comes from an observation of the relationship between the Higgs and Coulomb branches of a particular set of quivers.

Consider the affine a-type, d-type and e-type quivers. For each of these, their Higgs branch will be an ADE Kleinian singularity and their Coulomb branch will be the corresponding closure of a minimal nilpotent orbit. For instance, the the affine quiver with Coulomb branch a_7, its Higgs branch will be A_7 and for the affine quiver with Coulomb branch e_6 its Higgs branch will be E_6.

With these quivers then, we can define the operation of 'inversion' of their Hasse diagram such that if we take their Higgs branch Hasse diagram, turn it upside-down and change all Kleinian singularities to their corresponding minimal nilpotent orbit closures, we get the Hasse diagram for the Coulomb branch (we can go from the Coulomb branch Hasse diagram to the Higgs branch Hasse diagram by inverting these setps). Of course, since these quivers have Hasse diagrams that consist of only one transverse slice, it might not seem like we've done all that much. The real power comes however when we realise that this method will remain valid for a much wider class of quivers that have a Coulomb branch built from a-type, d-type or e-type nilpotent orbit closures (or correspondingly a Higgs branch Hasse diagram built from ADE Kleinian singularities).

Then it is a matter of combining these Hasse diagrams (taking care to understand which directions along the Coulomb, Higgs or mixed branches remain open at each leaf) to find the Hasse diagram for the *entire* moduli space [14].

0.2.6. BRANE METHODS. In this paper we will primarily consider Type IIB configurations of D5, NS5 and D3-branes, in which 8 of the original 32 supercharges are preserved [31] and the IR physics of the D3-brane contains a 3d $\mathcal{N} = 4$ gauge theory [3]. The branes are extended in 10-dimensional Minkowski space as shown in Fig. 1 [14]. Let's begin our

	x^0	x^1	x^2	x^3	x^4	x^5	x^6	x^7	x^8	x^9
D1	x							x		
F1	x			x						
NS5	x	x	x	x	x	x				
D5	x	x	x					x	x	x
D3	x	x	x				x			

$$\underbrace{}_{SO(1,2)} \quad \underbrace{}_{SU(2)_C} \quad \underbrace{}_{SU(2)_H}$$

Figure 1: This diagram shows the dimensions the various branes extend in. We see the R-symmetry of the theory corresponding to rotations of the NS5- and D5-branes.

description of brane systems with Fig. 1. This Type-IIB setup involves D5-branes infinite in the $\boldsymbol{k} = (x^7, x^8, x^9)$ directions and NS5-branes infinite in the $\boldsymbol{w} = (x^3, x^4, x^5)$ directions. The D5-branes are localised at specific points along $\boldsymbol{w}$ and x^6 and likewise for the NS5-branes along $\boldsymbol{k}$ and x^6. We can then suspend D3-branes between fivebranes in three inequivalent

configurations.

The first involves two D5-branes coincident along the $\boldsymbol{w}$ but generically seperated along x^6. Suspending a D3-brane between them along x^6 can be interpreted as parametrising a generic position on the Higgs branch moduli space. In other words, moving the D3-brane off the origin in the $\boldsymbol{k}$ direction corresponds to the tuning of massless moduli.

The second configuration consists of D3-branes suspended between two NS5-branes that are coincident along the $\boldsymbol{k}$ but separated along the $\boldsymbol{w}$ and x^6 directions. Now the movement of the D3-branes off the origin in the $\boldsymbol{w}$ directions corresponds to a generic point in the Coulomb branch.

The third configuration is when we have a D3-brane that is suspended between a D5-brane and an NS5-brane. In this configuration the D3-brane is frozen. We should add that between any D5-brane and NS5-brane, only one D3-brane can be suspended between them [3].

0.2.6.1. LINKING NUMBERS. Linking numbers are important quantities that allow us to characterise a brane configuration and quiver corresponding to it. For a 3d $\mathcal{N} = 4$ setup with unitary gauge nodes we define the linking number l of a fivebrane as [3]:

$$\ell = n_R^{D3} - n_L^{D3} + n_L^5 \tag{16}$$

where n_R^{D3} denotes the number of D3-branes ending form the right on the fivebrane, n_L^{D3} denotes similarly from the left and n_L^5 denotes the number of fivebranes of opposite type to the left of the fivebrane we are considering (where we are spuriously referring to NS-branes and D-branes being of 'opposite type'). Linking numbers are always preserved for a given brane configuration.

Although (16) works for unitary gauge groups, we also must consider another case that we will expand on later in this report. For quivers with orthosymplectic gauge groups, the corresponding brane systems will have orientifold planes (in the 3d case we are considering in this report these will be $\mathcal{O}3$ planes). When calculating linking number we have to include these $\mathcal{O}3$ planes in our counting (apart from the $\mathcal{O}3^-$ plane, which makes no contribution [25]). We will introduce orientifold planes in due course. For 3d $\mathcal{N} = 4$ systems, we can define the vectors $\boldsymbol{\ell}_s$ for the linking numbers of all NS5-branes in the system and $\boldsymbol{\ell}_d$ for the linking numbers of all D5-branes.

0.2.6.2. HANANY-WITTEN TRANSITION. The Hanany-Witten transition, first described in [31], describes a process by which we change the relative positions of D5 and NS5-branes while maintaining the same linking numbers of the branes involved and thus keeping the same theory.

Let's begin by considering the brane setup in Fig. 2 (**i**). We have two NS5-branes, one

D3-brane and one D5-brane. Now consider that we were able to move the D5 through the rightmost NS5-brane without changing the theory. As the authors consider in [31], the naive approach might be to simply push the D5-brane through the NS5-brane with no further changes - this is incorrect because it does not preserve the linking numbers of the brane system. In fact, the correct method is to create a new D3-brane that is suspended between the D5-brane we are moving and the NS5-brane it moves through. This is shown in Fig. 2 (ii) where an extra D3-brane has been created.

For the phase of the system where the D3-branes are now free to move along D5-branes we have the same logic at play. As we see in Fig. 2 (iii) & (iv), the transition proceeds by passing the NS5-brane through the D5-brane and creating a D3-brane to preserve the linking numbers of the D5 and NS5-branes. Extensions to more complicated brane systems follow naturally - the Hanany-Witten transition is solely concerned with the fivebrane we are moving and the other fivebrane it moves through. The only further complication comes from considering orientifold $\mathcal{O}3$ planes, since in these cases the linking numbers for the fivebranes now include the $\mathcal{O}3$ planes and so there are cases when we can transition D3-branes through fivebranes and it turns out that the preservation of linking number requires we transition one of our $\mathcal{O}3$ planes instead of creating a D3-brane. This special case will be considered below, however it is strictly limited to the brane systems of orthosymplectic quivers.
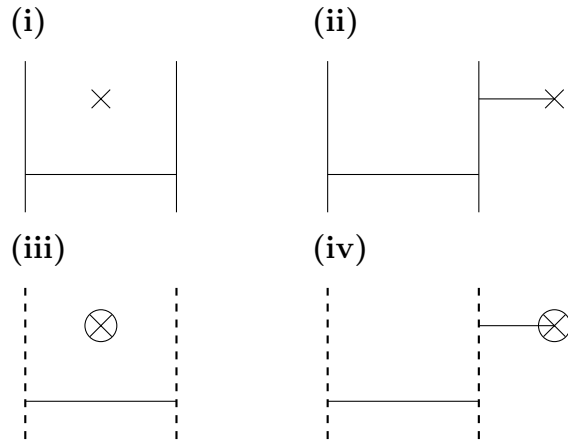

Figure 2: The Hanany-Witten transition for two example brane systems, one in which D3-branes are free to move along NS5-branes and one in which D3-branes are free to move along D5-branes. (i). The original brane system with one D5-brane and one D3-brane. (ii). The system after we have pushed the D5-brane through the rightmost NS5-brane - an extra D3-brane has been created to preserve linking number. (iii). The system with two D5-branes and one NS5-brane. (iv). The system after we have pushed the NS5-brane through the D5-brane, creating a D3-brane in the process.
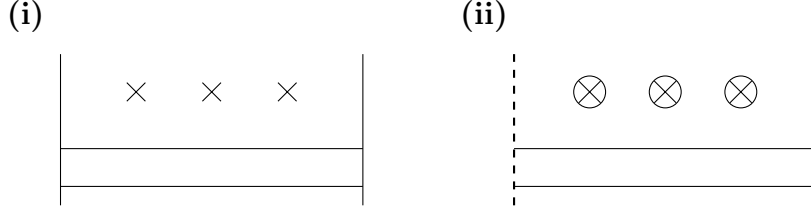
Figure 3: An example of 3d mirror symmetry on a generic 3d $\mathcal{N} = 4$ brane system. **i**. The original brane system. **ii** The brane system after performing 3d mirror symmetry, in which NS5-branes now have been replaced with D5-branes and vice versa.

0.2.6.3. 3D MIRROR SYMMETRY. One of the most important brane methods at our disposal is 3d mirror symmetry, first described in [32]. This duality explores Coulomb and Higgs branches that correspond to the same algebraic variety. For a given brane system, we can perform 3d mirror symmetry to find the 3d-mirror pair whose Higgs branch is the same variety as the Coulomb branch of the original brane system. An example of this is given in (3).

Hence, from the perspective of string theory, 3d mirror symmetry correspond to S-duality [33] and we can use the technology of brane systems to find 3d mirror pairs by swapping D5 and NS5-branes and keeping D3-branes invariant. This graphical representation further allows us to intuit that 3d mirror symmetry swaps the actions of D5 and NS5-branes under their $SU(2) \times SU(2)$ R-symmetry [33], since we have already seen that this global symmetry can be thought of as rotating the fivebranes in their respective three-dimensional sub-manifolds.

0.2.6.4. BRANE TRANSITIONS. In this section we consider the process by which we can move between the Coulomb and Higgs branches of a $3d$ $\mathcal{N} = 4$ brane system. In the Coulomb branch, the brane system in in the phase where all D3-branes not able to be annihilated via a Hanany-Witten transition are suspended between NS5-branes. In this setup, the quaternionic dimension of the brane system is equal to the number of these D3-branes. Similarly, the Higgs branch corresponds to the brane system whereby all D3-branes not able to be annihilated via a Hanany-Witten transition are suspended between D5-branes. Again, the quaternionic dimension of the Higgs branch is equal to the number of these D3-branes.

The question then arises of how we switch between the two brane systems. The main idea is to move the branes such that we go from a system where the D3-branes are suspended between NS5-branes to one in which they are suspended between D5-branes. In order for this to be so, we generally want to perform Hanany-Witten transitions on a given brane system so that the number of D3-branes between any adjacent pair of NS5-branes is the same. We

given examples of doing this throughout this report and these explicit manipulations might be most helpful in understanding the procedure. Often, we might make Hanany-Witten transitions to some D5-branes in a brane system to move them through NS5-branes while leaving other D5-branes alone.

Performing a rotation about the x^6 axis means that the vertical direction now denotes the x^7, x^8, x^9 dimensions and the horizontal direction denotes the x^3, x^3, x^5 dimensions. We represent this by changing each cross denoting a D5-brane with a dashed vertical line and changing each solid vertical line representing an NS5-brane with a circled cross. A step-by-step example of this process is provided in Fig. 8. For the case involving $\mathcal{O}3$ planes we will find that the general method presented here is largely unchanged.

0.2.6.5. ORIENTIFOLD PLANES & ORTHOSYMPLECTIC COMPLICATIONS. Following the analysis of [33], this section will introduce orientifold planes and describe their dyanmics in brane systems. We can understand the effect of orientifold planes intuitively by first recalling the argument for why we consider a stack of k coincident D-branes to host a $U(k)$ gauge theory on the open strings with Neumann-Neumann boundary conditions between them. For a generic open string suspended between the D-branes, we have k possibilities for the number of D-branes each end of the open string can end on; we call the indices that denote this the Chan-Paton factors. This gives rise to a $k \times k$ matrix that tells us that the string is in the adjoint representation of $U(k)$.

However, we can extend this analysis to include orientifold planes and induce a non-trivial orbit for the end-points of the string that correlates its end-points under a $\mathbb{Z}_2$ action. Then, assigning the Chan-Paton factors again, we find that the matrices that result are either $k \times k$ symmetric or $k \times k$ antisymmetric, giving the adjoint representations of $SO(k)$ or $Sp(k)$ respectively. For 3d $\mathcal{N} = 4$ systems we consider four types of $\mathcal{O}3$ planes: $\mathcal{O}3^+$, $\mathcal{O}3^-$, $\widetilde{\mathcal{O}3}^+$ and $\widetilde{\mathcal{O}3}^-$.

Of course, in all generality we can consider $\mathcal{O}N$ planes in brane systems with D-N branes; in this report we will be considering $\mathcal{O}3$ planes since we are in three dimensions.

In the brane systems we consider the $\mathcal{O}3$ planes will span the x^1, x^2 and x^6 dimensions and remain at the origin in the other six, so they will appear as horizontal lines in our conventional brane diagrams [25].

We also have to consider a further complication to the brane system through the addition of orientifold planes. Since in general an $\mathcal{O}N$ plane will induce a non-trivial $\mathbb{Z}_2$ orbit in the points that aren't coincident with it, the D5-branes we will consider in our brane system will have to be *half* D5-branes [33]. Let's consider this a little more carefully. Starting with a half D5-brane that is associated under $\mathbb{Z}_2$ action with another half D5-brane on the other side of an $\mathcal{O}3$ plane, we can ask what happens when we choose to move both half D5-branes

	NS5	D5
$\mathcal{O}3^+$	$\mathcal{O}3^-$	$\widetilde{\mathcal{O}3^+}$
$\mathcal{O}3^-$	$\mathcal{O}3^+$	$\widetilde{\mathcal{O}3^-}$
$\widetilde{\mathcal{O}3^+}$	$\widetilde{\mathcal{O}3^-}$	$\mathcal{O}3^+$
$\widetilde{\mathcal{O}3^-}$	$\widetilde{\mathcal{O}3^+}$	$\mathcal{O}3^-$

Figure 4: The transition of $\mathcal{O}3$ planes when they meet NS5-branes and D5-branes. We ca summarise this by stating that when an $\mathcal{O}3$ plane meets an NS5-brane a '+' becomes a '−' and when an $\mathcal{O}3$ plane meets a D5-brane it gains a tilde if it doesn't have one already and loses a tilde if it does.

such that they coincide with the $\mathcal{O}3$ itself. Instead of the D5-branes joining together, they can move independently in a phenomenon called *splitting*. We won't give a full treatment of splitting here, the interested reader is pointed towards [33]. It will suffice to note that, as in [25], we will consider all half D5-branes in brane systems with $\mathcal{O}3$ planes to be at the origin in the x^2 dimension.

Turning to the construction of brane systems involving $\mathcal{O}3$ planes, we specify in Fig. 4 the rules for how orientifold planes change as they pass through half D5-branes and NS5-branes. In our brane system diagrams, we will denote $\mathcal{O}3^+$ planes using red lines, $\widetilde{\mathcal{O}3^-}$ planes using blue lines, $\widetilde{\mathcal{O}3^+}$ using green lines and $\mathcal{O}3^-$ with no line. All orientifold planes will be located at the origin and D3-branes will as usual be denoted by black lines.

We also have to fix our convention regarding $\mathcal{O}3$ planes. When given a quiver it is simple to infer the orientifold planes, as will be discussed below. However, we can also directly construct brane systems with moduli spaces that correspond to particular minimal nilpotent orbits of $\mathfrak{so}_n$ and $\mathfrak{sp}_n$; for these cases we must defer to the prescription found in [25]. An important point here however is that, for a brane system with no $\mathcal{O}3$ planes, we need only specify the type of one $\mathcal{O}3$ plane to be able to infer the rest. From this we can use the results in Fig. 4 to find all other orientifold planes. This procedure is precisely what we must do when we enact an S-duality (i.e. $3d$ mirror symmetry) on our brane system - upon following the standard procedure with NS5-branes and D5-branes, we again enforce that the rightmost orientifold plane is $\mathcal{O}3^-$ and then follow the transitions through to specify the orientifold planes for the rest of the brane system [25]. Finally, we come to the process of reading a brane system from a quiver and vice versa. Given a brane system with D3-branes suspended between NS5-branes and with orientifold planes, to read a quiver we need to first ensure that any $\mathcal{O}3^-$ planes ending on D5-branes that can instead end on NS5-branes after a Hanany-Witten transition are moved such that they do. We call this the *collapse* transition

[25]. Once this is done, we can use the following rules to construct the quiver.

For a brane system (where we are in the phase where D3-branes are suspended between NS5-branes) with multiple 'chambers' (where we informally define a 'chamber' to be the space between two NS5-branes), Let's consider the quiver below.

$$
\begin{array}{ccc}
O_2 & & O_2 \\
\square & & \square \\
| & & | \\
\bigcirc - \bigcirc - \bigcirc \\
C_1 & C_1 & C_1
\end{array}
\tag{17}
$$

We show the transition from the brane system where D3-branes are suspended between NS5-branes to the brane system in which D3-branes are suspended between D5-branes in Fig. 5, along with an example of how we can use the collapse transition to read the quiver from the brane system.

0.2.7. MAGNETIC QUIVER. We have seen that the technology of 3d mirror symmetry relates the Higgs and Coulomb branches of different 3d $\mathcal{N} = 4$ theories. It turns out that we can extend this insight of the Higgs branch of one theory being the Coulomb branch of another using the the concept of the *magnetic quiver*. The magnetic quiver Q_M, discussed extensively in [16], [17], [19], for a given electric quiver Q_E, has the property,

$$
\mathcal{H}^d(Q_E) = \mathcal{C}^3(Q_M).
\tag{18}
$$

That is, the Higgs branch of an electric quiver in $d = 3, 4, 5, 6$ with eight supercharges is the same algebraic variety as the Coulomb branch of the magnetic quiver in $d = 3$. This is a particularly powerful insight that allows for the Higgs branch of theories that can be expressed in, for instance, Type IIA brane systems to be calculated using the monopole formula in the $3d$ $\mathcal{N} = 4$ case.

Let us further treat a subtlety here regarding unframed quivers. In this case we have to ungauge a node on the quiver, diagrammatically corresponding to turning a circle into a square. In the brane construction, we can think of this as picking a centre of mass to decouple from the rest of the system [25]. Given that our magnetic quivers can have many gauge nodes, we might rightly worry about the implications of ungauging different nodes on the Coulomb branch. For simply-laced cases, it can be shown that all different choices of ungauging yield the same Hilbert series via the monopole formula [34]. For non-simply-laced cases there are more subtleties and the reader is instructed to consider [34].
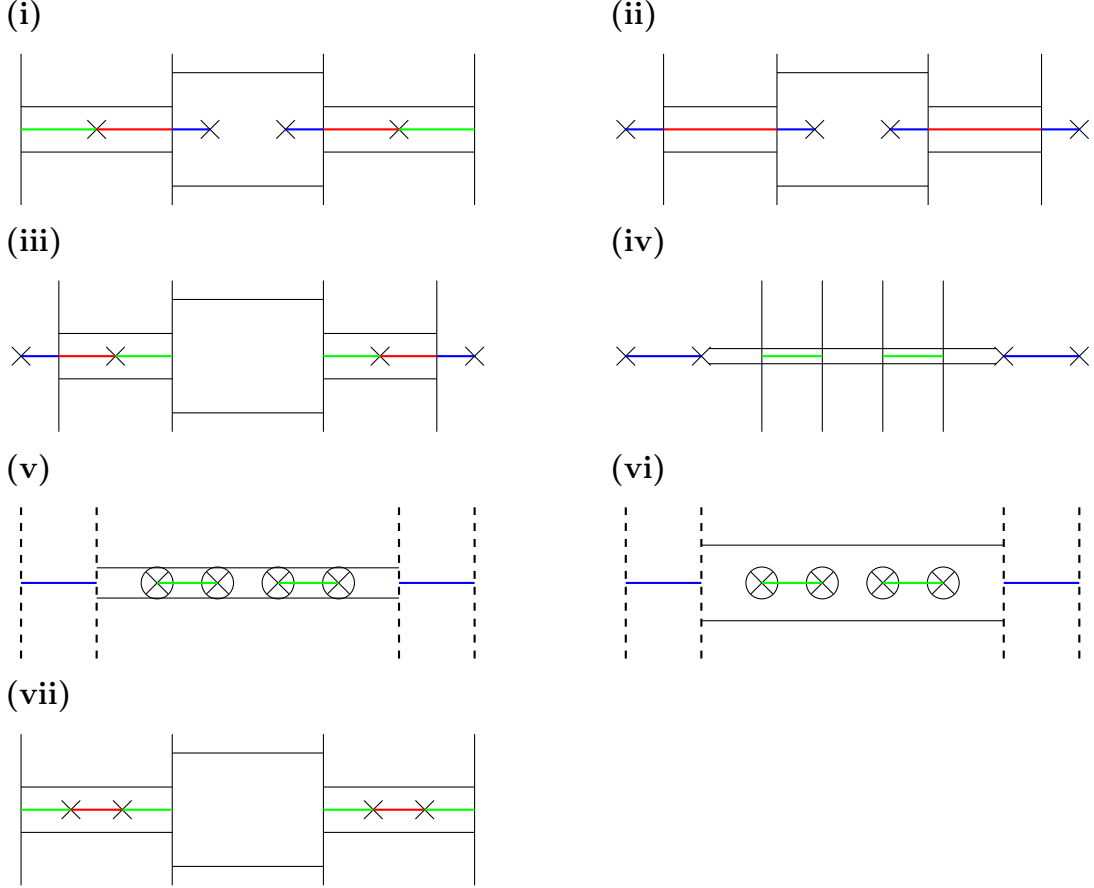
(i)

(ii)

(iii)

(iv)

(v)

(vi)

(vii)

Figure 5: The transition from the Coulomb branch to the Higgs branch of the quiver and the collapse transition. (**i**). The original brane system. (**ii**). First Hanany-Witten transition to move two of the D5-branes. Note that we have not had to create half D3 branes to preserve linking numbers here. (**iii**). Second Hanany-Witten transition to move two more D5-branes. We have again created no new half D3-branes. (**iv**). Third Hanany-Witten transition. Now we have all D3-branes ending on half D5-branes and we have had to create two half D3-branes to maintain linking numbers. we have also moved all half D3-branes to the origin. (**v**). Rotate the brane system along the x^6 dimension. The orientifold planes remain the same. (**vi**). Move the half D3-branes away from the origin such that we move into a generic point in the Higgs branch. (**vii**). This shows the collapse transition, allowing us to read the quiver.

0.3. Higgs Mechanism and Representations. We begin with a consideration of how we can use the Higgs mechanism on the Higgs branch. For these classical calculations we will use the technology of representation theory to construct Hasse diagrams for some simple quivers. Although enlightening, we will find that the methods become cumbersome as the examples become more complicated. Throughout this section, we will proceed in the spirit of [15], although we will consider a different example.

0.3.1. $SU(5)$ WITH 10 FUNDAMENTAL HPLETS. Let us begin by considering the quiver in (19).

$$
\begin{array}{c}
10 \\
\square \\
| \\
\circ \\
SU(5)
\end{array}
\tag{19}
$$

We see that we have one Hplet in the fundamental representation of $SU(5)$ and one Vplet in the adjoint representation. This $3d\ \mathcal{N}=4$ theory is easier to work with if we project into $3d\ \mathcal{N}=2$. Recall that $3d\ \mathcal{N}=4$ Vplets become one Vplet and one Cplet in $3d\ \mathcal{N}=2$ and Hplets in the fundamental representation of the gauge group become two Cplets, one in the fundamental representation and one in the antifundamental representation. There are many subgroups of $SU(5)$ we might consider here - the computation is made much easier when we consider that only a few are accessible through Higgsing. First let's consider Higgsing to $SU(4)$,

$$
\begin{aligned}
[1,0,0,0]_{A_4} &= [1,0,0]_{A_3} + [0,0,0]_{A_3} \\
[0,0,0,1]_{A_4} &= [0,0,1]_{A_3} + [0,0,0]_{A_3} \\
[1,0,0,1]_{A_4} &= [1,0,1]_{A_3} + [0,0,1]_{A_3} + [1,0,0]_{A_3} + [0,0,0]_{A_3}
\end{aligned}
\tag{20}
$$

where the above shows the decomposition of $SU(5)$ representations (labelled by their highest weight) into $SU(4)$ representations; we've shaded blue the parts that will receive a mass under the Higgs mechanism. To complete the process, we need to now consider what matter representations we end up with. Recall that we will have ten fundamental Hplets in the $3d\ \mathcal{N}=4$ theory becoming ten fundamental Cplets and ten antifundamental Cplets in the $3d\ \mathcal{N}=2$ theory and an adjoint Vplet in the $3d\ \mathcal{N}=4$ theory becoming an adjoint Vplet and an adjoint Cplet in the $3d\ \mathcal{N}=2$ theory,

$$
\begin{aligned}
10([1,0,0,0]_{A_4} + [0,0,0,1]_{A_4}) &- 2([0,0,1]_{A_3} + [1,0,0]_{A_3} + [0,0,0]_{A_3}) \\
&= 18[0,0,0]_{A_3} + 8([1,0,0]_{A_3} + [0,0,1]_{A_3}).
\end{aligned}
\tag{21}
$$

We ignore the contribution $18[0,0,0]_{A_3}$ since these correspond to free Hplets and instead we focus on the eight fundamental Hplets in the $3d$ $\mathcal{N}=4$ theory given by the contribution $8[1,0,0]_{A_3} + 8[0,0,1]_{A_3}$. Hence we recover the quiver,

$$
\begin{array}{c}
8 \\
\square \\
\vert \\
\bigcirc \\
SU(4)
\end{array}
\tag{22}
$$

It's now a simple task to repeat this for the case of $SU(4)$ breaking to $SU(3)$. We have the representations,

$$
\begin{aligned}
[1,0,0]_{A_3} &= [1,0]_{A_2} + [0,0]_{A_2} \\
[0,0,1]_{A_3} &= [0,1]_{A_2} + [0,0]_{A_2} \\
[1,0,1]_{A_3} &= [1,1]_{A_2} + [1,0]_{A_2} + [0,1]_{A_2} + [0,0]_{A_2}
\end{aligned}
\tag{23}
$$

where again we have shaded blue the parts of the adjoint representation decomposition that will receive a mass. Again we subtract these from the (anti-)fundamental Cplet contributions,

$$
\begin{aligned}
8([1,0,0]_{A_2} + [0,0,1]_{A_2}) &- 2([1,0]_{A_2} + [0,1]_{A_2} + [0,0]_{A_2}) \\
&= 14[0,0]_{A_2} + 6([1,0]_{A_2} + [0,1]_{A_2}).
\end{aligned}
\tag{24}
$$

We now recover the quiver,

$$
\begin{array}{c}
6 \\
\square \\
\vert \\
\bigcirc \\
SU(3)
\end{array}
\tag{25}
$$

Using the Higgs mechanism again to transition from $SU(3)$ to $SU(2)$ is simple,

$$
\begin{aligned}
[1,0]_{A_2} = [0,1]_{A_2} &= [1]_{A_1} + [0]_{A_1} \\
[1,1]_{A_2} &= [2]_{A_1} + 2[1]_{A_1} + [0]_{A_1}.
\end{aligned}
\tag{26}
$$

Note that the factor of two in the decomposition of $[1,1]_{A_2}$ above has appeared because the fundamental and antifundamental representations for A_1 are the same. Finding the matter content we have left,

$$
6([1,0]_{A_2} + [0,1]_{A_2}) - 2(2[1]_{A_1} + [0]_{A_1}) = 10[0]_{A_1} + 8[1]_{A_1}
\tag{27}
$$

Hence we recover the quiver

$$
\begin{array}{c}
4 \\
\square \\
| \\
\bigcirc \\
SU(2)
\end{array}
\tag{28}
$$

Now, it appears we can still use the Higgs mechanism to move to a theory with a $U(1)$ gauge group. However, when we try to calculate this in terms of representations,

$$
\begin{aligned}
[1]_{A_1} &= p + p^{-1} \\
[2]_{A_1} &= p^2 + 1 + p^{-2}
\end{aligned}
\tag{29}
$$

and we see that there is no way for us to break the $SU(2)$ gauge group further without breaking it fully. To do this last transition therefore, we use the fact that each representation of the remaining $SU(2)$ gauge group of dimension d decomposes into d irreducible representations of the trivial group. Hence we perform the calculation,

$$
4([1]_{A_1} + [1]_{A_1}) - 2([2]_{A_1}) = 10,
\tag{30}
$$

giving a ten complex-dimensional slice (so five quaternionic dimensions) and arrive at the Hasse diagram for the Higgs branch of the original quiver (19).

$$
\begin{array}{cc}
& \bullet\ 26 \\
5 & | \\
& \bullet\ 21 \\
5 & | \\
& \bullet\ 16 \\
7 & | \\
& \bullet\ 9 \\
9 & | \\
& \bullet\ 0
\end{array}
\tag{31}
$$

Although we have claimed to have found the Hasse diagram for the quiver (19), this is highly unconvincing unless we explain why we couldn't have Higgsed to the subgroups $SU(2) \times SU(2)$, $SU(3) \times SU(2)$, $Sp(2)$ and all subgroups involving $U(1)$.

The argument as to why $U(1)$ doesn't appear in our subgroups is simple - (32) shows the decomposition of $[1, 0, 0, 1]_{A_4}$ under two symmetry breaking patterns. In both cases we have terms with $U(1)$ charges p of order 5 and -5 - these terms would become massive under the Higgs mechanism, however we don't have any p^5 or p^{-5} terms in the decomposition of

$[1,0,0,0]_{A_4}$ or $[0,0,0,1]_{A_4}$ to accommodate them. As a result, these transitions are forbidden. Similar arguments hold for all other cases in which a $U(1)$ is present.

$$\begin{aligned}
\hookrightarrow SU(2) \times SU(3) \times U(1): \quad & (\cdots) + p^{-5}[1]_{A_1} \otimes [1,0]_{A_2} + p^5[1]_{A_1} \otimes [0,1]_{A_2} \\
\hookrightarrow SU(4) \times U(1): \quad & (\cdots) + p^5[1,0,0]_{A_3} + p^{-5}[0,0,1]_{A_3}
\end{aligned} \tag{32}$$

As for the case of $Sp(2)$, we have the decompositions,

$$\begin{aligned}
[1,0,0,0]_{A_4} = [0,0,0,1]_{A_4} &= [0,1]_{C_2} \\
[1,0,0,1]_{A_4} &= [2,0]_{C_2} + [0,2]_{C_2}
\end{aligned} \tag{33}$$

where we've shaded in red the term from the decomposition of the adjoint representation of $SU(5)$ that would become massive; in this case too there are no corresponding terms from the decompositions of the (anti-)fundamental and so we see the transition is forbidden.

0.4. Affine Grassmannian. Despite the Higgs branch of $3d$ $\mathcal{N} = 4$ theories being understood for some time as a hyper-Kähler quotient, a more general understanding of the Coulomb branch remained elusive before the work of Nakajima and collaborators. [1]

The affine Grassmnnian is the arena in which we can consider ADE quivers and transverse slices that are either A_n Kleinian singularities or minimal nilpotent orbits. Although this gives us the ability to understand the mathematical structure from which many Coulomb branches arise, it is not exhaustive. However, Nakajima and collaborators have considered generalised cases in [35].

The utility of the affine Grassmannian is as follows. We see that there is a bijection between orbits in the affine Grassmannian pertaining to a group G and the dominant coweights of the G. We can then construct quivers corresponding to transverse slices in the affine Grassmannian through specifying pairs of coweights (one dominant) and recover their Hasse diagrams. This beautifully illuminates the emergence of Hasse diagrams for a large family of quivers [21].

Our treatment will broadly follow that given in [21]. Let us begin by recalling the construction of a lattice from a real vector space V. Given a basis $(a_1, a_2, \cdots, a_n)$ (taking $dim(V) = n$) we can construct a lattice by taking all linear combinations of the basis elements with integer coefficients [21]; this subset of V will be isomorphic to $\mathbb{Z}^n$. Notice that we can take the product of any basis element with an integer and retain the same lattice. With our understanding of these n-dimensional lattices being constructed by n-tuples from a real vector space V, we can capture all such n-dimensional lattices in $GL(n, \mathbb{R})$ if we in-

---

[1]The author is indebted to Antoine Bourget for his illuminating seminar on the affine Grassmannian.

terpret each column in the matrix $A \in GL(n, \mathbb{R})$ as being a basis vector for the lattice. Again, we notice that each element of $GL(n, \mathbb{R})$ does not correspond to a *unique* lattice, as multiplication on the right of an element $A \in GL(n, \mathbb{R})$ by an element $B \in GL(n, \mathbb{Z})$ gives us columns in $A \cdot B$ that are integer-coefficient linear combinations of columns in A. Consider the simple two-dimensional example below,

$$A \cdot B = \begin{pmatrix} a & b \\ c & d \end{pmatrix} \begin{pmatrix} 2 & 3 \\ 4 & 5 \end{pmatrix} = \begin{pmatrix} 2a + 4b & 3a + 5b \\ 2c + 4d & 3c + 5d \end{pmatrix} \tag{34}$$

Clearly, we need to use this equivalence relation on the $GL(n, \mathbb{R})$ in order that each element of the remaining group correspond to a unique lattice. This is achieved by taking the following quotient,

$$GL(n, \mathbb{R})/GL(n, \mathbb{Z}). \tag{35}$$

Note a subtlety in the above analysis. The general linear group is defined over a field, but $\mathbb{Z}$ is a ring. We hence define

$$GL(n, \mathbb{Z}) = \left\{ A \in GL(n, \mathbb{R}) \middle| \det(A) = 1, A_{ij} \in \mathbb{Z} \; \forall \; i, j = 0, \cdots, n \right\} \tag{36}$$

Now we may ask the following question: how does this object change when we define the general linear group over a different field? Making a judicious choice of the field, we find that we are led to the construction of the affine Grassmannian.

Consider the following two objects:

- The *discrete valuation ring* $\mathbb{C}[[t]] = \left\{ f(t) = \sum_{i=0}^{N} a_i t^i \middle| N \in \mathbb{N}, a_i \in \mathbb{C} \right\}$

- The field $\mathbb{C}((t)) = \left\{ \frac{f(t)}{g(t)} \middle| f(t), g(t) \in \mathbb{C}[[t]], g(t) \neq 0 \right\}$

The field $\mathbb{C}((t))$ allows us to define the general linear group $GL(n, \mathbb{C}((t)))$ of $n \times n$ matrices with coefficients in $\mathbb{C}((t))$. As before, we can define $GL(n, \mathbb{C}[[t]])$ so long as we ensure that every element $A(t)$ satisfies $\det(A(t)) = 0 \; \forall t$, including $t = 0$.

With these definitions in mind, we can define the affine Grassmannian for an algebraic subgroup $G \subset GL(n, \mathbb{C})$ as,

$$Gr_G = G(\mathbb{C}((t)))/G(\mathbb{C}[[t]]), \tag{37}$$

where we define G(C((t)))

0.4.1. ORBITS & SLICES. Let us begin our discussion of orbits in the affine Grassmannian by considering why we quotiented on the left in (37). The reason, quite simply, comes from

our decision to associate the columns of a matrix in $GL(n, \mathbb{C}((t)))$ with the basis vectors of its associated lattice. We could just as well decided to associate the rows of such a matrix with the basis vectors of the lattice, and in such a case it would be multiplication from the *left* by an element of $GL(n, \mathbb{C}[[t]])$ that would define an equivalence relation on $GL(n, \mathbb{C}((t)))$. With this in mind, we consider now the action of multiplying an element in Gr_G by an element in $GL(n, \mathbb{C}((t)))$ on the left - we find it defines an *orbit* in the affine Grassmannian. Though we will not show it rigorously here, we note two essential points. The first is that each element of the affine Grassmannian corresponding to the group G can be labelled by a coweight λ of G, $M^\lambda \in Gr_G$. Secondly, we can decompose the affine Grassmannian corresponding to a group G into orbits labelled by specific coweights of G [21],

$$Gr_G = \bigsqcup_{\lambda \in \Lambda^+} [Gr_G]^\lambda \tag{38}$$

where we impress that this union is disjoint and identify Λ^+ as the set of all coweights that lie in the principal Weyl chamber of the weight lattice (as we've mentioned above, we could alternatively describe Λ^+ as the set of all coweights that admit a decomposition into a linear combination of fundamental coweights with non-negative coefficients). We can call the coweights $\lambda \in \Lambda^+$ that lie in the principal Weyl chamber the *dominant coweights*. Each $[Gr_G]^\lambda$ is called a *Schubert cell* and is an orbit in Gr_G where,

$$[Gr_G]^\lambda = G[[t]] \cdot M^\lambda \cdot G[[t]], \quad M^\lambda \in C((t)), \quad M^\lambda \cdot G[[t]] \in Gr_G. \tag{39}$$

Note that in the above equation the multiplication on the right of M^λ by $G[[t]]$ creates the equivalence class of lattices and the multiplication on the left of M^λ by $G[[t]]$ defines the orbit of the element $M^\lambda \cdot G[[t]]$ in the affine Grassmannian.

Having considered orbits in the affine Grassmannian, we are now in the position to define transverse slices. These are the objects that can be mapped to the Coulomb branches of good quivers where the gauge nodes form the Dynkin diagram of a simple Lie algebra [21]. Before doing this however, let us adopt the notation of $\mathscr{R}^\vee$ being the coroot lattice of the group G and make the following observation: we can define a partial order $<$ on the coweights α, β such that $\alpha \leq \beta$ iff $\exists \gamma \in \mathscr{R}^\vee$ where γ is the sum of fundamental coroots with non-negative integer coefficients. It turns out that this is the partial order obeyed by leaves in the Hasse diagrams that we extract from the affine Grassmannian.

0.4.2. CONSTRUCTING QUIVERS & BRANE SYSTEMS. Having introduced the affine Grassmannian and considered its basic properties, we are now in the position to introduce how we can associate quivers and brane systems with transverse slices of Gr_G.

The identification proceeds as follows, as in [21]:

Let us begin with the process of constructing a quiver from the affine Grassmannian. Firstly, for Gr_G, the quiver we construct will have gauge nodes that are the Dynkin diagram of $\mathfrak{g}$, the Lie algebra of G. Take a dominant coweight α and another coweight β such that $\beta \leq \alpha$. Then the ith gauge node in the quiver has a rank equal to $\langle \omega_i, \alpha - \beta \rangle$ where ω_i is the ith fundamental coweight of G. This gauge node will also have a flavour node connected to it of rank equal to $\langle \gamma_i^\vee, \beta \rangle$, where $\gamma_i^\vee$ is the ith fundamental coroot of G.

This identification might appear obscure - we'll now try to alleviate this with some examples. Consider the algebra A_2, where we note that the coroot and root lattices for algebras A_n are the same since the group $U(n)$ is GNO-dual to itself.

Consider, in the basis of fundamental (co-)weights, the dominant coweight $\lambda = [4, 0]$ for the algebra A_2. We'll pick our other coweight (which happens to also be dominant) $\mu = [1, 0]$. The difference is $\lambda - \mu = [3, 0]$ and we can compute the gauge node ranks by using the inverse Cartan matrix for A_2, M_{Cartan},

$$M_{Cartan}^{-1} = \frac{1}{3} \begin{pmatrix} 2 & 1 \\ 1 & 2 \end{pmatrix}, \tag{40}$$

so

$$\frac{1}{3} \begin{pmatrix} 2 & 1 \\ 1 & 2 \end{pmatrix} \cdot \begin{pmatrix} 3 \\ 0 \end{pmatrix} = \begin{pmatrix} 2 \\ 1 \end{pmatrix}, \tag{41}$$

giving the quiver in (42).

$$\tag{42}$$

where we have found the gauge node rank to be equal to μ in the basis of fundamental (co-)weights.

We can take another example in the algebra $\mathfrak{g}_2$. Take a dominant coweight $\lambda = [2, 0]$ and this time our $\mu = [0, 0]$. We perform the simple calculation,

$$\begin{pmatrix} 2 & 1 \\ 3 & 2 \end{pmatrix} \cdot \begin{pmatrix} 2 \\ 0 \end{pmatrix} = \begin{pmatrix} 4 \\ 6 \end{pmatrix}, \tag{43}$$

where we identify the matrix on the left hand side of (43) as the inverse Cartan matrix of $\mathfrak{g}_2$. This now corresponds to the quiver in (44).

$$
\begin{array}{c}
\underset{4}{\circ}\!\!\Lleftarrow\!\!\underset{6}{\circ}
\end{array}
\tag{44}
$$

We have presented here an account of how we can use slices in the Affine Grassmannian to find quivers and their Coulomb branches. This naturally extends to a brane description by representing the quivers as Type IIB brane systems. This lies outside of the scope of our discussion, however it is a natural extension and the interested reader is directed towards [21] for a clear exposition.

0.5. 3d $\mathcal{N} = 4$ Moduli & Methods.

0.5.1. SQED & MORE MONOPOLE EXAMPLES. Consider a $U(1)$ gauge group with an $SU(N)$ flavour node, with the corresponding quiver (45) as shown in Fig. 6.

$$
\begin{array}{c}
N \\
\square \\
| \\
\circ \\
1
\end{array}
\tag{45}
$$

This is the theory of *SQED with N flavours*, a simple system that nevertheless allows us to develop a technology for finding the Hasse diagrams for more complicated simply-laced unitary quivers.

The computation of the Hilbert series of the Coulomb branch of $U(1)$ with N flavours is a rite for any student of quiver gauge theory. We reproduce it here as follows.

First, we consider the conformal dimension (7) for the case of $U(1)$. We know that the Langlands dual group for $U(N)$ is itself and so we see that $\Gamma_{G^V} = \mathbb{Z}$ [4], hence our sum in (6) becomes simply a sum over the integers. We also see that the vector of magnetic charges is hence one-dimensional, m, and so we can write the conformal dimension as

$$
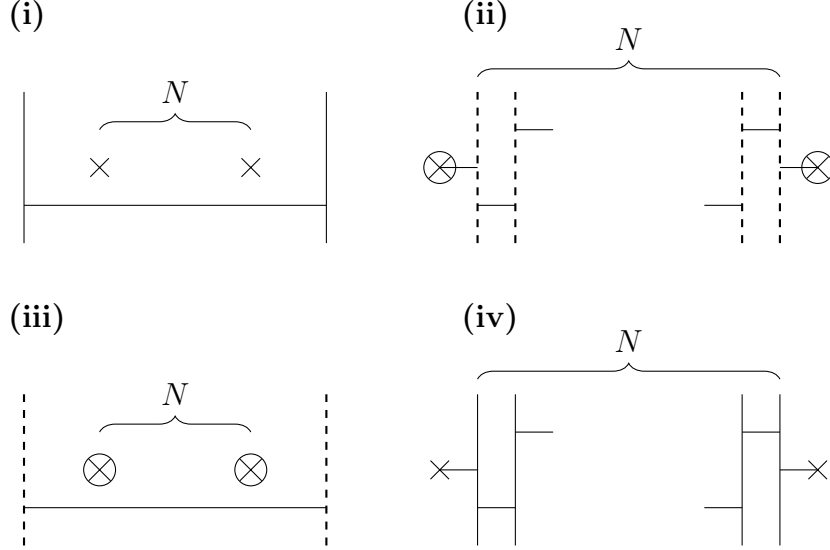\Delta(m) = \frac{N}{2}|m|
\tag{46}
$$

32

Figure 6: (**i**). The brane system representing a generic point on the Coulomb branch of $U(1)$ with N flavours - the singularity A_{N-1}. (**ii**). The brane system representing a generic point on the Higgs branch of $U(1)$ with N flavours - the singularity a_{N-1}. (**iii**). The brane system corresponding to the Higgs branch A_{N-1}. (**iv**). The brane system corresponding to the Coulomb branch a_{N-1}.

and thus our Hilbert series becomes,

$$
\begin{aligned}
HS_{\mathcal{M}_{U(1)}} &= \frac{1}{1-t^2} \sum_{m \in \mathbb{Z}} t^{N|m|} z^m = \frac{1}{1-t^2} \left[\sum_{m=1}^{\infty} \left(\frac{t^N}{z} \right)^m + \sum_{m=1}^{\infty} \left(t^N z \right)^m \right] \\
&= \frac{1-t^{2N}}{(1-t^2)(1-t^N z)(1-\frac{1}{t^N z})}
\end{aligned}
\tag{47}
$$

Importantly, upon setting $N = 1$ we find that the Hilbert series describes the

$$
\begin{array}{c}
\overset{1}{\bullet} \qquad \overset{N-1}{\bullet} \\
A_{N-1} \diagdown \qquad \diagup a_{N-1} \\
\bullet
\end{array}
\tag{48}
$$

We note two things here. The first is that the Hasse diagram of (48) possesses a manifest inversion symmetry. The second is that we can observe the brane systems that correspond to the singularities A_{N-1} and a_{N-1}, given in Fig. 6.

0.5.1.1. COULOMB BRANCH OF $U(4)$ WITH 8 FLAVOURS. The calculation of $U(1)$ with N flavours is the classic example of the monopole formula in action. We'll now consider a slightly more non-trivial case.

Consider the theory given by the quiver (49).

$$
\begin{array}{c}
8 \\
\square \\
| \\
\bigcirc \\
4
\end{array}
\tag{49}
$$

We'll use (6) to compute the Hilbert series of the Coulomb branch of this theory, starting by considering the conformal dimension (7). We begin by assigning four magnetic charges to the $U(4)$ gauge node, $m = (m_1, m_2, m_3, m_4)$. We also have a conserved topological charge $J(\boldsymbol{m}) = m_1 + m_2 + m_3 + m_4$. There are 8 Hplets in this theory and so we can reduce the sum over them in the Hplet contribution to a multiplicative factor of 8, while also making the identification $\sum_{\rho_i \in R_i} |\rho_i(\boldsymbol{m})| = \sum_{i=1}^{4} |m_i|$. Considering also the Vplet contribution, we are led to the expression for the conformal dimension given in (50).

$$
\Delta(m) = 4 \sum_{i=1}^{4} |m_i| - \sum_{i<k} |m_i - m_k|
\tag{50}
$$

Now we must consider the dressing function. For a general good theory with $U(k)$ gauge group and N flavours, our dressing function takes the form given in (51).

$$
P_k(\boldsymbol{m}; t) =
\begin{cases}
\frac{1}{(1-t)^k}, & m_1 \neq m_2 \neq \cdots \neq m_k \\
\frac{1}{(1-t)^{k-1}(1-t^2)}, & m_1 = m_2 \neq m_3 \neq \cdots \neq m_k \\
\frac{1}{(1-t)^{k-2}(1-t^2)(1-t^3)}, & m_1 = m_2 = m_3 \neq m_4 \neq \cdots \neq m_k \\
\vdots & \vdots \\
\frac{1}{(1-t)^{k-I+1}(1-t^2)\cdots(1-t^I)}, & m_1 = m_2 = \cdots = m_I \neq m_{I+1} \neq \cdots \neq m_k \\
\vdots & \vdots \\
\frac{1}{(1-t)(1-t^2)\cdots(1-t^k)}, & m_1 = m_2 = \cdots = m_k
\end{cases}
\tag{51}
$$

Now, for the $U(4)$ case, we clearly have,

$$
P_4(\boldsymbol{m}; t) =
\begin{cases}
\frac{1}{(1-t)^4}, & m_1 \neq m_2 \neq m_3 \neq m_4 \\
\frac{1}{(1-t)^3(1-t^2)}, & m_1 = m_2 \neq m_3 \neq m_4 \\
\frac{1}{(1-t)^2(1-t^2)(1-t^3)}, & m_1 = m_2 = m_3 \neq m_4 \\
\frac{1}{(1-t)(1-t^2)(1-t^3)(1-t^4)}, & m_1 = m_2 = m_3 = m_4
\end{cases}
\tag{52}
$$

34

Note than in both (52) and (51) we make no distinction between *which* of the m_i are equal to each other and are only interested in the number that are equal to each other. In other words, permutations of the m_i in these expressions for the dressing functions are immaterial. We can introduce the fugacity z with index $J(\boldsymbol{m})$ defined above and hence come to the final part of (6), where we sum over the principal Weyl chamber $\Gamma_{G^\vee}/W$ - this corresponds to summing over the dominant weights of the Langlands dual group $G^\vee$, or equally the dominant coweights of G. We can use the fact that the group $U(k)$ is Langlands dual to itself to arrive at the Hilbert series for the Coulomb branch, (54).

$$HS_{U(4),8}(t;z) = \sum_{m_4 \le m_3 \le m_2 \le m_1} P_4(\boldsymbol{m};t) t^{2\Delta} z^{(m_1+m_2+m_3+m_4)} \tag{53}$$

$$
\begin{aligned}
&= \frac{1}{(1-t)^4} \sum_{m_4<m_3<m_2<m_1} t^{2\Delta} z^{(m_1+m_2+m_3+m_4)} \\
&+ \frac{1}{(1-t^2)(1-t)^3} \sum_{m_4<m_3<m_1} t^{2\Delta} z^{(2m_1+m_3+m_4)} \\
&+ \frac{1}{(1-t)^2(1-t^2)(1-t^3)} \sum_{m_4<m_1} t^{2\Delta} z^{(3m_1+m_4)} \\
&+ \frac{1}{(1-t)(1-t^2)(1-t^3)(1-t^4)} \sum_{m_1} t^{2\Delta} z^{(4m_1)}
\end{aligned}
$$

$$\tag{54}$$

An explicit calculation of this gives the Hilbert series [12],

$$HS_{U(4),8}(t;z) = (1-t^8)(1-t^7)(1-t^6)(1-t^5) \prod_{i=1}^{4} \left(\frac{1}{(a-t^i)(1-zt^i)(1-z^{-1}t^i)} \right) \tag{55}$$

0.5.2. KRAFT-PROCESI TRANSITION. The Kraft-Procesi transition, so-named after the authors of [36], was introduced in its present physical context in [3] for unitary quivers and developed in [25] for the orthosymplectic case. Simply, the transition corresponds to moving from a theory with gauge group G to a Higgsed theory in which the gauge group has been broken to a subgroup of G. By utilising these transitions, we obtain a method for understanding the moduli space of a theory through its brane system and, for non-Lagrangian theories, are able to make conjectures about its moduli space through the technology of quiver subtraction. It is important to note here that we can perform this on either the Higgs or Coulomb branches, and in our examples we will consider both cases.

In the language of Hasse diagrams, we see that each Kraft-Procesi transition can be thought of as moving along an elementary transverse slice between adjacent leaves (recall that there

is a tautology here - a slice is defined to be elementary if the leaves are adjacent). In particular, we find that the singularities associated with these transitions are either Kleinian singularites of type A_n or minimal nilpotent orbits.

In this section we will give the prescription for the Kraft-Procesi transition for brane systems with unitary gauge nodes and consider an example

0.5.2.1. $\mathfrak{sl}_n$. We begin by exploring the Kraft-Procesi transition in the simplest case - that for the algebra $\mathfrak{sl}_n$. In performing the transition, we find that the moduli we tune during each transition correspond either to a minimal nilpotent orbit a_n or a Kleinian singularity A_n. We give the following explanation for a brane system where D3-branes are free to move along NS5-branes however it naturally applies to configuration where it is the D5-branes that the D3-branes are free to move along also - in this latter setup, we'd maximally split D3-branes between NS5-branes. Consider the following steps:

(i) Begin with a general brane configuration where D3-branes are suspended between NS5-branes. By 'general', we imagine that we have some brane system with D5, D3 and NS5-branes. If necessary, perform Hanany-Witten transitions such that all D3-branes should start and end on NS5-branes only.

(ii) Choose one D3-brane and take it into the origin whereby it intersects D5-branes.

(iii) Maximally split the D3-brane such that there are now two D3-branes suspended between D5 and NS5-branes and the rest of the split D3-branes start and end on D5-branes.

(iv) Take the D3-branes suspended between D5-branes to infinity along the D5-branes. In our diagram of the brane configurations, we no longer draw these D3-branes.

(v) Perform Hanany-Witten transitions to again recover a brane system where D3-branes are suspended between NS5-branes. This is the brane system of the new quiver corresponding to the adjacent leaf.

By repeating this process we can transition between nodes on the Hasse diagram. For the example in Fig. 7 we see that the transverse slice between the quivers in parts (A) and (C) is merely the Coulomb branch of SQED with three flavours, or A_2 - we can represent this on a Hasse diagram as in Fig. 56.

We can take this further. Kraft-Procesi transitions for unitary simply-laced quivers will correspond to removing moduli parametrised by D3-branes; these are singularities of type a_N or A_N; the former is the singularity associated with the Higgs branch of SQED with N flavours and the latter the Coulomb branch. Of course, we can use 3d mirror symmetry to

36

speak exclusively in terms of Higgs or Coulomb branches. The main point is that we can use this identification of brane systems with their singularities to reduce the process of taking Kraft-Procesi transitions to merely spotting the relevant SQED branches.

Considering Fig. 7, we can see only one D3-brane that we can take onto the origin, in which case it would intersect one D5-brane. Hence the relevant transverse slice in this case would be A_0, corresponding to $\mathbb{C}^2$.

$$A_2 \quad \vcenter{\hbox{\includegraphics{}}} \tag{56}$$

In [3] and [25] Kraft-Procesi transitions were considered as transitions between two Higgs branch phases corresponding to different nilpotent orbits of some classical algebra. Hence the structure of our Hasse diagrams is simply the structure of the partitions under the 'partial sum' partial ordering. In other words, we can determine the Hasse diagram skeleton by the method above without any recourse to brane systems or quiver dynamics - from the brane perspective the Kraft-Procesi transition corresponds to moving between these partitions.
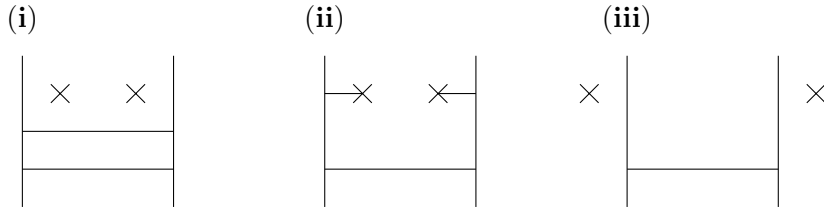

Figure 7: (**i**). The configuration after one D3-brane has been moved onto the origin. (**ii**). The D3-branes are split maximally and the D3-branes suspended between D5-branes are removed. (**iii**). A Hanany-Witten transition is taken to remove D3-branes suspended between D5 and NS5-branes.

As an example of the Kraft-Procesi transition in action on brane systems, as well as giving insight into how to transition a brane system from one phase to another, we will consider the Hasse diagram in (3.7) of [14]. This Hasse diagram is presented without the corresponding brane system - we'll work it out here. Firstly, consider the quiver in (57).

$$\tag{57}$$

The brane system with D3-branes suspended between NS5-branes is easy to read off from (57) and we can explicitly transition to the phase where all free D3-branes can move along D5-branes as shown in Fig. 8. From here, it is simply a matter of recognising the singularities
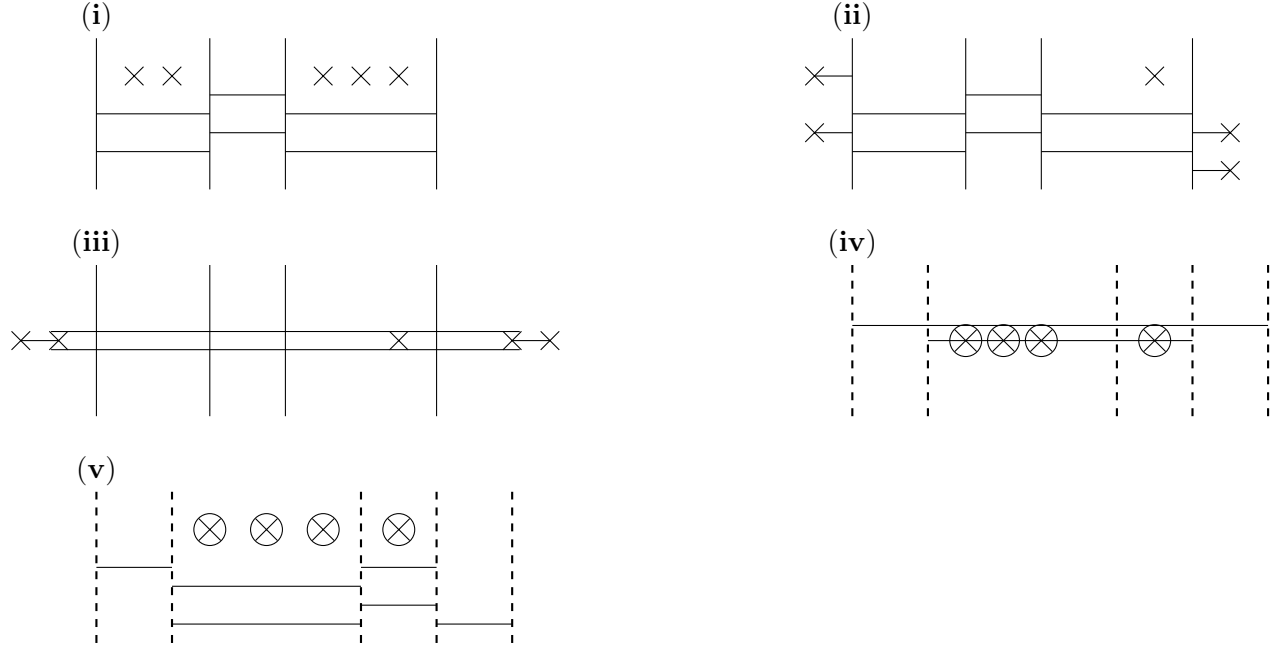
Figure 8: The phase transition from the phase where all free D3-branes are suspended between NS5-branes (**i**) to the phase where all free D3-branes are suspended between D5-branes (**v**) for the quiver (57).

in the brane systems to construct the Hasse diagram, which we do in Fig. 9. This exercise is made all the more simple by our identification in Fig.

0.5.2.2. $\mathfrak{so}_n$ & $\mathfrak{sp}_n$. The Kraft-Procesi transition for the case of orthosymplectic quivers is broadly similar to the case of unitary gauge nodes. The main complication when considering manipulations at the level of brane systems is unsurprisingly the presence of orientifold planes. We know that when we have $\mathcal{O}3$ planes in our brane system the D3-branes will become half D3-branes under the orientifold planes' $\mathbb{Z}_2$ action. Hence, the single whole D3-branes that we'd split in the Kraft-Procesi transition in the $\mathfrak{sl}_n$ case become two half D3-branes in the orthosymplectic case.

One more subtlety to keep aware of is the possibility of the Kraft-Procesi transition to break the supersymmetry of the brane system when applied incorrectly. This is particular to the orthosymplectic case and the particulars will be beyond the scope of our discussion. The reader is pointed towards [25] for more discussion. In this report we will focus only on the case corresponding to the algebra $\mathfrak{sl}_n$.
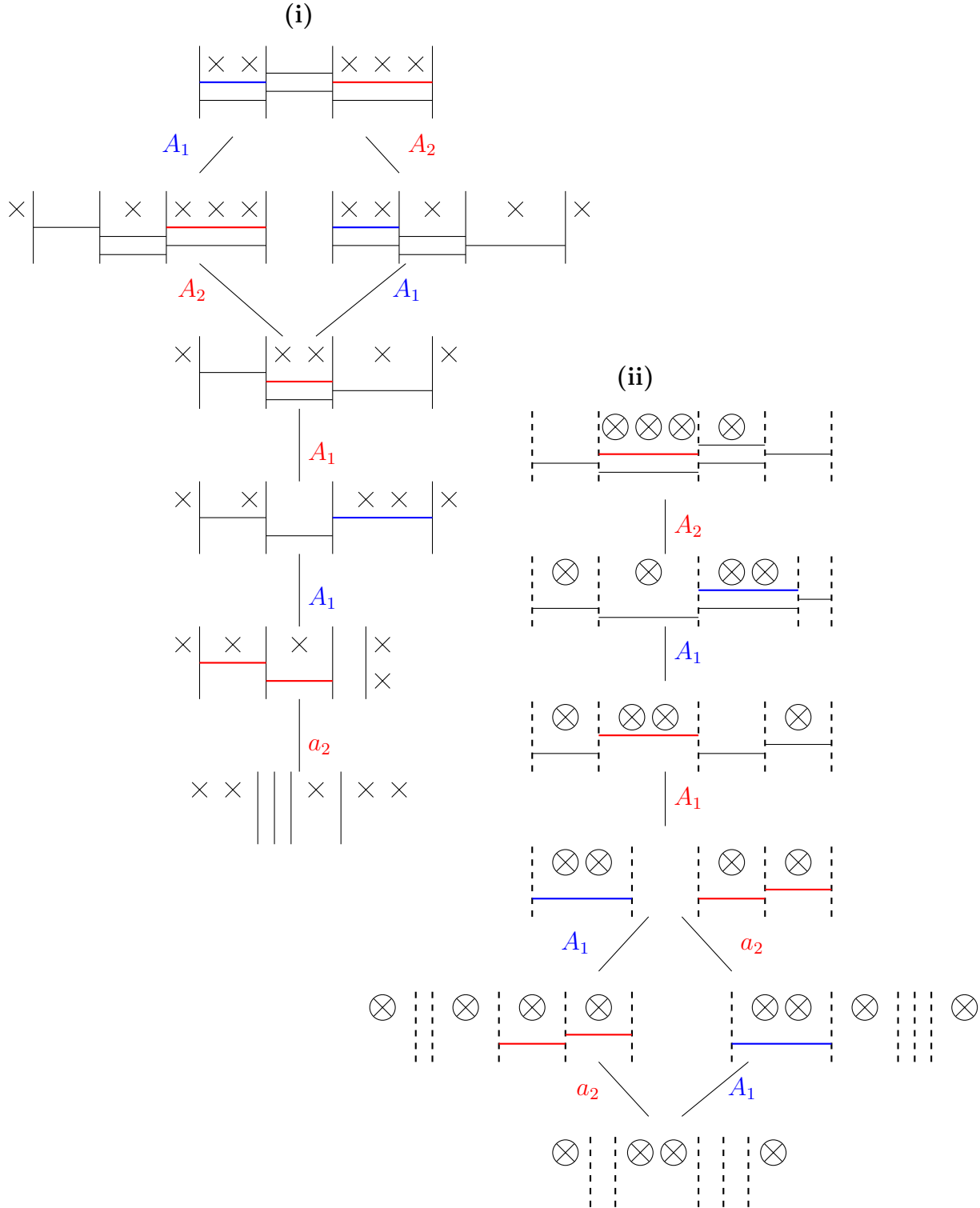
Figure 9: Kraft-Procesi transitions for the brane systems given by suspending the D3-branes between NS5-branes of D5-branes. We explicitly see the process of Hasse diagram inversion here, as is expected since the slices are either nilpotent orbits or Kleinian singularities of ADE-type.

0.5.3. BRANE CONFIGURATIONS & NILPOTENT ORBITS. Given that we know that the Higgs branch of SQED with N flavours corresponds to the minimal nilpotent orbit a_n, we might consider the question now of whether there are any other quivers whose branches, Coulomb or Higgs, we might be able to associate with the closure of a nilpotent orbit.

It turns out that there are. For the algebra $\mathfrak{sl}_n$ we can use linking numbers to specify brane systems with Higgs branches that correspond to a particular nilpotent orbit (identified by its partition λ), shown in Fig. 0.5.3 [3] [25]. Let us consider the quiver whose Coulomb branch corresponds to the maximal nilpotent orbit of $\mathfrak{sl}_n$, shown in (58).

Orbit Type	n_s, n_d	ℓ_s	ℓ_d	$\mathcal{O}3$ Type
A_n	n	λ^T	$(n-1, \cdots, n-1)$	-
B_n	$2n+1$	$Even(d_{BV}(\lambda))$	$(2n, \cdots, 2n)$	$\mathcal{O}3^-$
C_n	$2n+1$	$Odd(d_{BV}(\lambda))$	$(2n+1, 2n-1, 2n+1, 2n-1, \cdots)$	$\widetilde{\mathcal{O}3}^+$
D_n	$2n$	$Odd(d_{BV}(\lambda))$	$(2n-1, \cdots, 2n-1)$	$\mathcal{O}3^-$

Figure 10: This table shows the data required to construct Type IIB brane systems whose Higgs branch corresponds to the closure of the nilpotent orbit corresponding to the partition λ. Note that the rightmost column refers to the type of the rightmost $\mathcal{O}3$ plane in the brane system. The other $\mathcal{O}3$ planes follow by considering the relevant boundary conditions given in 4. The issue of the Coulomb branch is simple under $3d$ mirror symmetry for A_n-type partitions - for the other cases it is more subtle - see [37].

Let us also consider how we can identify Higgs and Coulomb branches of particular theories with the nilpotent orbits of $\mathfrak{so}_n$ and $\mathfrak{sp}_n$ algrbras. These are a little more complicated from the brane perspective than the $\mathfrak{sl}_n$ case since they involve orientifold planes, however the logic of the partition-nilpotent orbit perspective remains largely unchanged, save for some additions regarding the Lusztig-Spaltenstein and Barbasch-Vogan maps.

The main point to consider is that there is still an algorithmic way to go from a partition to the linking numbers of a brane system. In Fig. 0.5.3 we use the functions $Even()$ and $Odd()$, as well as the Barbash-Vogan map $d_{BV}()$.

First the Barbash-Vogan map:

- When λ is a partition of $2n+1$ for the B-type orbit, d_{BV} corresponds to first subtracting 1 from the first entry in the partition (ordered from smallest to largest) and then considering the following options. (Note that now we will have a partition of $2n$, not $2n + 1$.) If λ has odd parts with odd multiplicity, we replace λ with λ', where λ' is the largest partition of $2n$ such that $\lambda' \le \lambda$ and λ' has odd parts that have even multiplicity.

40

- When λ is a partition of $2n$ for the D-type orbit, d_{BV} corresponds to the following. If all even parts of λ have even multiplicity then we do nothing; if λ has even parts with odd multiplicity we replace it with the partition of $2n$ λ' where λ' is the largest partition of $2n$ such that $\lambda' \leq \lambda$ and all even parts of λ' occur with even multiplicity.

- When λ is a partition of $2n$ for the C-type orbit we first add 1 from the last entry in the partition (ordered from smallest to largest) and then consider the following. (Note again that now we will have a partition of $2n + 1$.) If λ has all even elements with even multiplicity we do nothing. If λ has any even elements with odd multiplicity we replace λ with λ' where λ' is the largest partition of $2n$ such that $\lambda' \leq \lambda$ and all even parts of λ' occur with even multiplicity.

Now consider the $Even()$ and $Odd()$ maps.

- For the $Even()$ map we are considering partitions of $2n$ where after applying the Barbash-Vogan map we will have recovered a partition where all odd parts occur with even multiplicity. First ensure that the partition is written such that it only contains elements like a^b where a is the partition element and b is its multiplicity. Now split each odd element o^b into two elements $o^{\frac{1}{2}b}$. For the first element $o^{\frac{1}{2}b}$ add 1 to it and the second element $o^{\frac{1}{2}b}$ subtract 1 from it. The multiplicities will remain the same. Reorder the partition from smallest to largest. Hence in the new partition all elements will be even.

- For the $Odd()$ map we are considering partitions of $2n + 1$ where after applying the Barbash-Vogan map we will have recovered a partition where all even parts occur with even multiplicity. First ensure that the partition is written such that it only contains elements like a^b where a is the partition element and b is its multiplicity. Now split each even element e^b into two elements $e^{\frac{1}{2}b}$. For the first element $e^{\frac{1}{2}b}$ add 1 to it and the second element $e^{\frac{1}{2}b}$ subtract 1 from it. Reorder the partition from smallest to largest. Hence in the new partition all elements will be odd.

The Higgs branch of the quiver below corresponds to the maximal nilpotent orbit of $\mathfrak{sl}_N$.

$$
\underset{1}{\circ}\!\!-\!\!\underset{2}{\circ}-\ \cdots\ -\!\!\underset{\text{N-1}}{\circ}\!\!-\!\!\underset{\text{N}}{\square}
$$

(58)

We will now go through some examples of the Kraft-Procesi transition.

0.5.3.1. TRANSITIONS IN $\mathfrak{sl}_6$. Let us provide some examples of using the relationship between the partition of an $\mathfrak{sl}_n$ algebra and the Kraft-Procesi transition. We'll look at two

elementary transverse slices in the Hasse diagram given in (13). Let us begin by considering the transition between the theory with Higgs branch equal to the singularity $\bar{\mathcal{O}}_{[1,5]}$ and that with Higgs branch $\bar{\mathcal{O}}_{[2,4]}$ - we see that in this case we need to find the $3d\ \mathcal{N} = 4$ brane system for which we have the linking numbers $\boldsymbol{\ell}_d = (5,5,5,5,5,5)$ and $\boldsymbol{\ell}_s = (0,1,1,1,1,2) = (1,5)^T$ such that $\boldsymbol{\ell}_s = \lambda^T$. We then construct the branes as in Fig. 11. Using Fig. 6 **iii** we can identify the four NS5-branes in the initial brane system with an A_3 transition and split the D3-brane shaded in blue along the NS5-branes. We end up with the second brane system shown in Fig. 11. We can check that this transition is correct by computing the linking numbers for the brane system we end up with - we find $\boldsymbol{\ell}_s = (0,0,1,1,2,2)$ and $\boldsymbol{\ell}_d = (5,5,5,5,5,5)$ and so by making the identification $\lambda^T = \boldsymbol{\ell}_s$ we end up with $\lambda = (2,4)$ as expected.
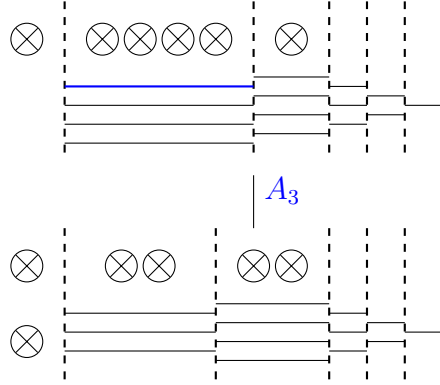

Figure 11: The transition between the brane systems with Higgs branch corresponding to the singularities $\bar{\mathcal{O}}_{[1,5]}$ and $\bar{\mathcal{O}}_{[2,4]}$. The D3-brane labelled in blue is the brane we take to perform the transition on giving an elementary transverse slice A_3.

For our second example we will consider the transition from the brane system with Higgs branch corresponding to the singularity $\bar{\mathcal{O}}_{[1,2,3]}$ of $\mathfrak{sl}_6$ to that corresponding to $\bar{\mathcal{O}}_{[2^3]}$. As we observe in Fig. 14, we can find an a_2 transition associated to the D3-branes shaded in red in the initial brane configuration. Again, we have used Fig. 6 **ii** to spot this and we can perform the simple brane manipulation to obtain the second brane system of Fig. 14. To check our result we again note the linking numbers $\boldsymbol{\ell}_s = (0,0,0,0,3,3) = \lambda^T$ and $\boldsymbol{\ell}_d = (5,5,5,5,5,5)$ giving $\lambda = (2^3)$ as expected. This completes our examples of Kraft-Procesi transitions between brane systems whose Coulomb or Higgs branches correspond to the closure of a nilpotent orbit of $\mathfrak{sl}_6$.
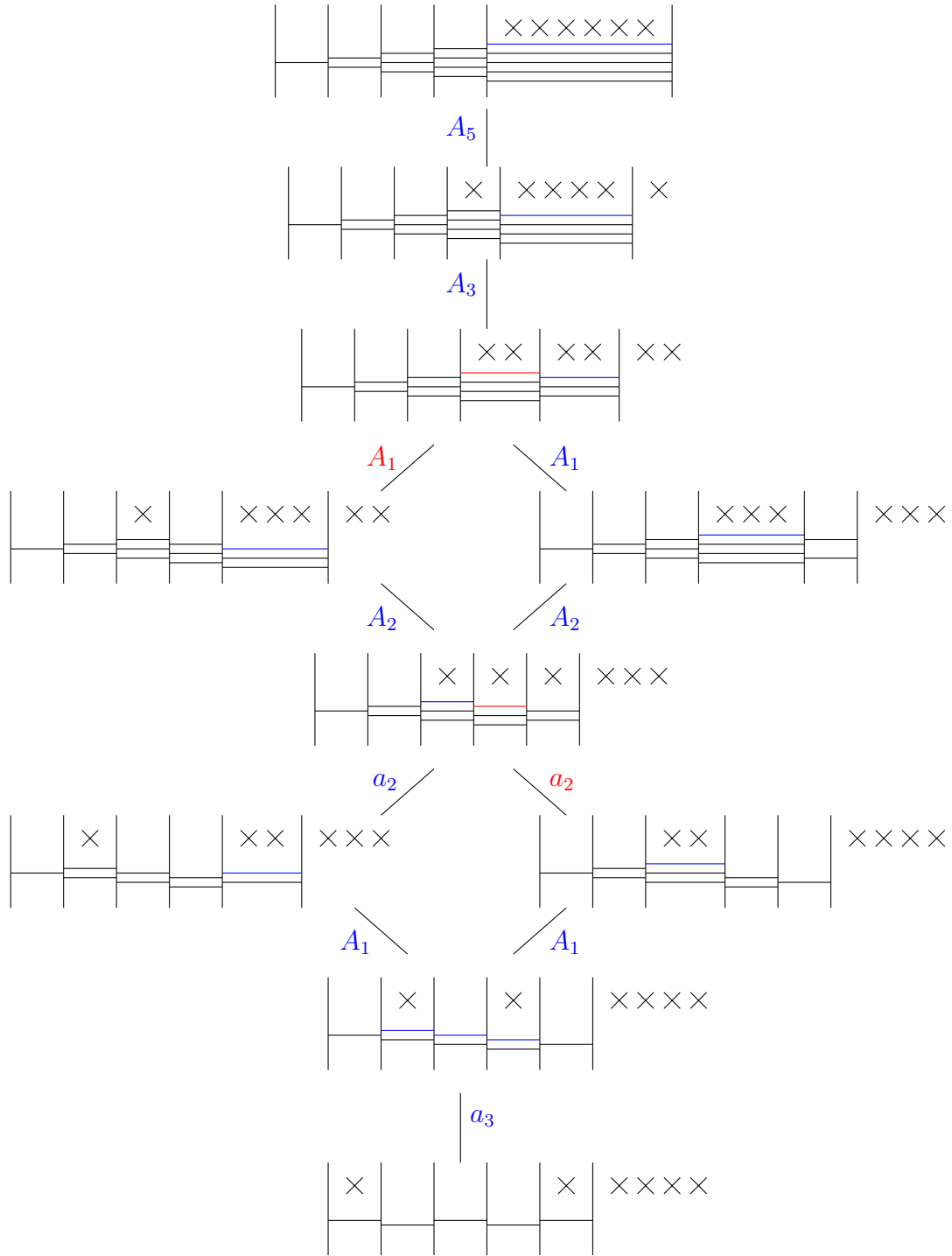
Figure 12: Kraft-Procesi transitions on the brane system corresponding to the Coulomb branch of the theory (58). Here we have used the process given in [3]. The coloured D3-branes correspond to the branes we are performing the Kraft-Procesi transition on (i.e. the branes that give the same-colour transverse slices coming out of the brane system).
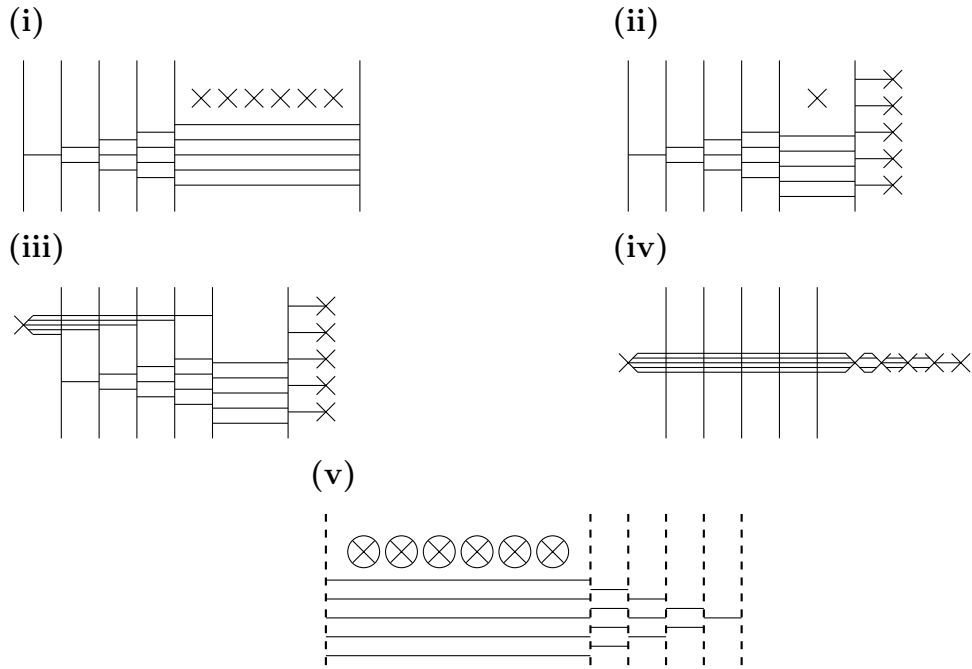
Figure 13: This shows the process of taking the brane system corresponding to the quiver (58) for $N = 6$ and manipulating it such that the D3-branes end on D5-branes. We can clearly see that this process is the same as what we'd get if we performed $3d$ mirror symmetry on the brane system - we conclude that this theory is self-dual. This means that its Higgs and Coulomb branches correspond to the same algebraic variety and so we can perform Kraft-Procesi transitions on the brane system in the phase i and recover the same Hasse diagram as if we were to perform the transitions on v
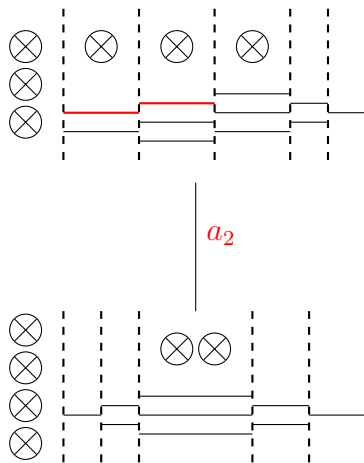

Figure 14: The Kraft-Procesi transition between the brane systems with Higgs branch corresponding to the singularities $\bar{\mathcal{O}}_{[1,2,3]}$ and $\bar{\mathcal{O}}_{[2^3]}$. The branes shaded in red correspond to the D3-branes we take the transition on, giving an elementary transverse slice a_2.

44

(i)

(iia) **(iib)**

(iic) **(iid)**

(iiia) **(iib)**

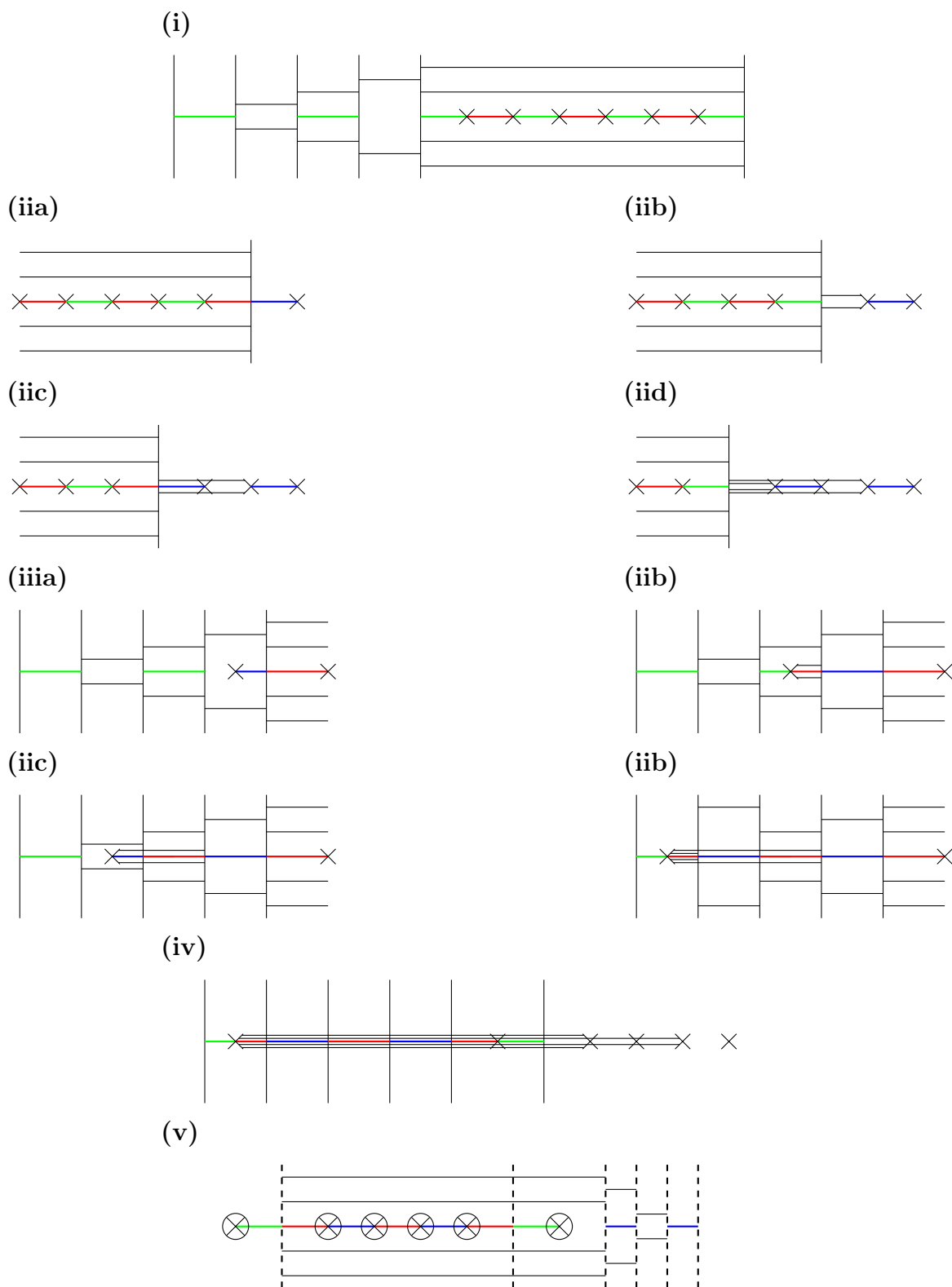**(iic)** **(iib)**

(iv)

(v)

Figure 15: This shows the procedure to change from the phase in which all D3-branes are suspended between NS5-branes to that in which all D3-branes are suspended between D5-branes for the theory given by the quiver corresponding to the highest nilpotent orbit of so_6.

45

0.6. Type IIA Brane Systems & 6d Theories. So far, we've considered $3d$ $\mathcal{N} = 4$ theories and their associated Type IIB brane systems. We've also considered $3d$ mirror symmetry and introduced the idea of the magnetic quiver. We'll now treat this more comprehensively using Type IIA brane systems derived from M-theory brane configurations on specific singularities. We'll find that we can calculate the Hasse diagram for certain theories using Type IIA considerations that were heretofore inaccessible.

Let us take a moment to stress exactly what's going on here. Recall that $3d$ $\mathcal{N} = 4$, $5d$ $\mathcal{N} = 1$ and $6d$ $\mathcal{N} = (1,0)$ theories all have eight supercharges - whether we have Hplets, Vplets or Tplets depends on the dimension. For their Higgs branches, we know that at finite coupling the renormalisation theorem protects us against quantum corrections (at infinite coupling in six-dimensions we can have quantum corrections. Hence by constructing brane systems in six dimensions we can use the technology of the magnetic quiver to associate these Higgs branches with Coulomb branches in $3d$ $\mathcal{N} = 4$ and thus find the algebraic variety corresponding to the Higgs branch of the theory we are investigating in six dimensions. We'll introduce Type IIA brane constructions by first considering systems of M5-branes and an M9 plane. The basic picture corresponding to the change from the M-theory setup to

	x^0	x^1	x^2	x^3	x^4	x^5	x^6	x^7	x^8	x^9	x^{10}
M5	x	x	x	x	x	x					
M9	x	x	x	x	x	x		x	x	x	x
A_{k-1}	x	x	x	x	x	x	x				
NS5	x	x	x	x	x	x				N/A	N/A
D6	x	x	x	x	x	x	x			N/A	N/A
D8/$\mathcal{O}8^-$	x	x	x	x	x	x		x	x	x	N/A

Figure 16: The dimensions for various objects in the M-theory and Type IIA constructions. Note that M-theory is an eleven-dimensional theory while the Type-IIA theory is ten-dimensional - we have accordingly left 'N/A' in the eleventh dimension for the branes in the Type IIA construction.

the Type IIA setup is given in Fig. 17. Note that we will not be concerned with the M-theory setup here and we include it only to show that the $6d$ theory is obtained from the world-volume theory of the M5-branes which admits a dual description as a Type IIA theory. Under this dual description we obtain n $D6$ branes from an A_{n-1} singularity, m NS5-branes from m M5-branes and eight D8-branes along with an $\mathcal{O}8^-$-plane from the $M9$-plane [18]. In our analysis we will be only interested in manipulations of D6-, D8- and NS5-branes. It is important to consider how we transition from the M-theory to the Type IIA construction explicitly. By changing the M9-plane into eight D8-branes and an orientifold plane. We bring in a D8-brane from infinity such that the D6-branes end on it and thus parametrise
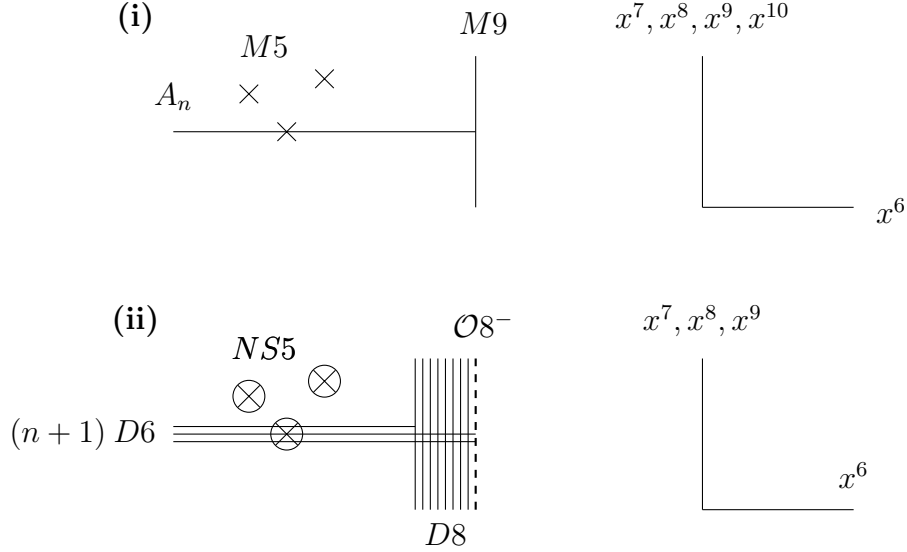
46

Figure 17: **i** The M-theory setup. The horizontal line denotes an A_n singularity, while the vertical line denotes an M9-plane and the crosses denote M5-branes. **ii** the dual Type IIA description. The circled crosses denote NS5-branes while the horizontal lines denote D6-branes, the vertical full lines D8-branes and the dashed vertical line an $\mathcal{O}8^-$ plane.

the Higgs branch.

0.6.1. SMALL e_8 INSTANTON TRANSITION. The distance of the NS5-branes from the orientifold plane along the x^6 direction is inversely proportional to the coupling. Hence moving the NS5-branes onto the orientifold transitions from finite coupling to infinite coupling. However, we see from (2) that we need to keep the numbers of unfrozen D6- and NS5-branes in the theory consistent for anomaly cancellation. In this 6d theory the movement of the NS5-branes along the x^6 direction will contribute a tensor multiplet to the theory and so in order for anomaly cancellation we'd hope that a transition to infinite coupling whereby the (half) NS5-branes become frozen on the orientifold, losing a tensor multiplet, would compensate by gaining 29 Hplets (D6-branes suspended between D8-branes). This is indeed the case and is called the *small e_8 instanton transition*.

Consulting Fig. 18, we see that while we lose one tensor multiplet when we transition to infinite coupling and the NS5-brane becomes two half NS5-branes on the orientifold, we compensate for this by gaining 29 Hplets in the new D6-branes that are now suspended between D8-branes. Hence we maintain anomaly cancellation given in (2). We should also note that in our drawings of these brane systems we will not depict the side on the right of the orientifold plane, although of course it is there. The four D6-branes that look to be 'bouncing' off the orientifold are in reality passing through the orientifold and ending on the
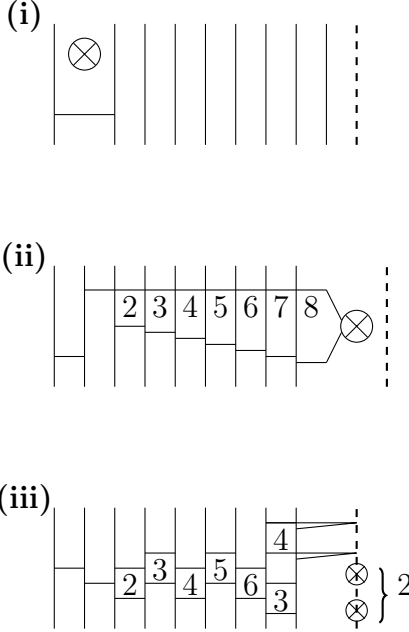
Figure 18: The small e_8 instanton transition. (**i**). The initial system with one NS5-brane and we have drawn one D6-brane between the two rightmost D8-branes. This is at finite coupling. (**ii**). Hanany-Witten transitions to bring the NS5-brane through so that it is now between the rightmost D8-brane and the orientifold plane. This is still at finite coupling. (**iii**). We have brought the NS5-brane onto the orientifold plane where it splits into two half NS5-branes. The D6-branes are now free to move between the D8-branes they span and so we lost one tensor multiplet but gain 29 Hplets.

mirror image of the D8-brane that they end on on the left-hand side. This is particular to the fact we have an $\mathcal{O}8^-$ plane, other types of orientifold plane would give different results.

0.6.2. Brane Construction of Magnetic Quivers. Following the method given in [18], we will now show how we construct 6d brane systems corresponding to specific magnetic quivers. Following the method espoused in [18], we will replace the M5-branes with NS5-branes and the M9-plane with eight D8-branes and an orientifold $\mathcal{O}8^-$ plane. The A_{k-1} singularity gives rise to k D6-branes along the x^6 direction. In practice, we will be constructing these Type IIA systems without discussion or recourse to the M-theory setup.

The motion of each D6-brane along the D8-branes gives corresponds to a Hplet and the motion of an NS5-brane along the x^6 direction gives a single tensor multiplet. Then the D6-branes are free to move between the D8-branes and the NS5-brane can only move in the (x^7, x^8, x^9) directions. Moving the NS5-brane onto the orientifold plane also transitions from finite to infinite coupling since the coupling is inversely-proportional to the x^6 distance between the NS5-brane and the orientifold plane.

We should also note a further parameter called the *Romans mass*. The Romans mass is the

difference between the number of D6-branes ending on the NS5-brane from the left and the number ending on it from the right. We'll note that the brane systems we draw are again consistent when we consider this parameter.

We'll now expound some of the general rules we use when drawing the brane systems corresponding to particular magnetic quivers. All the quivers we consider will be of a few types. The first corresponds to an 'affine e_8 shape' in which we have a long chain of nodes and then a bifurcation in the quiver, similar to how the rank-6 node in affine e_8 has rank-4 and rank-3 nodes attached to it (if we ignore the rank-5 node). The second type will be the affine

- k D6-branes suspended between two adjacent D8-branes will contribute a rank-k gauge node to the magnetic quiver. This is similar to the 3d case when we have k D3-branes suspended between NS5-branes contributing a $U(k)$ node to the electric quiver.

- K NS5-branes between two D8-branes (not considering any D6-branes ending on the NS5-brane) separated along the will contribute a $U(k)$ node with adjoint Hplet loop.

- K half NS5-branes on the orientifold plane will contribute a rank-k gauge node to the quiver.

0.6.3. TRANSITIONS BETWEEN THEORIES. If we have a particular Type IIA setup with D6-, D8- and NS5-branes, we can freeze specific D6-branes between NS5- and D8-branes, corresponding to a transition to a theory with a gauge group that is. subgroup of the original. In the brane systems we show, the positions of the D6-branes between D8-branes will parametrise generic points on the Higgs branch - we use the magnetic quivers associated with these theories to perform quiver subtraction.

The brane methods we used in the Type IIB case are broadly similar to the 6d case - for instance, the method to take a brane system from its magnetic to electric phase (going from the D6-branes suspended between D8-branes to suspended between NS5-branes) uses the same procedure. We will provide explicit examples of this in the following sections.

In the e_8 transitions we consider below, once we have frozen the D6-branes to end on an NS5-brane we will take the NS5-brane off the orientifold and perform Hanany-Witten transitions to recover a system in which the NS5-brane is between two D8-branes.

Although we haven't introduced these concepts yet, we note here the question of how to realise the Hasse diagrams for theories with magnetic quivers that have adjoint Hplets on gauge nodes. Later on, we will present the known Hasse diagrams for these theories, however it is useful to know how these transitions come about from the brane perspective. We do so by making these NS5-branes coincident, which in the decorated quiver corresponds to bringing several of the decorated nodes together into a short node.

0.7. Quiver Addition & Subtraction. Quiver subtraction is simply a way to articulate a Kraft-Procesi transition at the level of quiver diagrams [14]. This has several advantages over the brane perspective and it allows us to make conjectures regarding our expectation of the Hasse diagram structure of theories even if they are non-Lagrangian and do not admit a brane-system description [26].

In this section, we will describe the quiver subtraction algorithm that was first formalised in [38] and then developed further in [21] [26], [39], [14] amongst others. That these papers have been so recently published should belie any attempt to present the quiver subtraction algorithm as a completed process - it does not currently exist for all quivers and is frequently refined to meet the challenge of new examples [39].

Quiver addition, presented in [21], [26] gives the expected inverse operation to subtraction. As ever, there are complications. Primarily, quiver addition poses problems due to the fact that it is not unique. We here give the algorithm for implementing quiver subtraction on $3d$ $\mathcal{N} = 4$ magnetic quivers, as given in [26]. Note that we are limited in the quivers we can subtract to the magnetic quivers for elementary transverse slices. The most up-to-date list of these is presented in (A.1).

(i) Take two magnetic quivers, $\mathcal{Q}_1$ and $\mathcal{Q}_2$, where $\mathcal{Q}_1$ is our original leaf and $\mathcal{Q}_2$ an elementary slice. For us to be able to subtract $\mathcal{Q}_2$ from $\mathcal{Q}_1$ we require that $\mathcal{Q}_2$ is a connected subdiagram of $\mathcal{Q}_1$ with every unique node in $\mathcal{Q}_2$ corresponding to a unique node in $\mathcal{Q}_1$. Note that for $\mathcal{Q}_2$ to be a subdiagram of $\mathcal{Q}_1$, the rank each node in $\mathcal{Q}_2$ must be equal to or less than the rank of the node it corresponds to in $\mathcal{Q}_1$.

(ii) Align $\mathcal{Q}_2$ with $\mathcal{Q}_1$ and then subtract each node in $\mathcal{Q}_2$ from the node it corresponds to in $\mathcal{Q}_1$ to obtain the quiver $\mathcal{Q}_3'$.

(iii) We require that the nodes in $\mathcal{Q}_3'$ have the same balance (or unbalance) as they originally had in $\mathcal{Q}_1$. If this is not the case, we add a single $U(1)$ node to $\mathcal{Q}_3'$ and connect it to the nodes in $\mathcal{Q}_3'$ as follows:

   (a) If any of the nodes in $\mathcal{Q}_3'$ that have changed their balance from $\mathcal{Q}_1$ are *long* nodes, we add simply-laced links between these nodes and the added $U(1)$ until the nodes are balanced again.

   (b) If any of the nodes in $\mathcal{Q}_3'$ that have changed their balance are *short* nodes, we add non-simply-laced links between these nodes and the nodes in $\mathcal{Q}_1$ and the added $U(1)$ until the nodes are balanced again.

(iv) Once we've taken care of this posible extra $U(1)$, we recover the quiver $\mathcal{Q}_3$. This is our final result. Note that the $U(1)$ node we add to maintain the balance numbers for each

node does not itself need to be balanced, and in many cases will not be. However, if we then perform subsequent subtractions they will become the nodes of a new quiver $\mathcal{Q}_1$ and we'll have to possibly add more $U(1)$ nodes to main them.

This method works well for many calculations, however there is a subtlety we have overlooked. This is the case where we subtract the same elementary slice from the same set of nodes in a quiver twice in a row. In these cases, we do the following,

(a) If we are subtracting the same slice from the same nodes for the second time, we add an adjoint Hplet loop on to the $U(1)$ node that we added the first time and increase its gauge node rank to become a $U(2)$ node.

(b) If we are subtracting the same slice from the same nodes for more than the second time, we keep the adjoint Hplet that we added the first time and now simply increase the gauge node rank. For the nth subtraction, the gauge node has rank n.

Let's first consider as an example the following quiver,

$$(59)$$

Upon consultation of (A.1) we can see that there's a subdiagram in (59) corresponding to the magnetic quiver of a_2. Let's subtract this.

$$(60)$$

We've subtracted the two bottom rank-1 nodes of the a_2 magnetic quiver from the two rank-2 nodes of the original quiver to end up with two rank-1 nodes and the top-most node in the a_2 quiver has annihilated its counterpart in the original. Hence we've had to add a further $U(1)$ node and connect it to the left-most and right-most $U(1)$ nodes to restore their balance. The quiver we end up with has as its Coulomb branch a_4.

Let's now use the technology of quiver subtraction to check the Hasse diagram we found in

Fig. 31. The magnetic quiver corresponding to (19) is,

$$
\begin{array}{c}
\overset{\displaystyle 1\ \bigcirc \qquad \bigcirc\ 1}{} \\
\underset{1 \quad 2 \quad 3 \quad 4 \quad 5 \quad 4 \quad 3 \quad 2 \quad 1}{\bigcirc-\bigcirc-\bigcirc-\bigcirc-\bigcirc-\bigcirc-\bigcirc-\bigcirc-\bigcirc}
\end{array}
\tag{61}
$$
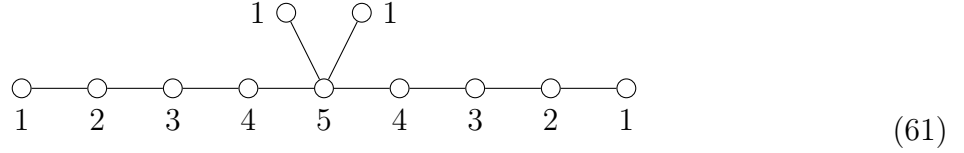
Immediately we see this agrees on dimensional grounds with the highest leaf of (31) - summing the ranks of our gauge groups in (61) gives 27 and we have to subtract one due to our $U(1)$ ungauging to see that the dimension of the Coulomb branch of (31) is 26 - the same as the Higgs branch of (19), its magnetic dual. The only elementary transverse slice we can subtract from this is a d_4, which has a quaternionic dimension of 5 and agrees with the topmost elementary transverse slice in (31). Subtracting this gives,
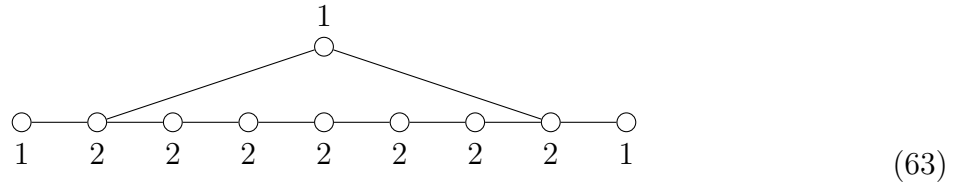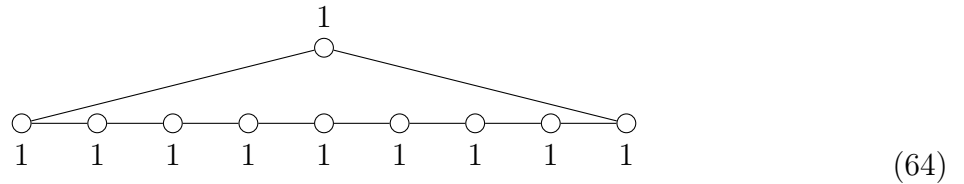
$$
\begin{array}{c}
\overset{\displaystyle 1}{\bigcirc} \\
\underset{1 \quad 2 \quad 3 \quad 3 \quad 3 \quad 3 \quad 3 \quad 2 \quad 1}{\bigcirc-\bigcirc-\bigcirc-\bigcirc-\bigcirc-\bigcirc-\bigcirc-\bigcirc-\bigcirc}
\end{array}
\tag{62}
$$
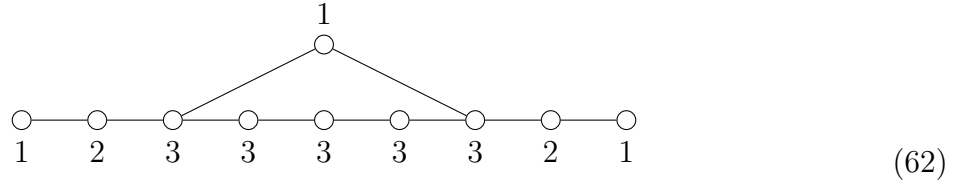
We can sum the gauge nodes and subtract one again to find that this Coulomb branch has quaternionic dimension 21, again the same as we found for its $3d$ mirror dual Higgs branch in 31. Now we can subtract an elementary transverse slice a_5 of quaternionic dimension 5 (again agreeing with the elementary slice dimension in 31) to get,

$$
\begin{array}{c}
\overset{\displaystyle 1}{\bigcirc} \\
\underset{1 \quad 2 \quad 2 \quad 2 \quad 2 \quad 2 \quad 2 \quad 2 \quad 1}{\bigcirc-\bigcirc-\bigcirc-\bigcirc-\bigcirc-\bigcirc-\bigcirc-\bigcirc-\bigcirc}
\end{array}
\tag{63}
$$

with quaternionic dimension 16, corresponding to the middle leaf of 31. Subtracting an a_7 leaves us with

$$
\begin{array}{c}
\overset{\displaystyle 1}{\bigcirc} \\
\underset{1 \quad 1 \quad 1 \quad 1 \quad 1 \quad 1 \quad 1 \quad 1 \quad 1}{\bigcirc-\bigcirc-\bigcirc-\bigcirc-\bigcirc-\bigcirc-\bigcirc-\bigcirc-\bigcirc}
\end{array}
\tag{64}
$$

which has a Coulomb branch corresponding to a_9 and thus has dimension 9, corresponding to the leaf second from bottom in 31. Hence we see that quiver subtraction on the magnetic quiver of 19 corresponds exactly to what we found using the explicit representations.
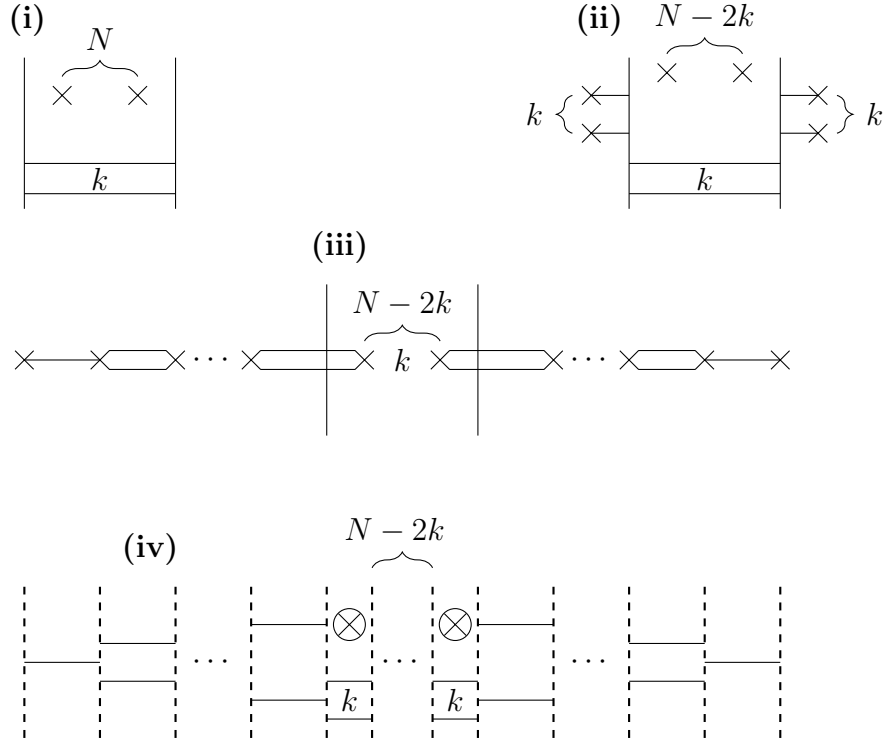
Furthermore, the fact that at each point we only have one elementary transverse slice to subtract (i.e. there are no bifurcations) implies that the gauge group transitions that we showed were proscribed by the decomposition of the representations are indeed unreachable. We also introduce quiver addition here using the prescription given for cases where we have adjoint Hplets [26],

0.8. Hasse Diagrams: Full Moduli Space. In this section we will show how we can construct the Hasse diagram of the full moduli space of various theories. This is achieved by performing quiver subtraction on the magnetic quiver corresponding to the Higgs branch of these theories and then using the technique of Hasse diagram inversion, explored recently in [14]. Although the technique of Hasse diagram inversion has been explored for a wider class of theories than the three types we will consider here, we believe that the import of the inversion technique conveyed by those we do cover. For these good theories we can use both the techniques of quiver subtraction and brane manipulation to understand their full moduli space, the interested reader is encouraged to consider [14] for greater depth.

0.8.1. $U(k)$ WITH N FLAVOURS. Let's begin by taking the magnetic quiver associated to $U(k)$ with N flavours, where $N \geq 2k$.

$$(65)$$

This can readily be found in the literature, but we should first make sure we understand its origin. For the theory of $U(k)$ with N flavours, we can straightforwardly construct the brane system that (when we configure it such that all D3-branes are suspended between D5-branes) corresponds to its the Higgs branch. Then, it's simply a case of using $3d$ mirror symmetry to find the brane system whose Coulomb branch gives the same algebraic variety. This is performed explicitly in Fig (19).

It should be clear that we can subtract an a_{N-2k+1} slice from this quiver, since the number

Figure 19: The process of transitioning the phase of the theory given of $U(k)$ with N flavours (where $N \geq 2k$) from the phase in which all D3-branes are suspended between D5-branes to the phase in which all D3-branes are suspended between NS5-branes.
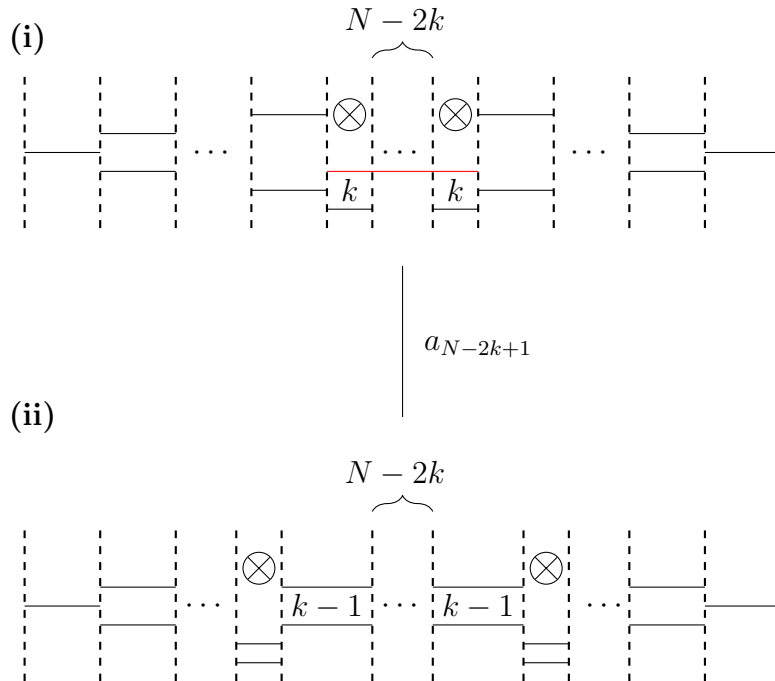

Figure 20: The first Kraft-Procesi transition on the theory given by (65).

of nodes in the middle bouquet is $(N - 1 - 2k + 2)$. We obtain the result below.

$$
\begin{array}{c}
\overset{1}{\circ} \\
\underset{k-1}{\nearwarrow} \quad \underset{k-1}{\nwarrow} \\
\underset{1}{\circ} - \underset{2}{\circ} - \cdots - \underset{k-1}{\circ} \underset{k-1}{\nearrow} \cdots \underset{k-1}{\circ} - \underset{k-1}{\circ} - \cdots - \underset{2}{\circ} - \underset{1}{\circ} \\
\underbrace{\qquad\qquad\qquad\qquad\qquad\qquad}_{N-1}
\end{array}
\tag{66}
$$

We have added a $U(1)$ gauge node in (66) in order to balance the left- and right-most $U(k-1)$ gauge nodes. This quiver clearly admits the subtraction of a a_{N-2k+3} elementary slice and we can observe that the quiver that will result will be identical to (66) except the two nodes connected to the top $U(1)$ will be $U(k-2)$ and we will have $(N - 2k + 5)$ $U(k-2)$ gauge nodes in the centre. We will be able to keep subtracting slices of the form a_{N-2k+m} (for odd m) until we reach $m = 2k - 1$ and we subtract the final slice a_{N-1}. The Hasse diagram that results, given in [15], can be written as below.

$$
\begin{array}{c}
\bullet \; k(N-k) \\
\Big| \; a_{N-2k+1} \\
\bullet \; (k-1)(N-(k-1)) \\
\Big| \; a_{N-2k+3} \\
\bullet \; (k-2)(N-(k-2)) \\
\vdots \\
\bullet \; N-1 \\
\Big| \; a_{N-1} \\
\bullet
\end{array}
\tag{67}
$$

Now, (67) is the Hasse diagram for the Coulomb branch of the theory. We can now use Hasse diagram inversion to find the Hasse diagram of the Higgs branch. Flipping (67) vertically and changing the nilpotent orbits to their associated Kleinian singularities, we find the Hasse diagram of the Higgs branch in (73).

$$
\begin{array}{c}
\bullet \\
\Big| \; A_{N-1} \\
\bullet \\
\vdots \\
\bullet \\
\Big| \; A_{N-2k+3} \\
\bullet \\
\Big| \; A_{N-2k+1} \\
\bullet
\end{array}
\tag{68}
$$

55

Now we can find the Hasse diagram of the full moduli space by taking the Hasse diagram of the Coulomb branch and, beginning with the lowest node in the diagram, we follow the following prescription: *for the kth node from the bottom of the Coulomb branch Hasse diagram, add to it the Hasse diagram corresponding to the transverse slice in the Higgs branch between the lowest node and the $(N-k)^{th}$ node.*

For the case of $U(k)$ with N flavours, we end up with the Hasse diagram given in (69).

$$(69)$$
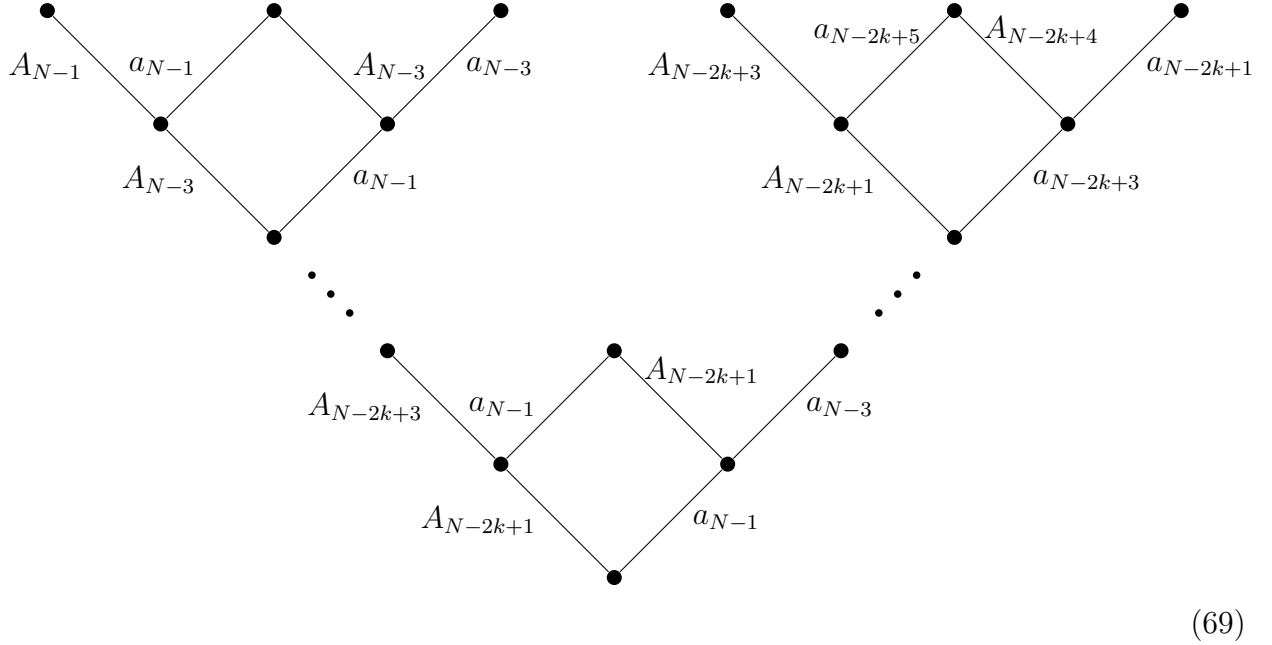
Consider that we can also verify our use of quiver subtraction here by performing explicit Kraft-Procesi transitions on the brane system in Fig. 19 ***iv***. Recalling Fig. 6 we see that the $(N-2k+2)$ D5-branes that are either side of the two NS5-branes in Fig. 19 ***iv*** give rise to an a_{N-2k+1} singularity which is precisely what we see using quiver subtraction.

### 0.8.2. $SU(K)$ with N Flavours. In this case our magnetic quiver is

$$(70)$$
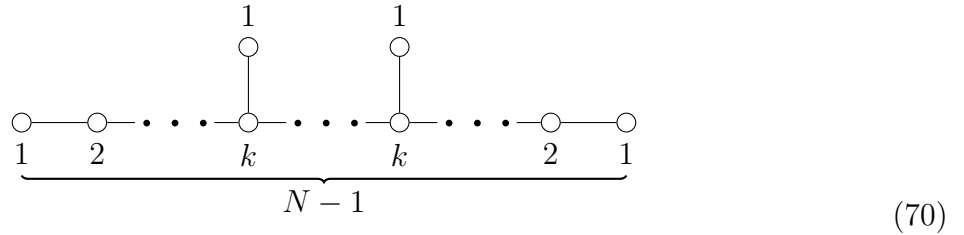
From the perspective of quiver subtraction, we can clearly remove a d_{N-2k+4} slice. The quiver we are left with is (71). Clearly from here we will follow the same path we did in the $U(k)$ case. We can subtract a further a_{N-2k+5} slice since the number of nodes in the middle
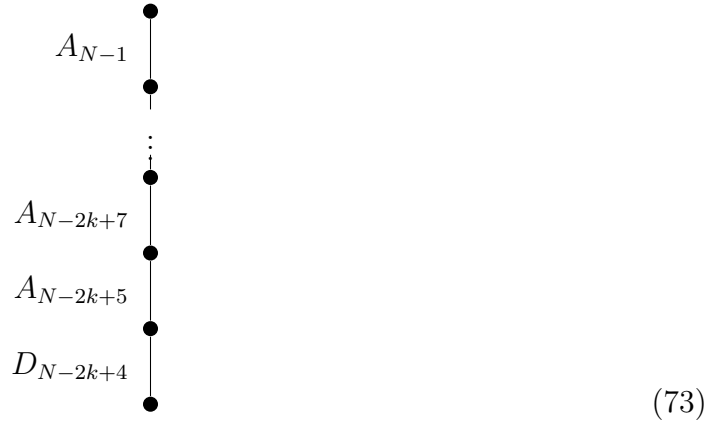
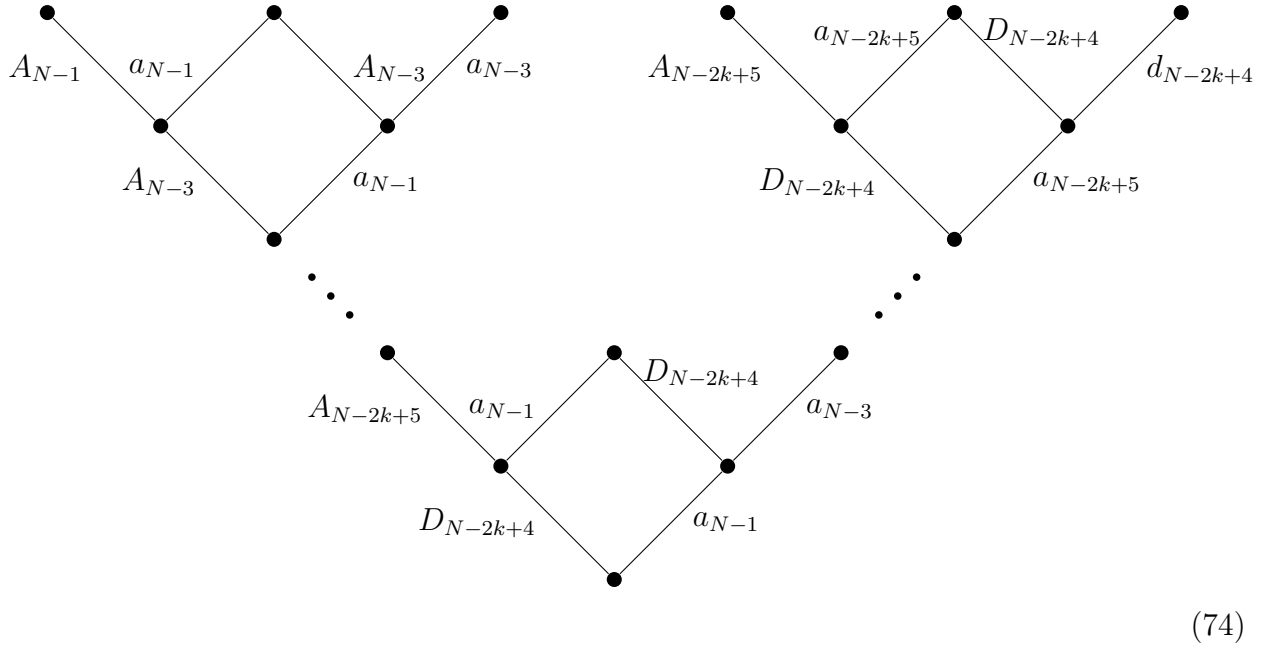bouquet is $(N - 1 - 2(k - 2) + 2)$.

$$\tag{71}$$
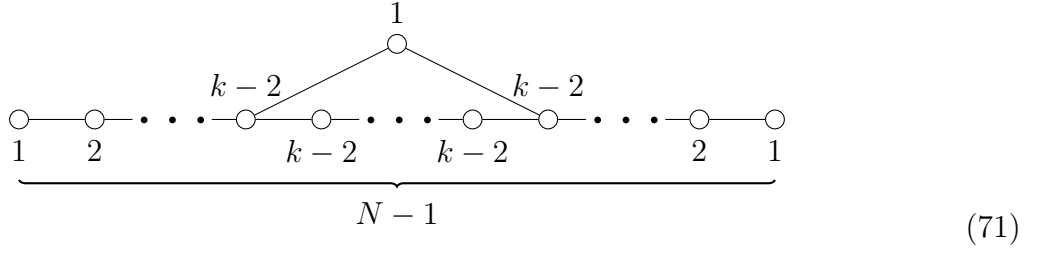
From here we obtain the same pattern of subtractions we had in the $U(k)$ case and the Hasse diagram for the Coulomb branch of the magnetic quiver (70) is (72).


$$\tag{72}$$
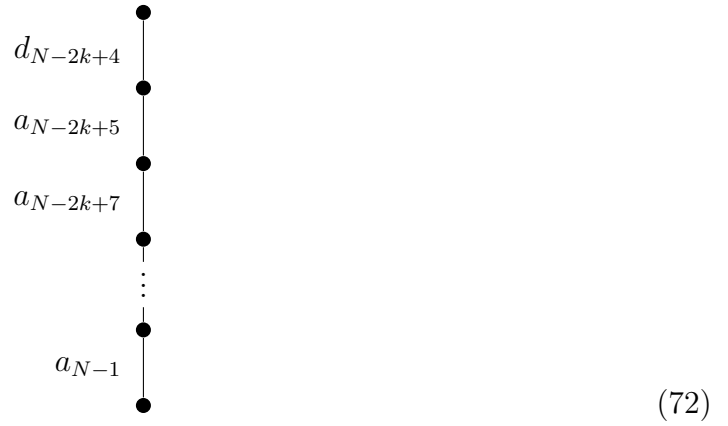
Now we can use Hasse diagram inversion since this only contains nilpotent orbits corresponding to A-type and D-type algebras. Performing a vertical inversion and relabelling the nilpotent orbits to Kleinian singularities we obtain (78), the Hasse diagram for the Coulomb branch of the theory.

$$\tag{73}$$

Now we find the Hasse diagram of the full moduli space to be (74).

$$
\begin{array}{c}
\text{(Hasse diagram)}
\end{array}
$$

with edge labels A_{N-1}, a_{N-1}, A_{N-3}, a_{N-3}, A_{N-3}, a_{N-1} on the left top; a_{N-2k+5}, D_{N-2k+4}, d_{N-2k+4}, A_{N-2k+5}, D_{N-2k+4}, a_{N-2k+5} on the right top; A_{N-2k+5}, a_{N-1}, D_{N-2k+4}, a_{N-3}, D_{N-2k+4}, a_{N-1} at the bottom.
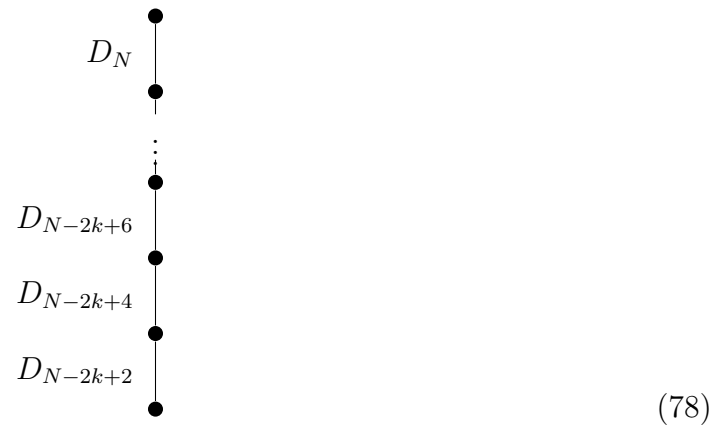
$$\tag{74}$$

0.8.3. $Sp(K)$ with $SO(2N)$ Flavour Group.

Again consulting [15], we find that the magnetic quiver for the theory of $Sp(k)$ gauge group with $SO(2N)$ flavour group, where $N \geq 2k$, is (75). Clearly we can subtract a slice d_{N-2k+2} from this, leaving us with the quiver (76).


$$\tag{75}$$

$$\tag{76}$$
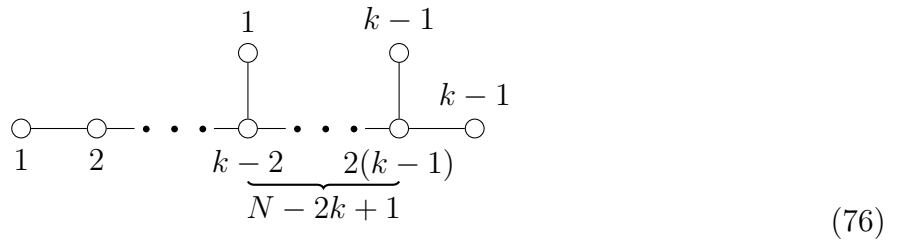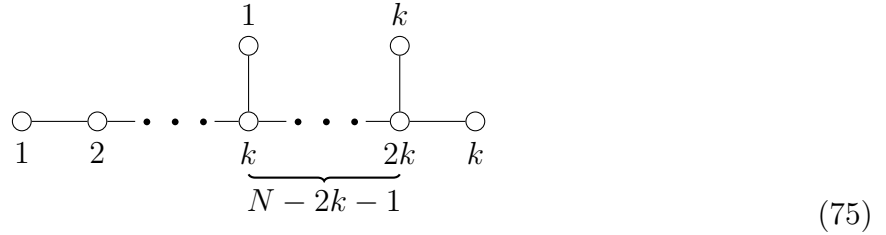
Clearly, we can continue to subtract d-type minimal slices and we generate the Hasse diagram (77).

$$
\begin{array}{r}
\bullet \\
d_{N-2k+2} \quad | \\
\bullet \\
d_{N-2k+4} \quad | \\
\bullet \\
d_{N-2k+6} \quad | \\
\bullet \\
\vdots \\
\bullet \\
d_N \quad | \\
\bullet
\end{array}
\tag{77}
$$

Again we can simply invert this to obtain the Hasse diagram for the Higgs branch of the theory of $Sp(k)$ with $SO(2N)$ flavour group (78).

$$
\begin{array}{r}
\bullet \\
D_N \quad | \\
\bullet \\
\vdots \\
\bullet \\
D_{N-2k+6} \quad | \\
\bullet \\
D_{N-2k+4} \quad | \\
\bullet \\
D_{N-2k+2} \quad | \\
\bullet
\end{array}
\tag{78}
$$

59

Now it is again a simple matter to combine these to obtain the Hasse diagram for the full moduli space, (79).


$$\tag{79}$$
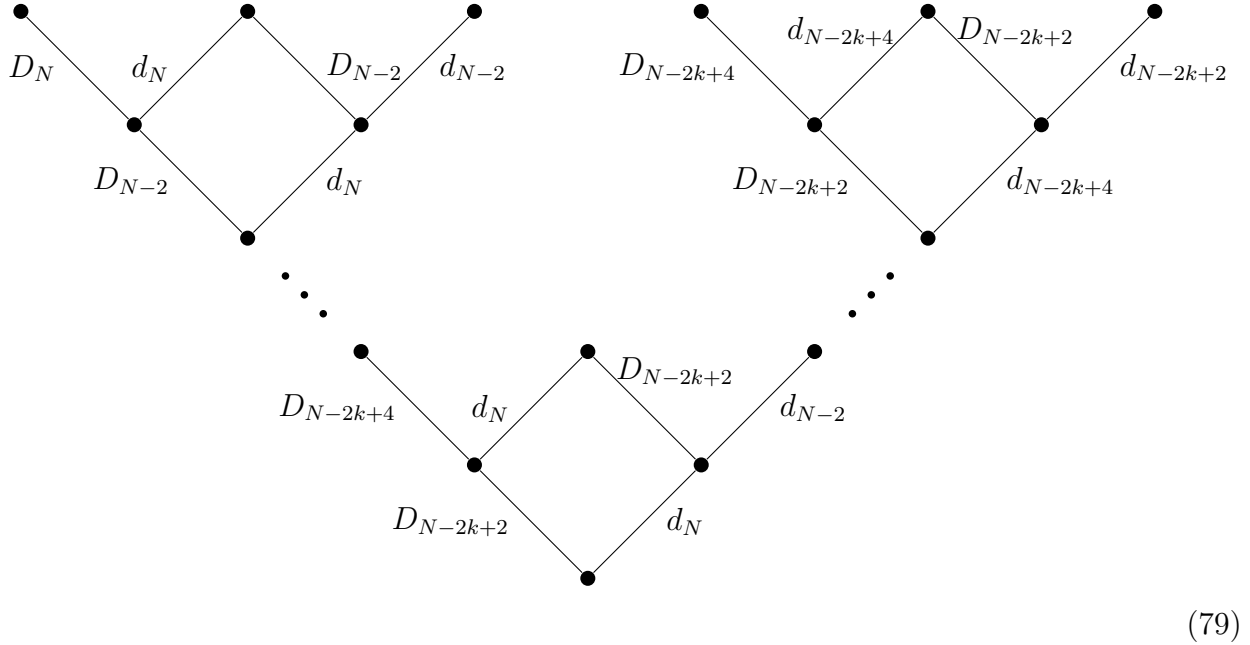
0.9. Multiple Subtractions & Decorations. Recent work [26], [39] has considered quivers containing Hplets in the adjoint representation of the gauge group (termed 'adjoint matter'). One of the main features of quivers of this type is the failure of the standard Coulomb branch global symmetry algorithm to find the full Coulomb branch global symmetry - a new algorithm has been proposed that finds the full symmetry group under this enhancement [26]. So too do complications occur for the quiver subtraction algorithm. When quiver addition is performed on them the ranks of the gauge nodes with adjoint Hplets reduce by one, and this has to be accounted for when going the other way with quiver subtraction by introducing the idea of a *decorated* quiver.

We'll now consider an example of the decoration. Take the quiver (80), studied in [26].

$$\tag{80}$$
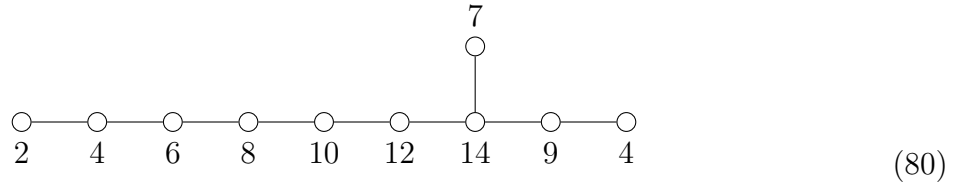
We see here that the only elementary slice that we can subtract is e_8. However, this is not as straightforward as it might appear. In reality, we can think of this quiver as having two decorated affine e_8 slices that have been added to an original quiver with adjoint matter. Subtracting an e_8 slice corresponds to contracting one of these added e_8 loops - we have a

choice as to which we contract and the decoration remains after the subtraction.

(81)
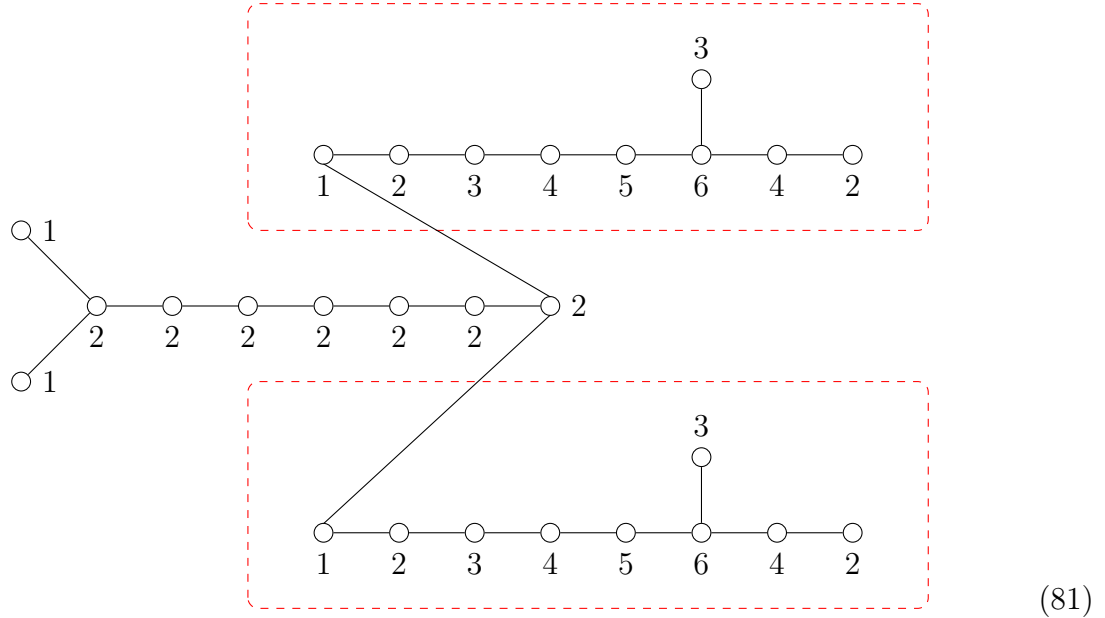
We see this at work in (81). The decorations are the red dashed lines around the e_8 slices. Performing an e_8 subtraction corresponds to contracting one of the decorated loops to a decorated $U(1)$ gauge node with adjoint loop (adjoint loops on $U(1)$ gauge nodes are trivial and their presence makes no difference to the physics, we can choose to include the adjoint loop to remind us that when we contract the other e_8 slice we'll end up increasing the rank of the node and the adjoint loop will no longer be trivial).

Contracting both decorated loops in (81) leaves us with the quiver (82). The two decorated $U(1)$ gauge nodes are conjectured to be equivalent to a single $U(2)$ gauge node with an adjoint Hplet. The quiver that results has Coulomb branch variety $d_9/\mathbb{Z}_2$ and has been studied in [26] - the Hasse diagram for this quiver can be found in Fig. 33.


(82)
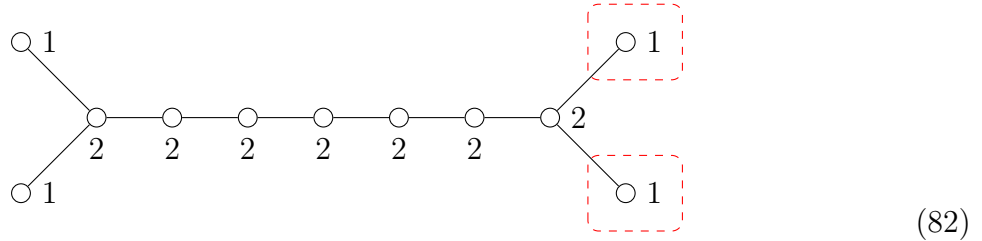
This might seem unconvincing if we remember that the rationale for quiver subtraction originally came from Kraft-Procesi transitions on brane systems and that such physical constructions played no argument in our reasoning. In the following we will do exactly this and check it using $6d$ brane systems.

0.9.1. HASSE DIAGRAMS FOR QUIVERS FROM ADJOINT MATTER. In this section we shall present Hasse diagrams calculated from the quivers studied in [26]. These are computations that have not been performed before on this particular set of quivers. At this time, further work to interpret and study these diagrams is difficult owing to the lack of understanding of the quivers the quivers the diagrams derive from. The complexity (high-rank) of these quivers means that only the first few terms in their Hilbert series can be calculated and the use of a somewhat novel technique - quiver decoration - means that there is at present no way to completely determine whether they are indeed the correct Hasse diagrams for the quivers in question. We have tried to amerliorate this by finding brane computations where possible to show that quiver subtraction does indeed provide the same answers as we would expect through Type IIA considerations. These brane methods have only been used for a particular set of the quivers in [26], however, and do not extend to every Hasse diagram presented.

In this section we will also use the term 'maximum height' to mean the longest path we can follow through the Hasse diagram using the partial ordering. It might be interesting to study this further by considering how it changes for different theories.

0.9.1.1. $\overline{\text{N.MIN } B_n}$, $n \geq 4$. We first consider the quiver given by (83). This has as its Coulomb branch the closure of the next-to-minimal nilpotent orbit of the algebra B_n, given by the Hasse diagram (84). The brane system corresponding to this is shown in Fig. (45) (*iii*). This quiver is the basis for the additions (and subsequent Hasse diagrams) given in Figs. (21) - (29). Broadly, as shown in [26], this causes a global symmetry enhancement from $SO(2n)$ to $SO(2n + 1)$ in the Coulomb branch. This is easily calculable given the enhanced global symmetry algorithm in [26], and we see agreement when we consider that the elementary slice(s) next to the lowest node in a Hasse diagram form a subset of the non-Abelian part of the global symmetry of the Coulomb branch.

$$(83)$$

$$(84)$$
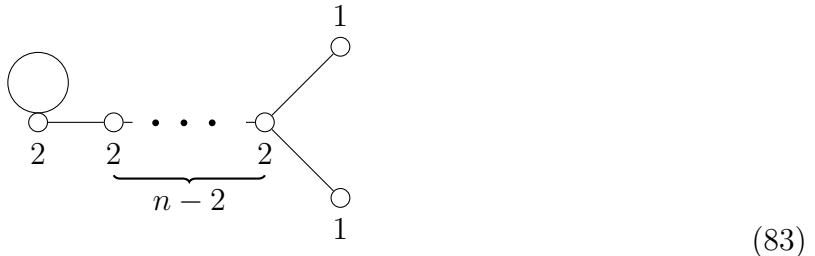
For the Hasse diagrams in Figs. 21 and 22, we can construct the quivers that generate them from adding the quivers corresponding to the usual minimal slices to the existing nodes of (83) twice. We end up with an enhancement from a D-type global symmetry to a B-type global symmetry for the Coulomb branch. These enhancements are explicitly observed in the lowest slices of the Hasse diagrams in Fig. 21 and 22 and we have reproduced the brane systems for the e_8 additions in Figs. 45 and 46.

In Fig. 21, following the procedure in [26], we have taken $n = 4$ for the Hasse diagram corresponding to a_k slice additions to (83), $n = 6$ for the e_6 addition, $n = 7$ for the e_7 addition and $n = 9$ for the e_8 addition. For the d_k addition we have $n = k + 1$.

We give a brane construction for the case of $SO(19)$ global symmetry in Fig. 45 where we explicitly see how we can construct the associated Hasse diagram using the freezing of branes.

Added Slice	a_3	$a_k,\ k \geq 4$	$d_k,\ k \geq 4$	e_6	e_7	e_8
Hasse Diagram	a_3 a_3 a_1 b_4	e_7 a_k a_{k-6} e_6 a_k a_1 a_{k-4} b_5	d_k d_k a_1 b_{k+1}	e_6 e_6 a_1 b_6	e_7 e_7 a_1 e_8 a_1 b_7	e_8 e_8 a_1 b_9
EGS	$SO(9)$	$SO(9) \times U(k-3)$	$SO(2k+3)$	$SO(13) \times U(1)$	$SO(15) \times SU(2)$	$SO(19)$

Figure 21: The Hasse diagrams generated from applying the quiver subtraction algorithm to the quivers given in Table 4 of [26]. We provide the constraints on the added slices in the first row and the enhanced global symmetry of the Coulomb branch in the last row. The original quiver the slices have been added to is given in (83). We give the explicit brane construction and computation of the Hasse diagram found from e_8 subtraction in Fig. 45 and the associated magnetic quivers in (102).

0.9.1.2. $\overline{\text{N.MIN } B_3}$. This case involves taking the $n = 3$ case of the quiver given in (83), which we show in (85). In the Hasse diagrams of Fig. 22 we have added the given affine quivers to either of the $U(1)$ gauge nodes of (85) (either can be used since they are equivalent under a $\mathbb{Z}_2$ action).

In Fig. 46 we have reproduced exactly the Hasse diagram that exists in Fig. 22 for the addition of an e_8 slice, we can also see that the skeleton of the Hasse diagram is the same for the cases of a_k addition and e_7 addition in Fig. 22, as well as for c_k addition in Fig. 23. Similarly, the structure of the Hasse digrams for b_k addition and d_k addition are identical. Consulting (86), we can identify the elementary slices in the Hasse diagrams next to the lowest nodes in Figs. 22 and 23 to match clearly with what we'd expect from global symmetry calculations in [26].
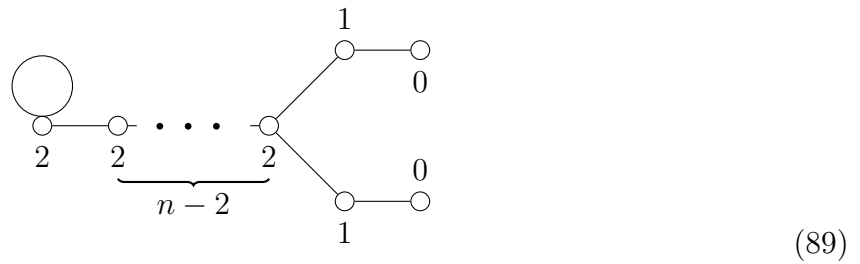

$$(85)$$

$$(86)$$

0.9.1.3. $\overline{\text{N.MIN } B_2}$. We here consider another special case of the next-to-minimal nilpotent orbit of the algebra B_n, now taking $n = 2$. In this case we have the quiver given in (87) with the corresponding Hasse diagram (88). In this case, we are adding slices to empty nodes of rank-0 either side of the rank-1 nodes in (87). For this to work (i.e. for us to be able to add nodes to each of the rank-1 nodes simultaneously) we are restricted to the slices whose quivers have a reflection symmetry - a_n, d_n, e_7 and e_6. The Hasse diagrams corresponding to the quivers we obtain after these additions are given in Fig. 24.

$$(87)$$

$$(88)$$

0.9.1.4. $\overline{\text{N.MIN } B_n}$, $\quad n \geq 3$: EMPTY NODE ADDITION. The last case corresponding to addition of minimal slices onto (83) concerns the addition onto rank-0 nodes that we imagine are attached to the rank-1 nodes. For the case of $n \geq 3$ we no longer have to stipulate that our added quivers have a reflection symmetry and so the full set of Hasse diagrams corresponding to these additions are given in Figs. 25 and 26.

Again, we can be comforted that the elementary slices of the Hasse diagram next to the lowest node do indeed give the non-Abelian part of the enhanced global symmetry of the Coulomb branch. Of course, this on its own is not enough to show that the Hasse diagrams are completely correct (further subtleties of the quiver decoration are likely to arise in the near future).

$$
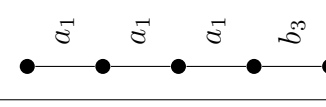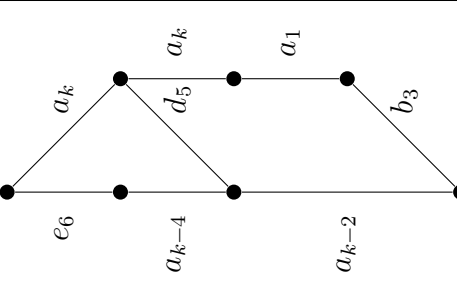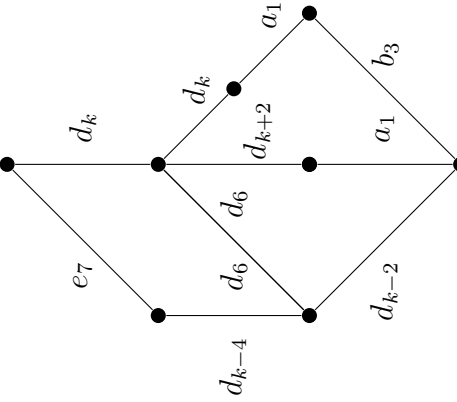\tag{89}
$$

We've shown this empty-node setup explicitly in (89).

Figure 22: The Hasse diagrams generated from applying the quiver subtraction algorithm to the quivers given in Table 5 of [26]. We provide the constraints on the added slices in the first row and the enhanced global symmetry of the Coulomb branch in the last row. The original quiver the slices have been added to is given in (85). We give the explicit brane construction and computation of the Hasse diagram found from e_8 subtraction in Fig. 46 and the associated magnetic quivers in (104).

Added Slice	$b_k, \quad k \geq 3$	$c_k, \quad k \geq 2$	f_4	g_2
Hasse Diagram				
EGS	$SO(7) \times SU(2) \times SO(2k-3)$	$SO(7) \times Sp(k-1)$	$SO(7) \times Sp(3)$	$SO(7) \times SU(2)$

Figure 23: The Hasse diagrams generated from applying the quiver subtraction algorithm to the quivers given in Table 6 of [26]. We provide the constraints on the added slices in the first row and the enhanced global symmetry of the Coulomb branch in the last row. The original quiver the slices have been added to is given in (86).
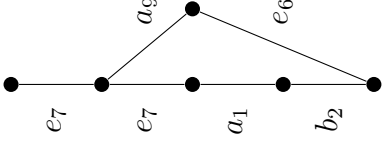
Added Slice	a_1	$a_k, \quad k \geq 2$	$d_k, \quad k \geq 4$	e_6	e_7
Hasse Diagram					
EGS	$SO(5) \times SU(2)$	$SO(5) \times SU(2) \times U(k-1)$	$SO(5) \times U(k)$	$SO(5) \times SO(10) \times U(1)$	$SO(5) \times E_6 \times U(1)$

Figure 24: The Hasse diagrams generated from applying the quiver subtraction algorithm to the quivers given in Table 7 of [26]. We provide the constraints on the added slices in the first row and the enhanced global symmetry of the Coulomb branch in the last row. The original quiver the slices have been added to is given in (88).

Added Slice	a_k, $k \geq 1$, $n \geq 3$	d_k, $k \geq 4$	e_6, $n \geq 3$	e_7, $n \geq 3$	e_8, $n \geq 3$
Hasse Diagram					
EGS	$SU(k+1) \times SO(2n+1)$	$SO(2k) \times SO(2n+1)$	$E_6 \times SO(2n+1)$	$E_7 \times SO(2n+1)$	$E_8 \times SO(2n+1)$

Figure 25: The Hasse diagrams generated from applying the quiver subtraction algorithm to the quivers given in Table 8 of [26]. We provide the constraints on the added slices in the first row and the enhanced global symmetry of the Coulomb branch in the last row. The original quiver the slices have been added to is given in (83).
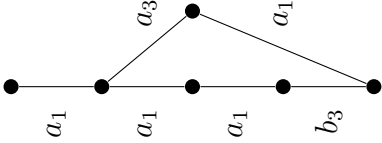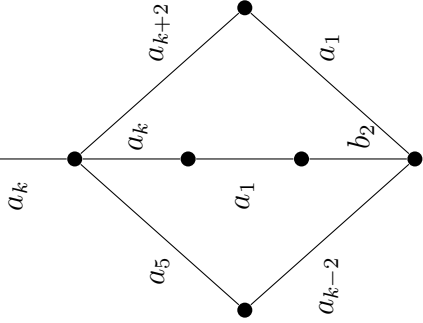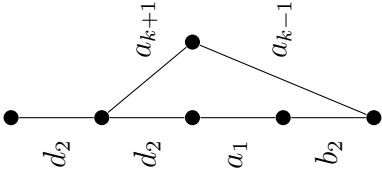
Added Slice	$b_k,\ k \geq 3,\ n \geq 3$	$c_k,\ k \geq 2,\ n \geq 3$	$f_4,\ n \geq 3$	$g_2,\ n \geq 3$
Hasse Diagram	diagram with labels b_{n+k-1}, d_{n+3}, b_k, b_{k-2}, a_1, d_{n+1}, b_k, a_1, b_n, b_k	diagram with labels b_{n+1}, c_k, c_{k-1}, d_{n+1}, c_k, a_1, b_n, c_k	diagram with labels d_{n+7}, f_4, f_4, c_3, d_{n+1}, f_4, a_1, b_{n+3}, f_4	diagram with labels g_2, g_2, a_1, d_{n+1}, g_2, b_2
EGS	$SO(2k+1) \times SO(2n+1)$	$Sp(k) \times SO(2n+1)$	$F_4 \times SO(2n+1)$	$G_2 \times SO(2n+1)$

Figure 26: The Hasse diagrams generated from applying the quiver subtraction algorithm to the quivers given in Table 9 of [26]. We provide the constraints on the added slices in the first row and the enhanced global symmetry of the Coulomb branch in the last row. The original quiver the slices have been added to is given in (83).
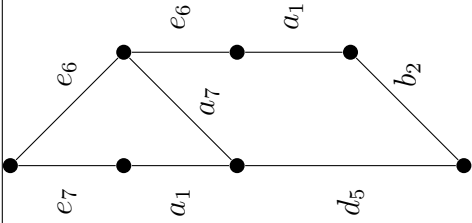
0.9.1.5. $\overline{\text{N.MIN } B_n}$, $\quad n \geq 3$: ADDITIONAL CASE. In this additional case we follow [26] in their consideration of the quiver (90). In this case we have added an A_1 slice such that the original two $U(1)$ legs have been combined into one with two connecting edges. For this quiver we get the Hasse diagram (91). This is simple to see via quiver subtraction - recall that an A_1 slice consists of two rank-1 nodes with two edges connecting them. We can subtract this from the $U(2)$ and $U(1)$ nodes connected by two edges in (90), the $U(1)$ node is removed and we have to add a further $U(1)$ node to the new rightmost $U(2)$ node to preserve balance.

$$\tag{90}$$

$$\tag{91}$$

In this case, the global symmetry enhancement of the Coulomb branch is now from $SU(n) \times U(1)$ to $SO(2n+1)$. For quiver addition in this case, we will be adding the quivers corresponding to minimal slices on to the leftmost nodes of (90).

As mentioned in [26], we can add many more slices to 83 and consider the various ways we can remove the adjoint Hplet through addirion of minimal slices. This would be an interesting prospect for further work, and it would be interesting to find the Hasse diagrams in these cases.

Figure 27: The Hasse diagrams generated from applying the quiver subtraction algorithm to the quivers given in Table 10 of [26]. We provide the constraints on the added slices in the first row and the enhanced global symmetry of the Coulomb branch in the last row. The original quiver the slices have been added to is given in (90).

Figure 28: The Hasse diagrams generated from applying the quiver subtraction algorithm to the quivers given in Table 10 of [26]. We provide the constraints on the added slices in the first row and the enhanced global symmetry of the Coulomb branch in the last row. The original quiver the slices have been added to is given in (90).

Added Slice	$b_k, \ k \geq 3$	$c_k, \ k \geq 2$	f_4	g_2
Hasse Diagram				
EGS	$SO(2k+1) \times SO(2n+1)$	$Sp(k) \times SO(2n+1)$	$F_4 \times SO(2n+1)$	$G_2 \times SO(2n+1)$

Figure 29: The Hasse diagrams generated from applying the quiver subtraction algorithm to the quivers given in Table 11 of [26]. We provide the constraints on the added slices in the first row and the enhanced global symmetry of the Coulomb branch in the last row. The original quiver the slices have been added to is given in (90).

75

0.9.1.6. $\overline{\text{S.REG } G_2}$, $\quad n \geq 4$. In this section we will consider the Hasse diagrams of quivers obtained from additions of minimal slices to the sub-regular nilpotent orbit of G_2. The quiver we begin with is given in (92). The corresponding Hasse diagram is given in (93), where we have used the non-normal slice m.

$$\text{(92)}$$

$$\text{(93)}$$

In this case we have an enhancement of the global symmetry of the Coulomb branch from $SU(3)$ to G_2. In Figs. 30 and 31 we have added minimal slices to the rank-1 and rank-2 nodes of (92). Whereas in the previous cases in this section it required the subtraction of two previously-added slices to reach the original quiver (92), the fact that the node with the adjoint Hplet is now third-rank means that we'll have to subtract the added slices three times. Hence the maximum height of the Hasse diagrams are now seven nodes, taking into account the two required subtractions of previously-added slices and the three slices making the Hasse diagram of the Higgs branch of (92). Recall by 'maximum height' we mean the longest path we can follow through the Hasse diagram obeying the partial ordering. In Figs. 32, 33 and 34 we will be adding the minimal slices to the rank-2 node of (92) and an empty rank-0 node we will imagine attached to it, as shown in (94). Again we find agreement between the enhanced global symmetry and the lowest slices of the calculated Hasse diagrams.

$$\text{(94)}$$

Added Slice	$a_k, \ k \geq 1$	$d_k, \ k \geq 4$	e_6	e_7	e_8
Hasse Diagram	(Hasse diagram with labels a_k, e_7, a_k, e_6, a_{k-6}, a_1, a_{k-4}, b_4, a_k, d_4, m, a_{k-2}, A_1)	(Hasse diagram with labels d_k, e_8, d_k, e_7, d_{k-6}, a_1, d_k, a_1, d_{k-4}, b_{k+1}, d_4, b_5, m, a_1, d_{k-2}, A_1)	(Hasse diagram with labels e_6, e_6, e_6, b_6, d_4, a_1, m, a_5, A_1)	(Hasse diagram with labels e_7, e_7, e_7, a_1, a_1, b_7, d_4, m, d_6, A_1)	(Hasse diagram with labels e_8, e_8, e_8, a_1, d_4, b_8, m, e_7, A_1)
EGS	$G_2 \times U(1)^\ell \times SU(k-1)$	$G_2 \times SU(2) \times SO(2k-4)$	$G_2 \times SU(6)$	$G_2 \times SO(12)$	$G_2 \times E_7$

Figure 30: The Hasse diagrams generated from applying the quiver subtraction algorithm to the quivers given in Table 12 of [26]. We provide the constraints on the added slices in the first row and the enhanced global symmetry of the Coulomb branch in the last row. The original quiver the slices have been added to is given in (92). We give the explicit brane construction and computation of the Hasse diagram found from e_8 subtraction in Fig. 47 and the associated magnetic quivers in (109).

Added Slice	$b_k, \; k \geq 3$	$c_k, \; k \geq 2$	f_4	g_2
EGS	$G_2 \times SU(2) \times SO(2k-3)$	$G_2 \times Sp(k-1)$	$G_2 \times Sp(3)$	$G_2 \times SU(2)$
Hasse Diagram				

Figure 31: The Hasse diagrams generated from applying the quiver subtraction algorithm to the quivers given in Table 13 of [26]. We provide the constraints on the added slices in the first row and the enhanced global symmetry of the Coulomb branch in the last row. The original quiver the slices have been added to is given in (92).

Added Slice		
$a_k, \quad k \geq 1$	$d_k, \quad k \geq 4$	e_6

Hasse Diagram for column 1 (EGS $G_2 \times SU(k+1)$), with edge labels: e_6, a_k, a_{k-4}, d_5, a_k, a_{k-2}, a_1, b_3, a_k, A_1, m, g_2.

Hasse Diagram for column 2 (EGS $G_2 \times SO(2k)$), with edge labels: d_k, e_7, d_{k-4}, d_6, d_{k+2}, a_1, d_{k-2}, d_k, d_k, a_1, b_3, d_k, A_1, m, g_2, d_k.

Hasse Diagram for column 3 (EGS $G_2 \times E_6$), with edge labels: e_6, e_6, e_6, d_7, a_1, e_6, a_5, b_3, A_1, e_6, m, g_2.

EGS		
$G_2 \times SU(k+1)$	$G_2 \times SO(2k)$	$G_2 \times E_6$

Figure 32: The Hasse diagrams generated from applying the quiver subtraction algorithm to the quivers given in Table 14 of [26]. We provide the constraints on the added slices in the first row and the enhanced global symmetry of the Coulomb branch in the last row. The original quiver the slices have been added to is given in (92).
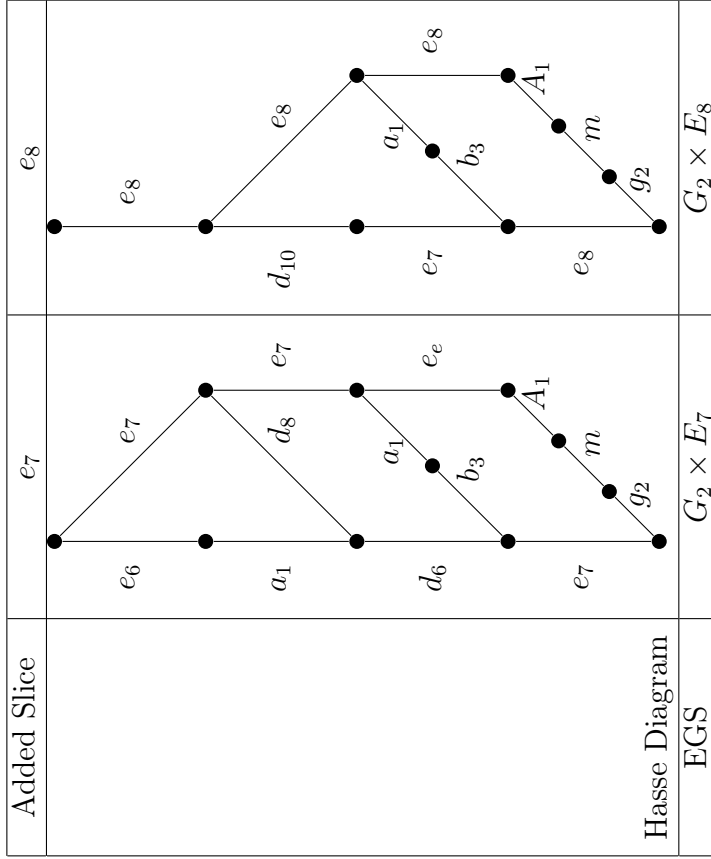
Figure 33: The Hasse diagrams generated from applying the quiver subtraction algorithm to the quivers given in Table 14 of [26]. We provide the constraints on the added slices in the first row and the enhanced global symmetry of the Coulomb branch in the last row. The original quiver the slices have been added to is given in (92). We give the explicit brane construction and computation of the Hasse diagram found from e_8 subtraction in Fig. 48 and the associated magnetic quivers in (110).
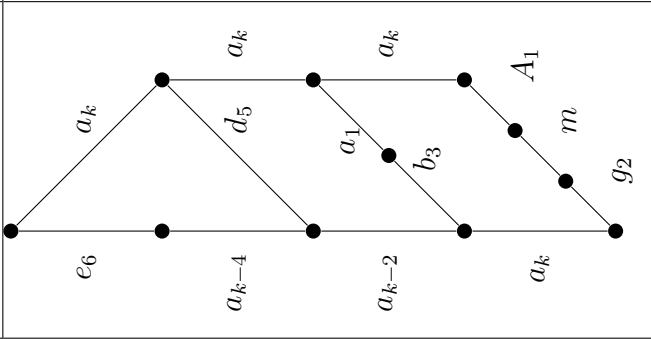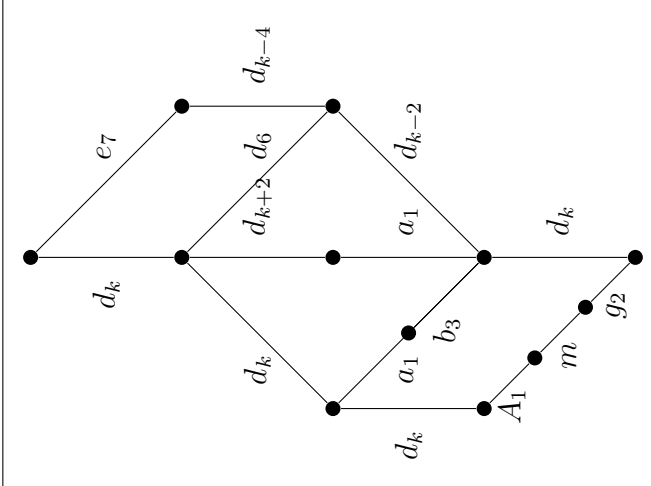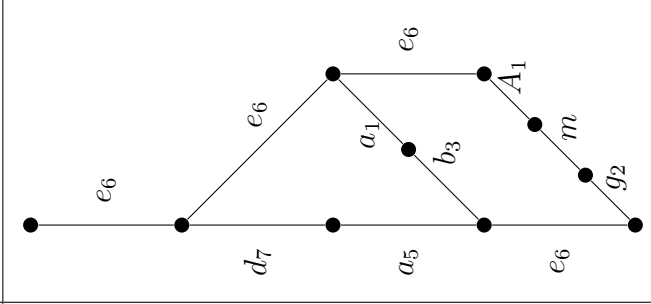
Figure 34: The Hasse diagrams generated from applying the quiver subtraction algorithm to the quivers given in Table 15 of [26]. We provide the constraints on the added slices in the first row and the enhanced global symmetry of the Coulomb branch in the last row. The original quiver the slices have been added to is given in (92).

0.9.1.7. $\overline{\text{N.MIN } D_n}$, $n \geq 3$. In this section we will consider the theory given by (95), which is the next-to-minimal nilpotent orbit of the algebra D_n. In this case we have the Hasse diagram of (95) given by (96) and a gauge enhancement of the Coulomb branch global symmetry from $SO(2n-1)$ to $SO(2n)$.

$$\tag{95}$$

$$\tag{96}$$

We must also be wary of the fact that the cases of $n \geq 3$ and $n = 2$ must be treated separately since we are now dealing with a non-simply laced quiver. The cases that treat $n \geq 3$ are given in Figs. 35, 36 and 37, while we consider the $n = 2$ case in Figs. 38 and 39. Note that in the $n = 2$ case we have a Coulomb branch global symmetry gauge enhancement to $SU(2) \times SU(2)$ now. the quiver and Hasse diagram for the $n = 2$ case are given in () and () respectively.

$$\tag{97}$$

$$\tag{98}$$

Of course, we now consider whether the symmetry enhancement is borne by the Hasse diagrams themselves. In the cases of Figs. 35 - 37 we clearly have agreement between the Coulomb global branch symmetry enhancement and the lowest slices on the Hasse diagrams. In the cases of Figs. 38 and 39 the reader may worry that the d_2 slices do not show the $SU(2) \times SU(2)$ global symmetry that we wish. However, we should recall that the $d_2 = a_1 \cup a_1$ and hence we indeed see the global symmetry enhancement at the level of the Hasse diagram.
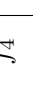
Added Slice		
Hasse Diagram	b_k, b_k, b_k, a_1, d_{k+2}	f_4, f_4, f_4, a_1, d_6
EGS	$SO(2k+4)$	$SO(12)$

Figure 35: The Hasse diagrams generated from applying the quiver subtraction algorithm to the quivers given in Table 16 of [26]. We provide the constraints on the added slices in the first row and the enhanced global symmetry of the Coulomb branch in the last row. The original quiver the slices have been added to is given in (95).

Added Slice	$a_k,\ k \geq 1,\ n \geq 3$	$d_k,\ k \geq 4$	$e_6,\ n \geq 3$	$e_7,\ n \geq 3$	$e_8,\ n \geq 3$
Hasse Diagram					
EGS	$SU(k+1) \times SO(2n)$	$SO(2k) \times SO(2n)$	$E_6 \times SO(2n)$	$E_7 \times SO(2n)$	$E_8 \times SO(2n)$

Figure 36: The Hasse diagrams generated from applying the quiver subtraction algorithm to the quivers given in Table 17 of [26]. We provide the constraints on the added slices in the first row and the enhanced global symmetry of the Coulomb branch in the last row. The original quiver the slices have been added to is given in (95).

84

Added Slice	$b_k,\ k \geq 3,\ n \geq 3$	$c_k,\ k \geq 2,\ n \geq 3$	$f_4,\ n \geq 3$	$g_2,\ n \geq 3$
Hasse Diagram				
EGS	$SO(2k+1) \times SO(2n)$	$Sp(k) \times SO(2n)$	$F_4 \times SO(2n)$	$G_2 \times SO(2n)$

Figure 37: The Hasse diagrams generated from applying the quiver subtraction algorithm to the quivers given in Table 18 of [26]. We provide the constraints on the added slices in the first row and the enhanced global symmetry of the Coulomb branch in the last row. The original quiver the slices have been added to is given in (95).

Added Slice	b_k, $k \geq 3$	c_k, $k \geq 2$	f_4	a_{2k-1}, $k \geq 3$
Hasse Diagram	(Hasse diagram with edges f_4, b_k, d_{k-2}, c_3, b_k, a_1, d_2)	(Hasse diagram with edges d_2, a_{2j+3}, $a_{2k-2j+3}$, d_2, c_{k-j-1}, a_1, c_{j-1}, c_{k-j}, d_2, c_j)	(Hasse diagram with edges f_4, e_6, a_1, c_4, f_4, a_1, b_4, d_2)	(Hasse diagram with edges a_{2k-1}, a_{2k-1}, c_{k+1}, a_1, c_k, d_2)
EGS	$SU(2)^2 \times SO(2k)$	$SU(2)^2 \times Sp(j) \times Sp(k-j)$	$SU(2)^2 \times SO(9)$	$SU(2)^2 \times Sp(k)$

Figure 38: The Hasse diagrams generated from applying the quiver subtraction algorithm to the quivers given in Table 19 of [26]. We provide the constraints on the added slices in the first row and the enhanced global symmetry of the Coulomb branch in the last row. The original quiver the slices have been added to is given in (97).

Added Slice	$d_{k+1}, \quad k \geq 2$	e_6
Hasse Diagram	*(diagram with labels f_4, d_{k+1}, b_{k-2}, c_3, d_{2k+1}, a_1, b_k, d_2)*	*(diagram with labels e_6, e_6, c_5, a_1, f_4, d_2)*
EGS	$SU(2)^2 \times SO(2k+1)$	$SU(2)^2 \times F_4$

Figure 39: The Hasse diagrams generated from applying the quiver subtraction algorithm to the quivers given in Table 19 of [26]. We provide the constraints on the added slices in the first row and the enhanced global symmetry of the Coulomb branch in the last row. The original quiver the slices have been added to is given in (97).

87

0.9.1.8. d_4/S_4. The final cases we consider consist of the quiver with Coulomb branch $\frac{d_4}{S_4}$, given by the quiver (99).

$$
\begin{array}{cc}
\bigcirc & \\
\circ\!-\!\!-\!\!-\!\circ & \\
4 \quad 2 &
\end{array}
\tag{99}
$$

Although the Hasse diagram for (99) is not given in [26], we can calculate it here. It follows from the brane system that we will construct in 6d.

The entire Hasse diagram for the Coulomb branch of the quiver (99) is not known, which is why we have kept the link in the Hasse diagrams in Figs. 41, 42 corresponding to this slice as d_4/S_4. However, we can form part of it in the way we have done in Fig. 40. Here we have performed transitions to show what we might expect by combining NS5-branes and then (at the end) freezing D6-branes on the NS5-branes. We find that we get the Hasse diagram given in Fig. 40 where the last brane system has as its magnetic quiver affine a_2, given in (100).

$$
\circ\!\!\!\Lleftarrow\!\!\!\circ \atop 1 \quad\quad 2
\tag{100}
$$

Let us also explain how we have found the transitions in Fig. 40. When we are combining two NS5-branes with the same charge of 1 we have an A_1 transition. When we combining two NS5-branes of different charge we have an m transition. When we are combining two NS5-branes each of charge 2 we have an $A_1 \cup A_1$ transition since the individual NS5-branes are identical objects.

The Hasse diagrams for the additions of elementary slices onto the quiver (99) are presented in Figs. 41, 42. In each of these we see the global symmetry after enhancement having an $SU(3)$ factor which corresponds with the lowest a_2 slice we see in Fig. 40. Hence although we cannot claim that the Hasse diagram Fig. 40 is complete, it stands to reason that the lowest slice of affine a_2 is the unique lowest node in the Hasse diagram.

We can also compute the electric quiver. Taking the D6-branes to now be suspended between NS5-branes we find the electric quiver (101), where we have included the parameter x because for different numbers of D8-branes we will find a different $SO(x)$ flavour group.

$$
\begin{array}{ccc}
SO(4) & & SO(x) \\
\square & & \circ \\
| & & | \\
\circ\!-\!\circ\!-\!\circ\!-\!\circ & & \\
1 \quad 2 \quad 1 \quad Sp(0) &
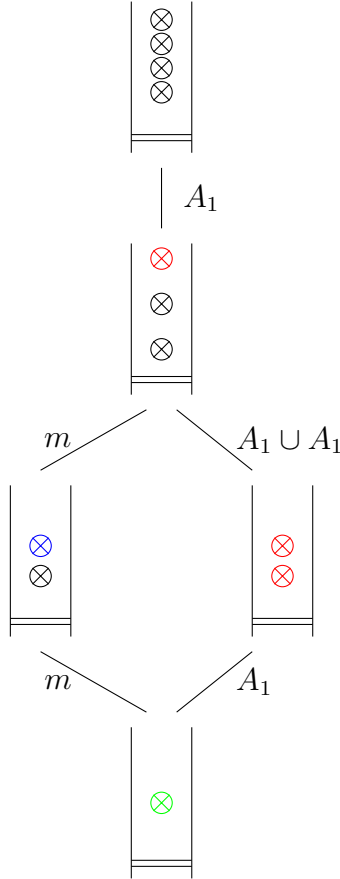\end{array}
\tag{101}
$$

Figure 40: The Hasse diagram for d_4/S_4 from a 6d brane system. We start with four NS5-branes between two D8-branes and the two D6-branes. We can make two NS5-branes coincident using an A_1 transition to the diagram below. Now the coincident NS5-branes are given in red. We now have two choices about the next transitions. The first choice is to bring the two remaining single NS5-branes to be coincident, which is an $A_1 \cup A_1$ transition as the NS5-branes are identical objects. The other way is to bring a third NS5-brane to be coincident with the two that are already coincident. This transition is a non-normal slice m and we colour the three coincident NS5-branes blue. We then can perform another m transition to bring the final single NS5-brane to be coincident with the other three to get four coincident NS5-branes, coloured in green. The final brane system is that of affine a_2.

Added Slice	$a_k, \quad k \geq 1$	$d_k, \quad k \geq 4$	e_6	e_7	e_8
Hasse Diagram	(diagram)	(diagram)	(diagram)	(diagram)	(diagram)
EGS	$SU(3) \times SU(k+1)$	$SU(3) \times SO(2k)$	$SU(3) \times E_6$	$SU(3) \times E_7$	$SU(3) \times E_8$

Figure 41: The Hasse diagrams generated from applying the quiver subtraction algorithm to the quivers given in Table 20 of [26]. We provide the constraints on the added slices in the first row and the enhanced global symmetry of the Coulomb branch in the last row. The original quiver the slices have been added to is given in (99).
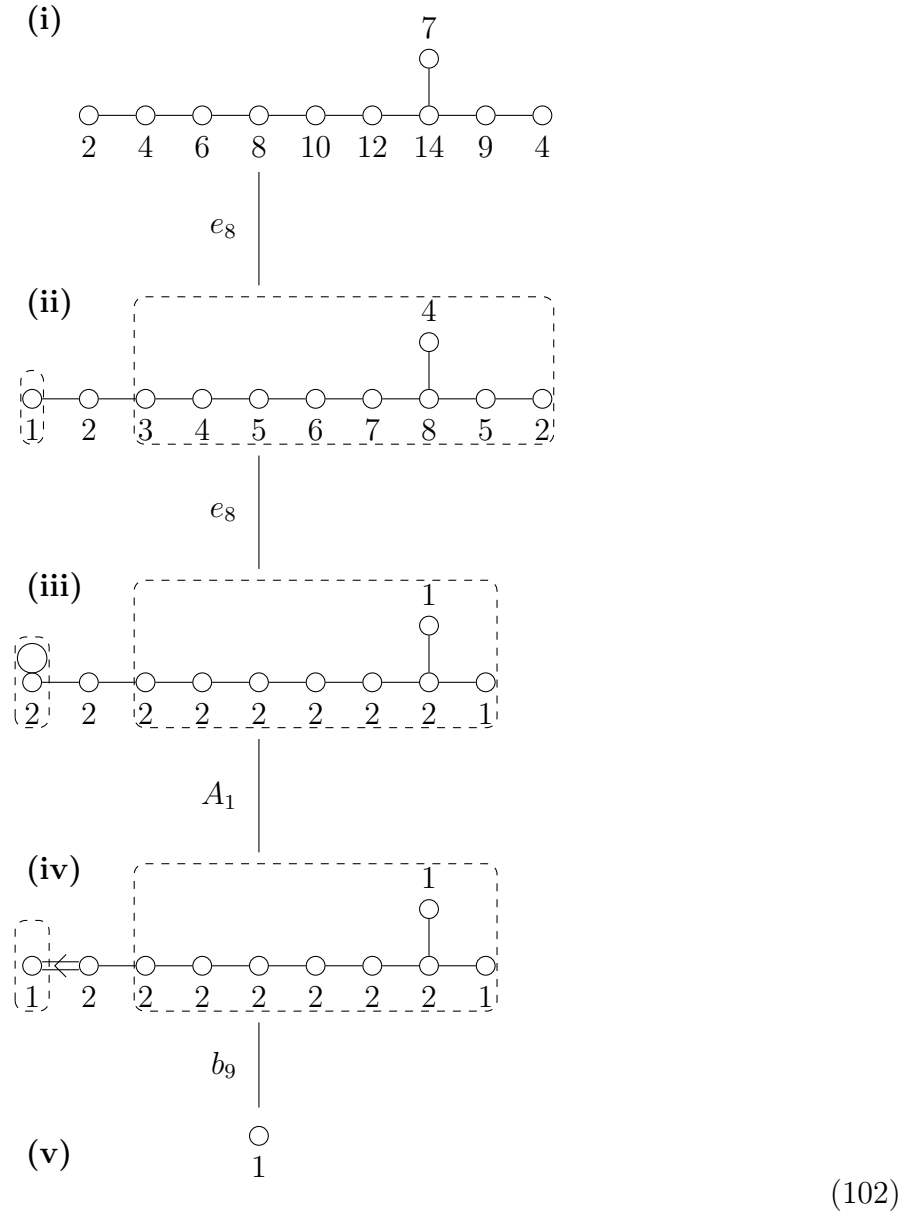
Figure 42: The Hasse diagrams generated from applying the quiver subtraction algorithm to the quivers given in Table 21 of [26]. We provide the constraints on the added slices in the first row and the enhanced global symmetry of the Coulomb branch in the last row. The original quiver the slices have been added to is given in (99).

0.9.2. e_8 ADDITION & EGS: BRANE PERSPECTIVE. We now come to the part of the report in which we present some new computations, following the methods of quiver subtraction and brane system manipulation presented in [15], [26]. In [26], the phenomenon of the enhancement of the global symmetry of the Coulomb branch of a special class of quiver was considered and these enhancements calculated. These enhancements are related to the presence of adjoint matter in particular magnetic quivers, although the adjoint Hplets can be removed through successive quiver addition. The magnetic quivers that result, despite having an enhanced global symmetry to their Coulomb branch, do not have any explicit adjoint Hplets. In Figs. 32 - 42 we present the Hasse diagrams for these quivers in full.

We will not give the algorithms here that allow us to compute enhanced global symmetry, we instead point the interested reader to [26] where they are given in full. Instead, our task is to take the results of [26] and compute the Hasse diagrams using quiver subtraction and compare them to those found using brane methods, which we explicitly compute. We do these brane computations because quiver subtraction is not on its own a convincing method for unequivocally stating the Hasse diagram for a generic quiver. We've seen how decorations have to be introduced for cases including adjoint matter and without explicit brane reasoning it is fair to doubt the accuracy of calculations.

0.9.2.1. $SO(19)$. Let's start with the quiver we gave in (80). We immediately see that we can freeze the D6-branes corresponding to an e_8 elementary slice. We then move to finite coupling by taking the NS5-brane off the orientifold (that is, we combine the two half NS5-branes to one before taking the full NS5-brane off the orientifold). Performing some Hanany-Witten transitions gives the final state of the brane system, shown in in Fig. 45 **ii**. The corresponding magnetic quiver is given in (102) **ii**. The leftmost NS5-brane contributes a $U(1)$ 'rebalancing' node to the magnetic quiver. Note that the rebalancing node in (102) **ii** has been coloured red to distinguish it. Furthermore, we have had to add a decoration to the magnetic quiver to keep track of the fact that this is a different moduli space than the moduli space that would be calculated from the magnetic quiver if the decoration was not

there.

(i)

7

○ ○ ○ ○ ○ ○ ○ ○ ○
2 4 6 8 10 12 14 9 4

e_8

(ii)

4

○ ○ ○ ○ ○ ○ ○ ○ ○ ○
1 2 3 4 5 6 7 8 5 2

e_8

(iii)

1

○ ○ ○ ○ ○ ○ ○ ○ ○
2 2 2 2 2 2 2 2 1

A_1

(iv)

1

○ ○ ○ ○ ○ ○ ○ ○ ○
1 2 2 2 2 2 2 2 1

b_9

(v)

○
1

$$(102)$$

It is now a matter of continuing this procedure for Fig. 45 **ii**. We have again taken an e_8 instanton transition and then taken the two half NS5-branes as one full NS5-brane off the orientifold. We now recover the system given by Fig. 45 **iii**. Clearly, this gives us the quiver in (102) **iii** where we now have a rank-2 node with adjoint Hplet. It is important to appreciate here that this brane construction allows us to explicitly see the transitions that make up this quiver. In the next step, we combine the two NS5-branes such that they are coincident, corresponding to an A_1 transition. Now, we have gone from two NS5-branes each of charge-1 to the D6-branes seeing a single NS5-brane of charge 2. In the magnetic quiver this corresponds to a short rank-1 node and we obtain the affine b_9 quiver, given in Fig. 45
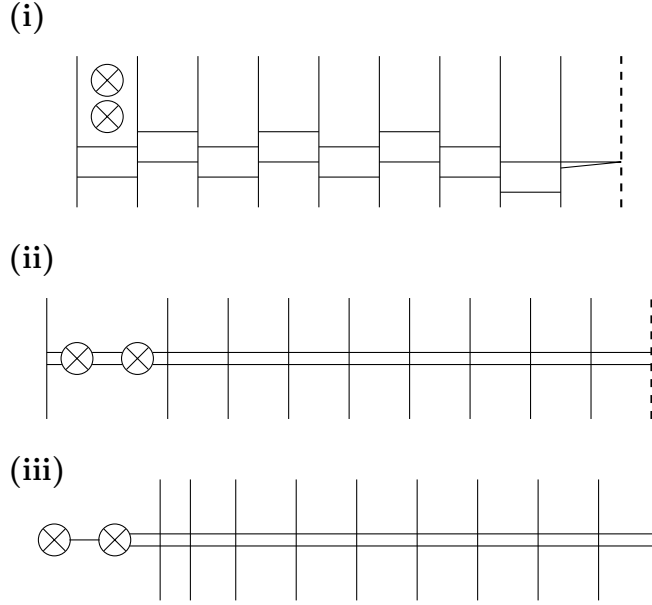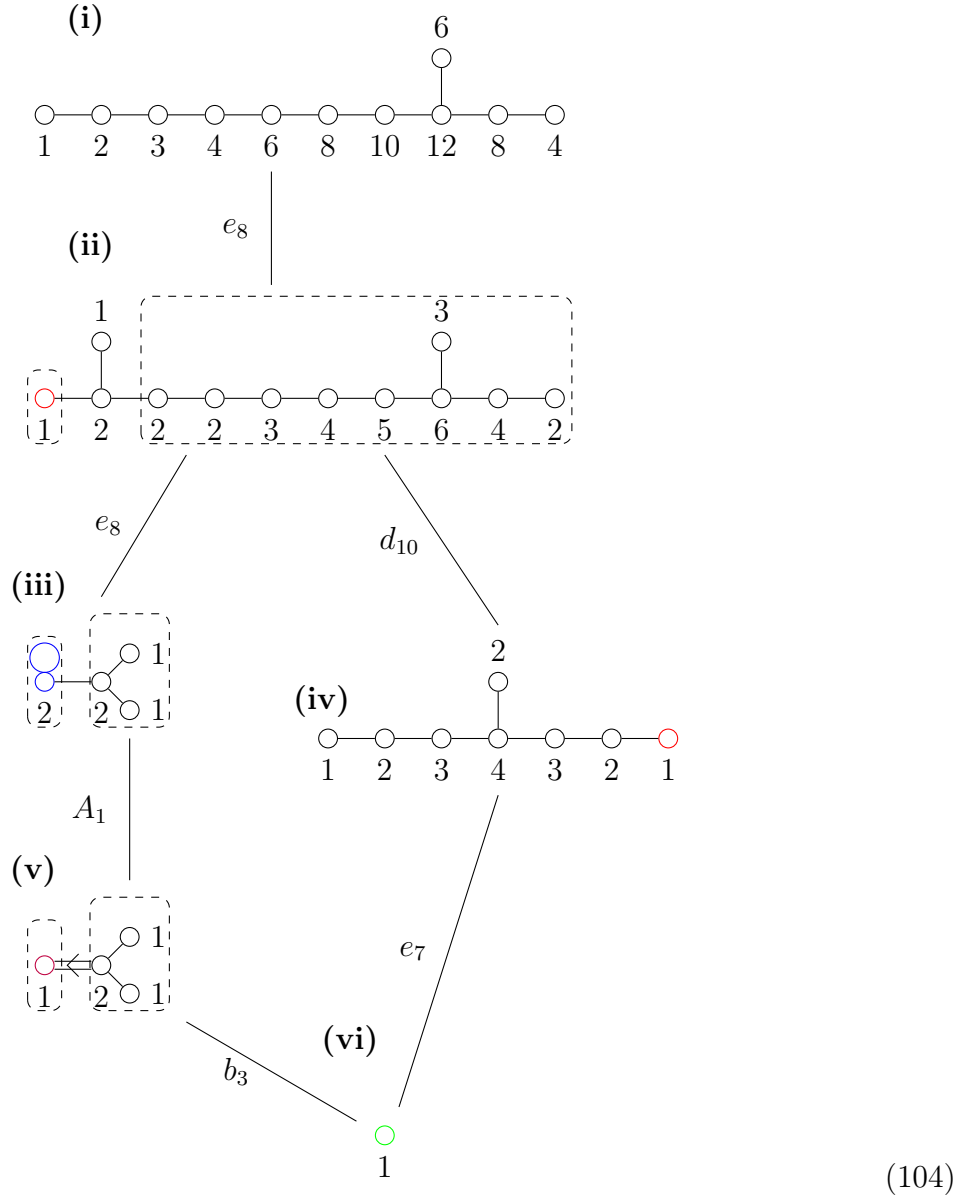
(i)

(ii)

(iii)

Figure 43: The manipulations to take the brane system with magnetic quiver (102 **i** to the phase where all D6-branes are suspended between NS5-branes. We can thus read off the electric quiver for this theory.)

iv. It is now a small task to freeze the remaining D6-branes, as we have done in Fig. 45 **v** to obtain the magnetic quiver given in 45 **v**. The power of this construction should be clear - we have seen an explicit physical realisation corresponding exactly to the quiver subtraction algorithm's results. However, we can extract even more information from this brane system - let's find the electric quiver corresponding to this system.

To do this we will need to take the NS5-branes off the orientifold, going to finite coupling, and consider again the system we see in Fig. 45 **iii**. We give the method to read off the electric quiver in Fig. 43. We see that we can read off the electric quiver as that given in (103).

$$\tag{103}$$

0.9.2.2. $SO(7) \times E_7$.

(i)

$$1 \quad 2 \quad 3 \quad 4 \quad 6 \quad 8 \quad 10 \quad 12 \quad 8 \quad 4$$

with node 6 above 12.

e_8

(ii)

$$1$$
$$1 \quad 2 \quad 2 \quad 2 \quad 3 \quad 4 \quad 5 \quad 6 \quad 4 \quad 2$$
with node 3 above 6.

e_8

d_{10}

(iii)

$$2 \quad 2 \quad 1 \quad 1$$

A_1

(iv)

$$1 \quad 2 \quad 3 \quad 4 \quad 3 \quad 2 \quad 1$$
with node 2 above 4.

(v)

$$1 \quad 2 \quad 1 \quad 1$$

e_7

b_3

(vi)

$$1$$

$$(104)$$

In similar fashion to the previous case with an $SO(19)$ enhanced global symmetry, we now consider the case of e_8 slice addition onto (85). Similar to the previous case, we begin with an e_8 instanton transition, taking the system from that given in Fig. 46 **i** to **ii**. Like before the NS5-brane becomes a rebalancing $U(1)$ node in the magnetic quiver (104) **ii**. Again we must add a decoration. We can see now from both the brane system and the quiver that there are two possibilities for further subtractions. The first is an e_8 slice that will correspond to an e_8 instanton transition in the brane system. The second is a d_{10} slice which will correspond to freezing D6-branes on the NS5-brane which we took off the orientifold in the previous step.

The e_8 instanton transition is shown in Fig. 46 **iii** where we end up with now two NS5-branes between the same two D8-branes. We recover the magnetic quiver given in (104) **iii**, where the two NS5-branes now exist as a rank-2 node with adjoint Hplet. We still have the decoration.

The d_{10} transition corresponds to freezing the D6- and NS5-branes as shown in red in Fig. 46 **iv**. These frozen branes contribute a $U(1)$ factor to the overall gauge group and we can read off the resulting magnetic quiver by realising that this $U(1)$ factor is connected to the $U(2)$ factor given by the half NS5-branes on the orientifold. From the perspective of quiver subtraction, this is seen by adding a rebalancing $U(1)$ node to the rightmost $U(2)$ node. This rebalancing $U(1)$ node is shown in red in (104) **iv**. Now let's consider the A_1 transition given between Fig. 46 **iii** and **v**. This, like before, corresponds to making the NS5-branes coincident so that the D6-branes see them as one NS5-brane of charge 2. This appears on the magnetic quiver as a short $U(1)$ node that will be attached to the $U(2)$ node given by the interval with two D6-branes. We see that the magnetic quiver is precisely affine b_3, shown in (104) **v**. It's a simple exercise to freeze the remaining D6-branes such as to be left with a single $U(1)$ node.

$$
\begin{array}{c}
SO(12)\ \square \qquad \square\ SO(8) \\
\vert \qquad\qquad \vert \\
\bigcirc \!-\!\!-\! \bigcirc \\
Sp(0) \quad 2
\end{array}
$$

(105)

As for the transition between the brane systems given by Fig. 46 **iv** and **vi**, we can freeze the remaining D6-branes and then move to finite coupling as we combine the half NS5-branes and movethem off the orientifold, then performing Hanany-Witten transitions to recover the same system as we did along the other route with the b_3 slice. This corresponds to an e_7 transition which is easily seen in the magnetic quiver (104) **vi**.

As before, this brane system gives us much more information than that pertaining to the magnetic quivers. We can also now find electric quivers for these theories.

$$
\begin{array}{c}
SO(20) \\
\bigcirc \\
\vert \\
\bigcirc \\
2
\end{array}
$$

(106)

We show in Fig. 44 the calculation of the electric quiver from the brane system by moving the D6-branes from being suspended between the D8-branes to being suspended between the NS5-branes. We find the electric quiver (105).
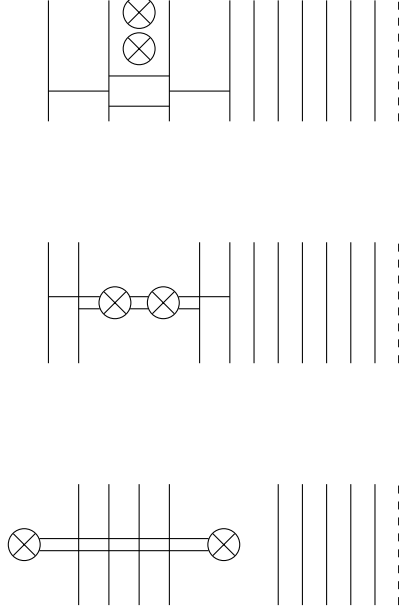
Figure 44: The transitions from the phase where the D6-branes are suspended between the D8-branes to the phase where the D6-branes are suspended between the NS5-branes for the theory defined by the magnetic quiver given in (104) **i**. We use this to compute the electric quiver.

The electric quiver (105) is that corresponding to the slice from the top to the bottom of the moduli space. The electric quiver corresponding to the slice from (104) **iv** to (104) **i** is given by (106).

0.9.2.3. $G_2 \times E_7$. For the case of the magnetic quiver with enhanced Coulomb branch global symmetry $G_2 \times E_7$, we have the brane system construction given in Fig. 47 **i**. We see that there is an e_8 instanton transition that leaves us with the brane system given in Fig. 47 **ii**. As before, we have taken the two half NS5-branes off the orientifold plane and then performed Hanany-Witten transitions until the NS5-brane no longer has any D6-branes ending on it. The NS5-brane then corresponds to the rebalancing $U(1)$ node we see in (109) **ii**. From here it is clear from looking either at the brane system or the magnetic quiver that we can perform another e_8 instanton transition and recover the brane system given by Fig. 47 **iii**. Since we now have two NS5-branes between the same two adjacent D8-branes we have an adjoint $U(2)$ node in the magnetic quiver, given by (109) **iii**.

Now we have a bifurcation in the Hasse diagram corresponding to the two transiions that we can make - either an A_1 transition in which the two NS5-branes are brought together to be coincident or another e_8 instanton transition.

First let's consider the A_1 transition. We label the new charge 2 NS5-brane in Fig. 47 **iv**, labelled red. The corresponding magnetic quiver is seen in (109) **iv**. This gives us a short

$U(1)$ node which allows for a b_9 transition by freezing the D6-branes labelled red in Fig. 47 **vi**. Clearly, either by consulting the magnetic quiver or the brane system, we have left an e_7 transition. Again we should note that the $U(1)$ node attached to the $U(2)$ node in the magnetic quiver given by the two half NS5-branes on the orientifold is seen by the frozen red branes ending (in our diagram) on the orientifold. This last e_7 transition involves freezing the D6-branes and then performing an e_8 instanton transition to recover the brane system seen in Fig. 47 **ix**. These frozen branes give a $U(1)$ gauge group, given by the magnetic quiver (109) **ix**.

The second route in the bifurcation corresponds to performing a third e_8 instanton transition. In this case we would now have a system in which we have a rank-3 node with adjoint Hplet, seen in the magnetic quiver (109) **v**. In this case we can perform an A_1 transition on the brane system by bringing two of the three NS5-branes together to become coincident, seen in Fig. 47 **vii**. This corresponds to the magnetic quiver (109) **vii**. Now we can bring the third NS5-brane to be coincident with the other two such that the D6-branes see a single NS5-brane with charge 3. This transition is the non-normal slice m. The corresponding change in the magnetic quivers can be seen in (109) **viii**. Now before we had the case of two coincident NS5-branes giving a short $U(1)$ node in the magnetic quiver with two edges linking it to its adjacent node; in the case where we have brought three NS5-branes together this short node has three edges connecting it to the adjacent node. In other words the magnetic quiver associated to the brane system Fig. 47 **viii** corresponds to affine g_2, shown in (109) **viii**.

Now for discussion about the corresponding electric quivers. The utility of these brane realisations of the transitions is that they allow us to bring the D6-branes between NS5-branes and show the electric quiver. For this brane system, a simple calculation along the lines of those we've done preciously shows the electric quiver to be that given in (107).

$$
\begin{array}{c}
SO(12)\ \square \qquad \square\ SO(6) \\
| \qquad\quad | \\
\circ\!-\!-\!-\!\circ\!-\!-\!-\!\circ \\
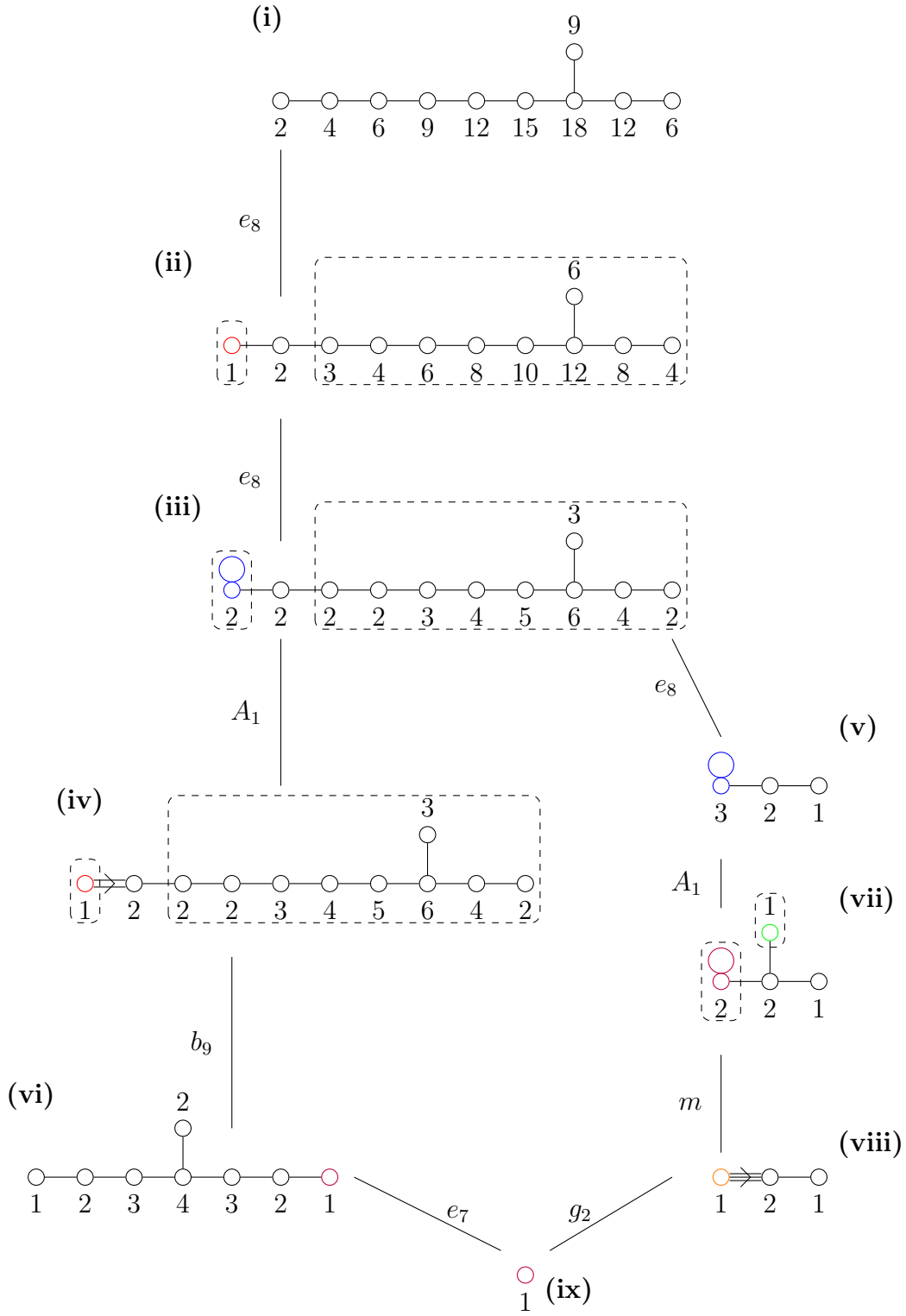Sp(0) \quad 2 \quad\; 1
\end{array}
\tag{107}
$$

0.9.2.4. $G_2 \times E_8$. In the case where we have the magnetic quiver with enhanced Coulomb branch symmetry to $G_2 \times E_8$ we consider the brane system given by Fig. 48 **i**. We can perform a first e_8 instanton transition to get to the brane system given by Fig. 48 **ii**, with associated magnetic quiver (110) **ii**. We see the NS5-brane as the rebalancing $U(1)$ node in the quiver and the decoration. We can then perform another e_8 instanton transition to get to the brane system given by Fig. 48 **iii** and the corresponding magnetic quiver (110) **iii**,

although we have a bifurcation as there is also the possibility of subtracting a d_{10} slice from the brane system given in Fig. 48 **ii**, where we now freeze D6-branes, coloured in red, to get to Fig. 48 **iv**. The associated magnetic quiver is given by (110) **iv**. Following this direction, we can perform a further e_7 transition to get to the brane system given in Fig. 48 **viii**, where we have frozen D6-branes and then taken the NS5-brane off the orientifold and performed Hanany-Witten transitions. The magnetic quiver is given in (110) **viii**. WE can also get to this brane system by taking the brane system given in Fig. 48 **iii** and performing an A_1 transition to bring two of the NS5-branes together, getting to Fig. 48 **vi**, before freezing D6-branes corresponding to a b_3 transition.
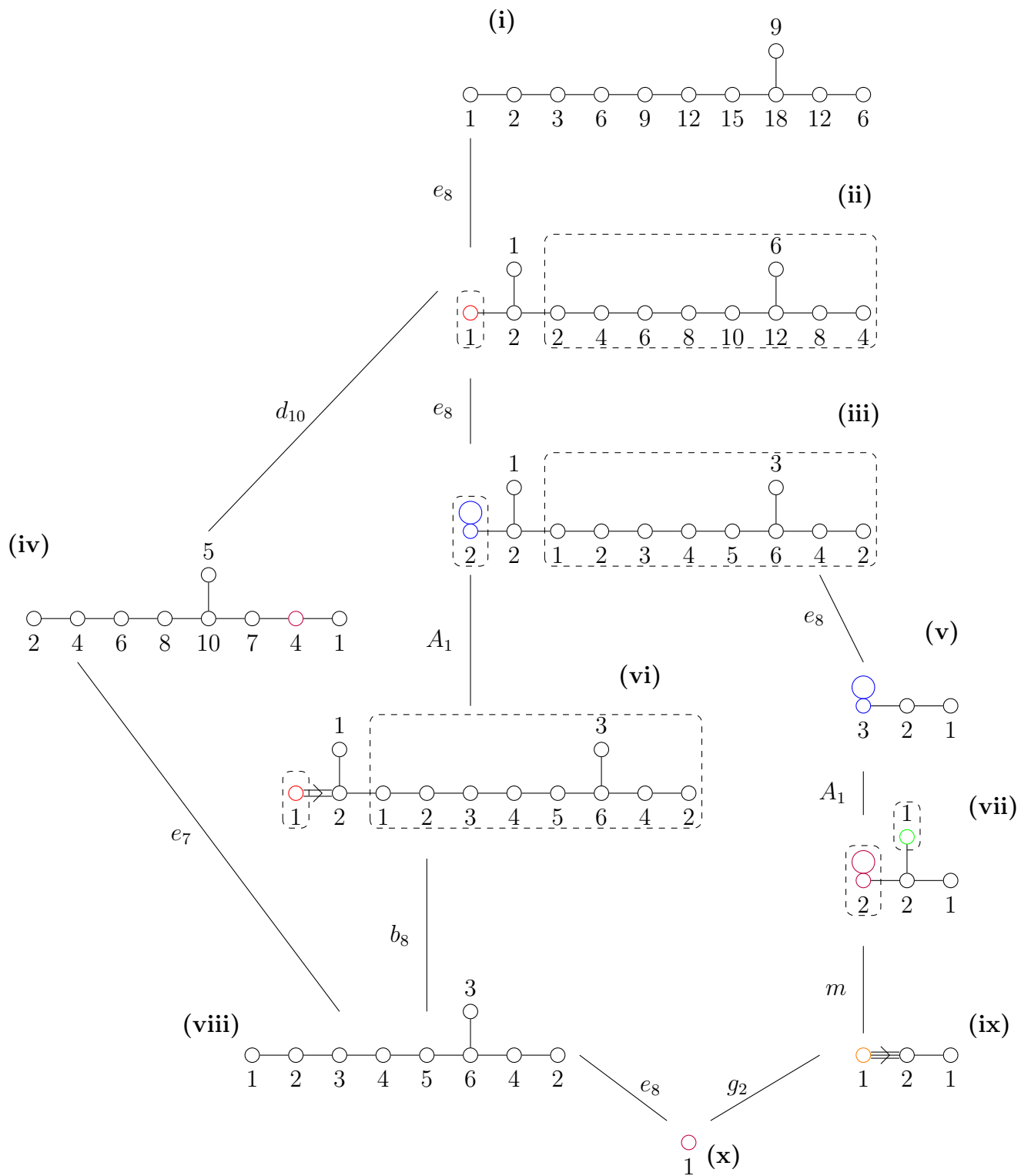
The other direction along the Hasse diagram corresponds to performing another e_8 instanton transition on Fig. 48 **iii** to get to the brane system Fig. 48 **v**, given by the magnetic quiver (110) **v**. As before, the magnetic quiver has a rank-3 node with adjoint Hplet. Now we can bring two of the NS5-branes to be coincident, corresponding to an A_1 transition, and recover the brane system Fig. 48 **vii** with corresponding magnetic quiver (110) **vii**. As we did for the $G_2 \times E_7$ global symmetry example, we can now bring the two coincident NS5-branes to be coincident with the third NS5-brane such that we end up with the brane system given by Fig. 48 **ix**, corresponding to the magnetic quiver (110) **ix** as it did in the $G_2 \times E_7$ global symmetry example. Again - it's a small matter of freezing the branes to recover a theory with $U(1)$ gauge group shown in Fig. 48 **x** and (110) **x**.

Now for the electric quiver. By performing a rearrangement of the brane system given in Fig. 48 **v** we see that the electric quiver is that given in (108). We should note an interesting fact about this - while it may seem that the magnetic quiver is the same as it was in the $E_7 \times G_2$ case, we have a different electric quiver since we have a different amount of D8-branes to the right of the rightmost D6-brane.

$$SO(14) \; \square \qquad \qquad \square \; SO(6)$$

$$
\underset{Sp(0)}{\bigcirc} - \underset{1}{\bigcirc} - \underset{2}{\bigcirc}
$$

$$(108)$$

(i)

9

2 4 6 9 12 15 18 12 6

e_8

(ii)

6

1 2 3 4 6 8 10 12 8 4

e_8

(iii)

3

2 2 2 2 3 4 5 6 4 2

e_8

(v)

3 2 1

A_1

A_1

(iv)

3

1 2 2 2 3 4 5 6 4 2

(vii)

1

2 2 1

b_9

m

(vi)

2

1 2 3 4 3 2 1

(viii)

1 2 1

e_7 g_2

1 **(ix)**

(109)

100

(i)

(ii)

(iii)

(iv)

(v)

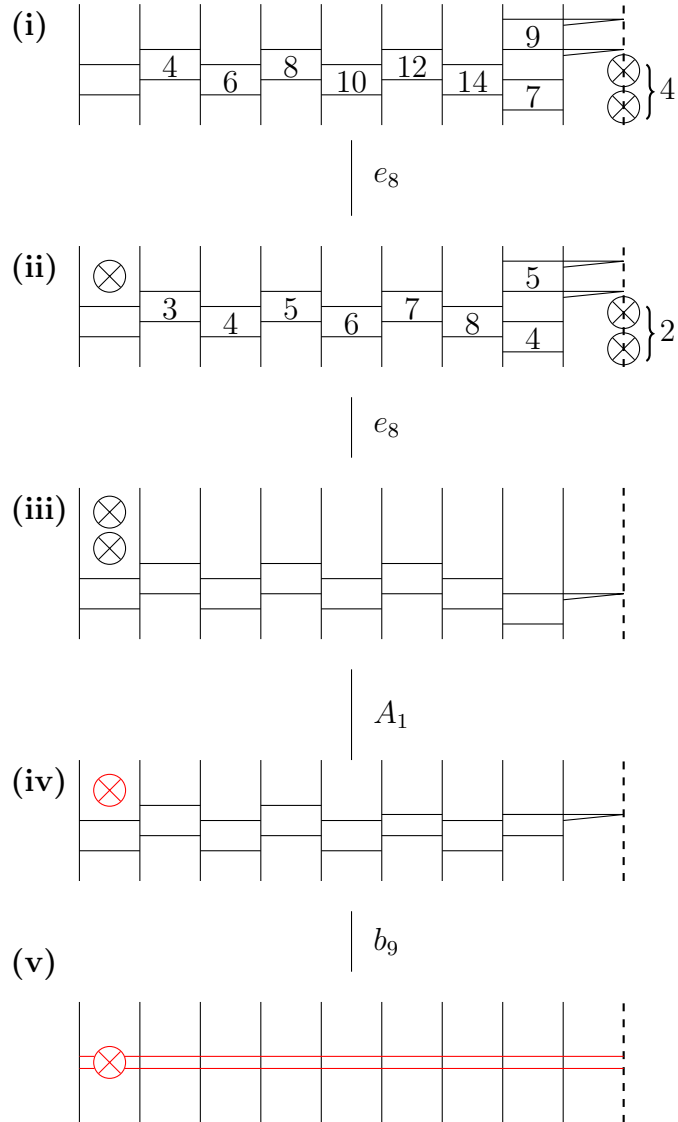**(vi)**

(vii)

(viii)

(ix)

(x)

(110)

Figure 45: The Hasse diagram calculated from freezing D6 branes in the brane system given in **i**. Full explanation is given under the subheading '$SO(19)$'.

Figure 46: The Hasse diagram calculated from performing quiver subtraction on the magnetic quiver shown in **i**. Full explanation is given under the subheading '$SO(7) \times E_7$'.
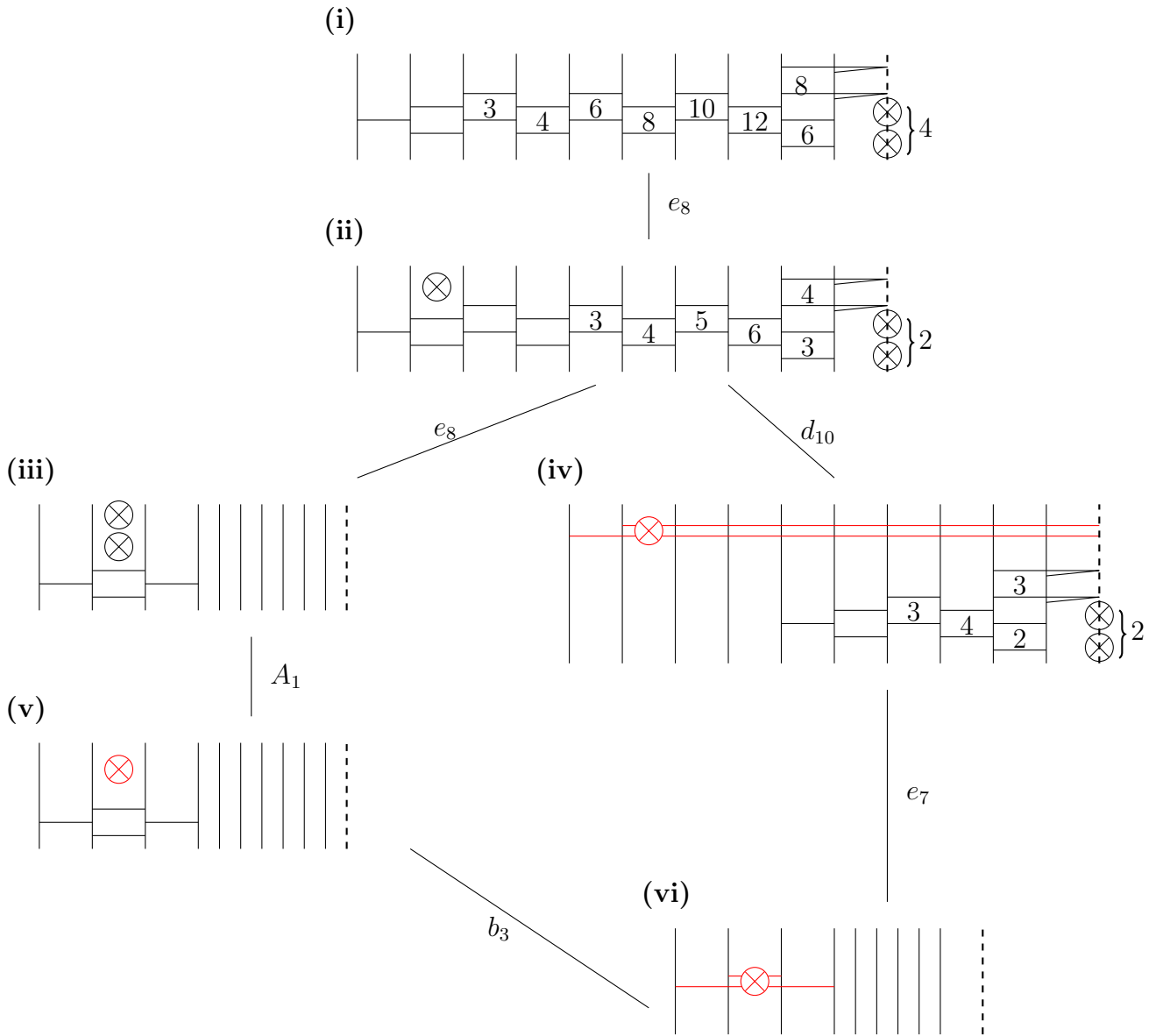
Figure 47: The Hasse diagram calculated from performing quiver subtraction on the magnetic quiver shown in **i**. Full explanation is given under the subheading '$G_2 \times E_7$'.
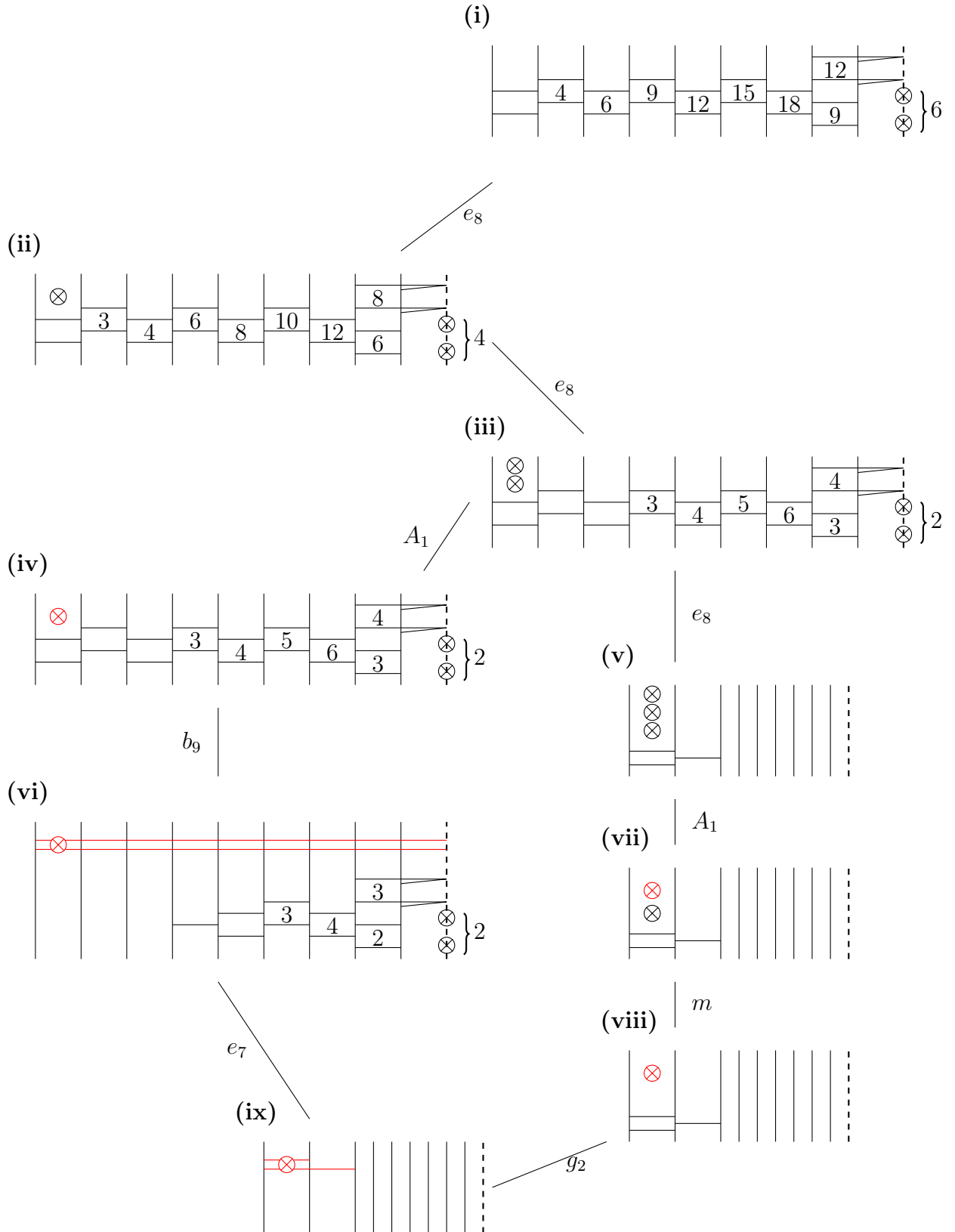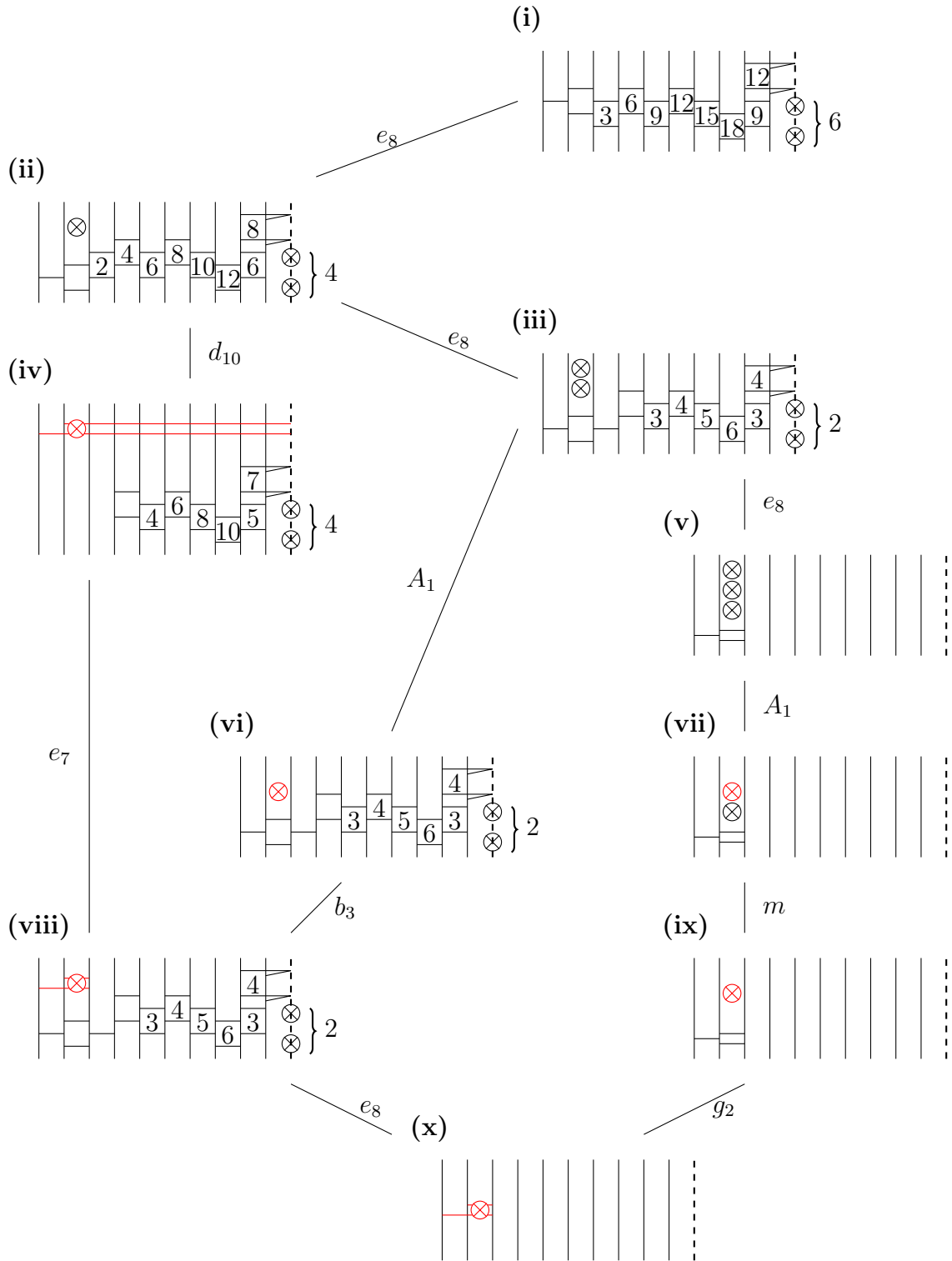
Figure 48: The Hasse diagram calculated from performing quiver subtraction on the magnetic quiver shown in **i**. Full explanation is given under the subheading '$G_2 \times E_8$'.

0.10. Conclusion. This report has provided an exposition on various aspects of Hasse diagrams and their uses in quiver gauge theory. A background of quiver gauge theory and the brane methods commonly used, the ideas of Hasse diagrams themselves and novel calculations have been provided. We began by considering the mathematical preliminaries needed for the subject, before looking further at the particular uses of Type IIB brane constructions and their associated supersymmetric gauge theories. We considered quivers with both unitary and orthosymplectic nodes and gave explicit realisations of Kraft-Procesi transitions on the former. This allowed us to give Hasse diagrams for the entire moduli spaces of various theories using the idea of Hasse diagram inversion, although this method cannot be used in all cases.

We later saw how we can use techniques from Type IIA brane constructions to provide explicit computations for quivers with decorations - we computed Hasse diagrams for a class of quivers given in [26] and checked some particular examples. We were also able to calculate some electric quivers and give an insight into how these are associated to different parts of the Hasse diagrams.

Of course, this survey gives only a particular insight into this topic and further discussion could be made of several of the areas we discussed. The interested reader might want to consider the further intricacies involved in Kraft-Procesi transitions on brane systems corresponding to theories with orthosymplectic nodes, given in [25], or the large complexity attributable to 6d theories, only some of which we used for our computations, given in [18]. Perhaps most important in our discussion has been decorated quivers. These are new objects that still are not understood fully. The brane constructions we have performed are the side that is known - further work in this area will undoubtedly attempt to define decoration more clearly.

Appendix A

Minimal Slices

Coulomb branch	Affine Quiver
a_k	A diagram with a top node labeled 1, connected to two bottom nodes each labeled 1, with $\cdots$ between them; the bottom row is braced as k.
b_k, $k \geq 3$	A top node 1 above a node 2; a horizontal chain $1 - 2 - \cdots - 2 \Rightarrow 1$; the middle nodes braced as $k-2$.
c_k, $k \geq 2$	A horizontal chain $1 \Rightarrow 1 - \cdots - 1 \Leftarrow 1$; the middle nodes braced as $k-1$.
d_k, $k \geq 4$	Two top nodes each 1 above nodes 2 and 2; horizontal chain $1 - 2 - \cdots - 2 - 1$; middle braced as $k-3$.
e_6	Vertical branch 1 above 2, attached to a horizontal chain $1 - 2 - 3 - 2 - 1$.
e_7	Vertical node 2 attached to horizontal chain $1 - 2 - 3 - 4 - 3 - 2 - 1$.
e_8	Vertical node 3 attached at node 6 of horizontal chain $1 - 2 - 3 - 4 - 5 - 6 - 4 - 2$.
f_4	Horizontal chain $1 - 2 - 3 \Rightarrow 2 - 1$.
g_2	Horizontal chain $1 - 2 \Rrightarrow 1$.

Figure A.1: The main set of minimal slices we use for quiver subtraction, reproduced from page 7 of [26].

Bibliography

[1] J. Wess and J. A. Bagger, "Supersymmetry and supergravity," 1992.

[2] S. Cremonesi, "3d supersymmetric gauge theories and Hilbert series," 2017.

[3] S. Cabrera and A. Hanany, "Branes and the Kraft-Procesi transition," *Journal of High Energy Physics*, vol. 2016, nov 2016.

[4] S. Cabrera, "Branes and the vacuum structure of supersymmetric gauge theories," 2019.

[5] N. Seiberg, "Non-trivial fixed points of the renormalization group in six dimensions," *Physics Letters B*, vol. 390, pp. 169–171, jan 1997.

[6] N. Seiberg and E. Witten, "Comments on string dynamics in six dimensions," *Nuclear Physics B*, vol. 471, pp. 121–134, jul 1996.

[7] B. C. Hall, *Lie Groups, Lie Algebras and Representations: An Elementary Introduction.* Springer Graduate Texts in Mathematics, Springer Cham, 2015.

[8] P. Tauvel and R. W. T. Yu, *Lie Algebras and Algebraic Groups.* Springer Berlin, Heidelberg, 2005.

[9] I. Kriz and S. Kriz, *Introduction to Algebraic Geometry.* Birkhauser Cham, 2021.

[10] J. Grimminger, "Real mass resolutions and complex mass deformations of 3d n=4 coulomb branches."

[11] A. Hanany and M. Sperling, "Coulomb branches for rank 2 gauge groups in 3d $\mathcal{N} = 4$ gauge theories," *Journal of High Energy Physics*, vol. 2016, aug 2016.

[12] S. Cremonesi, A. Hanany, and A. Zaffaroni, "Monopole operators and Hilbert series of Coulomb branches of 3d $\mathcal{N} = 4$ gauge theories," *Journal of High Energy Physics*, vol. 2014, jan 2014.

[13] A. Hanany and M. Sperling, "Algebraic properties of the monopole formula," *Journal of High Energy Physics*, vol. 2017, feb 2017.

[14] J. F. Grimminger and A. Hanany, "Hasse diagrams for 3d $\mathcal{N} = 4$ quiver gauge theories - Inversion and the full moduli space," *Journal of High Energy Physics*, vol. 2020, sep 2020.

[15] A. Bourget, S. Cabrera, J. F. Grimminger, A. Hanany, M. Sperling, A. Zajac, and Z. Zhong, "The Higgs mechanism - Hasse diagrams for symplectic singularities," *Journal of High Energy Physics*, vol. 2020, jan 2020.

[16] A. Bourget, J. F. Grimminger, A. Hanany, M. Sperling, and Z. Zhong, "Magnetic quivers from brane webs with O5 planes," *Journal of High Energy Physics*, vol. 2020, jul 2020.

[17] A. Bourget, S. Giacomelli, J. F. Grimminger, A. Hanany, M. Sperling, and Z. Zhong, "S-fold magnetic quivers," *Journal of High Energy Physics*, vol. 2021, feb 2021.

[18] S. Cabrera, A. Hanany, and M. Sperling, "Magnetic quivers, Higgs branches and 6d $\mathcal{N}$ =(1,0) theories)," *Journal of High Energy Physics*, vol. 2019, jun 2019.

[19] A. Bourget, J. F. Grimminger, A. Hanany, M. Sperling, G. Zafrir, and Z. Zhong, "Magnetic quivers for rank 1 theories," *Journal of High Energy Physics*, vol. 2020, sep 2020.

[20] A. Beauville, "Symplectic singularities," *Inventiones Mathematicae*, vol. 139, pp. 541–549, mar 2000.

[21] A. Bourget, J. F. Grimminger, A. Hanany, M. Sperling, and Z. Zhong, "Branes, Quivers, and the Affine Grassmannian," 2021.

[22] F. Carta and H. Hayashi, "Hilbert series and Mixed Branches of T[$SU(N)$] theories," *Journal of High Energy Physics*, vol. 2017, feb 2017.

[23] P. B. Kronheimer, "The construction of ALE spaces as hyper-Kähler quotients," *Journal of Differential Geometry*, vol. 29, no. 3, pp. 665 – 683, 1989.

[24] W. Lerche, C. Lütken, and C. Schweigert, "D-branes on ALE spaces and the ADE classification of conformal field theories," *Nuclear Physics B*, vol. 622, no. 1, pp. 269–278, 2002.

[25] S. Cabrera and A. Hanany, "Branes and the Kraft-Procesi transition: classical case," *Journal of High Energy Physics*, vol. 2018, apr 2018.

[26] K. Gledhill and A. Hanany, "Coulomb branch global symmetry and quiver addition," *Journal of High Energy Physics*, vol. 2021, dec 2021.

[27] W. Wang, "Dimension of a minimal nilpotent orbit," 1999.

[28] R. Suter, "Coxeter and dual Coxeter numbers," *Communications in Algebra*, vol. 26, no. 1, pp. 147–153, 1998.

[29] D. H. Collingwood, *Nilpotent orbits in semisimple Lie algebras*. Van Nostrand mathematics series, Van Nostrand Reinhold, 1993.

[30] A. Hanany and M. Sperling, "Resolutions of nilpotent orbit closures via Coulomb branches of 3-dimensional $\mathcal{N} = 4$ theories," *Journal of High Energy Physics*, vol. 2018, aug 2018.

[31] A. Hanany and E. Witten, "Type IIB superstrings, BPS monopoles, and three-dimensional gauge dynamics," *Nuclear Physics B*, vol. 492, pp. 152–190, may 1997.

[32] K. Intriligator and N. Seiberg, "Mirror symmetry in three dimensional gauge theories," *Physics Letters B*, vol. 387, pp. 513–519, oct 1996.

[33] B. Feng and A. Hanany, "Mirror symmetry by O3-planes," *Journal of High Energy Physics*, vol. 2000, pp. 033–033, nov 2000.

[34] A. Hanany and A. Zajac, "Ungauging schemes and Coulomb branches of non-simply laced quiver theories," *Journal of High Energy Physics*, vol. 2020, sep 2020.

[35] A. Braverman, M. Finkelberg, and H. Nakajima, "Coulomb branches of $3d\,\mathcal{N} = 4$ quiver gauge theories and slices in the affine Grassmannian (with appendices by Alexander Braverman, Michael Finkelberg, Joel Kamnitzer, Ryosuke Kodera, Hiraku Nakajima, Ben Webster, and Alex Weekes)," 2016.

[36] H. Kraft and C. Procesi, "On the geometry of conjugacy classes in classical groups," *Commentarii Mathematici Helvetici*, vol. 57, pp. 539–602, 1982.

[37] S. Cabrera, A. Hanany, and Z. Zhong, "Nilpotent orbits and the Coulomb branch of T (g," vol. 2017, nov 2017.

[38] S. Cabrera and A. Hanany, "Quiver subtractions," *Journal of High Energy Physics*, vol. 2018, sep 2018.

[39] A. Bourget, J. F. Grimminger, A. Hanany, and Z. Zhong, "The Hasse Diagram of the Moduli Space of Instantons," 2022.